Advanced thermal analysis of electrospun polymer nanofibers

Tasnim Missaoui

▶ **To cite this version:**

Tasnim Missaoui. Advanced thermal analysis of electrospun polymer nanofibers. Other [cond-mat.other]. Normandie Université, 2023. English. NNT : 2023NORMR006 . tel-04074820

HAL Id: tel-04074820
https://theses.hal.science/tel-04074820

Submitted on 19 Apr 2023

HAL is a multi-disciplinary open access archive for the deposit and dissemination of scientific research documents, whether they are published or not. The documents may come from teaching and research institutions in France or abroad, or from public or private research centers.

L'archive ouverte pluridisciplinaire **HAL**, est destinée au dépôt et à la diffusion de documents scientifiques de niveau recherche, publiés ou non, émanant des établissements d'enseignement et de recherche français ou étrangers, des laboratoires publics ou privés.

Normandie Université

THÈSE

Pour obtenir le diplôme de doctorat

Spécialité PHYSIQUE

Préparée au sein de l'Université de Rouen Normandie

Analyse thermique Avancée de nanofibres polymères

Présentée et soutenue par
TASNIM MISSAOUI

Thèse soutenue le 28/03/2023 devant le jury composé de		
MME VALÉRIE GAUCHER	PROFESSEUR DES UNIVERSITES, UNIVERSITE DE LILLE	Rapporteur du jury
M. FREDERIC HEIM	PROFESSEUR DES UNIVERSITES, UNIVERSITE DE HAUTE ALSACE	Rapporteur du jury
M. NICOLAS DELPOUVE	MAITRE DE CONFERENCES, Université de Rouen Normandie	Membre du jury
M. JOSEPH LEJEUNE	MAITRE DE CONFERENCES, ENS ARTS INDUST TEXT ROUBAIX	Membre du jury
MME ALLISSON SAITER-FOURCIN	PROFESSEUR DES UNIVERSITES, Université de Rouen Normandie	Membre du jury
M. ERIC DARGENT	PROFESSEUR DES UNIVERSITES, Université de Rouen Normandie	Directeur de thèse

Thèse dirigée par ERIC DARGENT (GROUPE DE PHYSIQUE DES MATERIAUX)

UNIVERSITÉ DE ROUEN NORMANDIE

ED 591 PSIME

GPM Groupe de Physique des Matériaux

Table of contents

Introduction

The application of nanostructured materials can be traced back to the prehistoric times. Little was known about their properties since their use was mostly related to life development on earth, starting from nanomaterials generated by volcanic ash, meteorites to weathering process of metal-containing rocks [1] [2]. One of the first applications of nanomaterials was in cave paintings that can be found in Sulawesi caves in Indonesia and in the Chauvet-Pont-d'Arc caves in France [3]. These paintings were made from carbon-based nanomaterials like graphene obtained from fire smock and soot. Another impressive example of the nanomaterial use in art is the Lycurgus Cup which is a dichroic glass displaying two different colors when exposed to different light wavelengths because of its composition containing gold and silver nanoparticles [4] [5]. Decades later, the scientific committee started gaining interest in nanotechnology due to the development of characterization techniques such as the scanning tunneling microscope (STM) and atomic force microscopy (AFM), and this interest increased with the development of nanoscaled carbon-based materials[1] [6].

To date, nanomaterials are widely used in several fields such as nanoparticles for the reinforcement of composite materials or alloys in order to have lighter weight with proper strength and hardness to be used in automotive and aerospace industries [7]. They are also used in medical field in tissue engineering, drug delivery and regenerative medicine among other fields related to civil and electric engineering [8] [9]. As a matter of fact, the high potential of use of nanoparticles, nanofibers and other forms of nanomaterials is thought to be related to their reduced size that triggers distinct properties compared to their bulk counterparts. Depending on the nature of the material, properties like conductivity, solubility, and even mechanical and thermal properties like the melting point can vary at the nano-scale. An example of this variation in properties has been reported for a solution containing gold (Au) which appears yellow in the bulk but becomes red or purple when Au nanoparticles are added [10]. Such modifications in fundamental properties are called the "size-effect" and are attributed to the high surface-to-volume ratio, the spatial confinement and in some cases less imperfections in the nanosized structure [5].

Among the above-mentioned nanomaterials, nanofibers are widely used and have an ever-growing interest. With a cross-section of tens to hundreds of nanometers and a macroscale length, nanofibers are expected to alleviate the problems related to the discontinuous nature of nanoparticles [11]. Various techniques have been used to develop nanofibers but the most commonly used is electrospinning because it is simple, can produce continuous nanofibers on

extremely short timelines and is suitable for almost any soluble polymer [12]. Their interest is also related to the tunability of their properties that were found to be size-dependent. One of the most impressive features of nanofibers is their compelling mechanical behavior which was noted to overcome that of bulk material. For example, studies conducted by Papkov et al [13] on electrospun PAN nanofibers revealed a simultaneous increase in elastic Modulus, strength and toughness as the diameter of the nanofibers decreased, contrarily to the classical strength/ductility trade-off. Subsequent investigations using a wide range of characterization techniques led to the conclusion that this behavior can be attributed to a high molecular orientation in nanofibers together with a low degree of crystallinity induced by the electrospinning process [14]. However, this explanation remains fragmentary and require further investigation of the structure-properties relationship of nanofibers due to difficulties related to the nanosized structure of nanofibers, the number of control parameters involved in electrospinning and to the physical properties of the electrospun polymer.

In this context, this research was carried out to better understand the behavior of electrospun nanofibers by studying their physical properties through an approach that combines spectroscopic and especially thermal techniques. This PhD work is realized within the framework of the project *Nanoscale Design* led by the international laboratory *Advanced Mechanics and Materials Engineering (AMME)* which is a joint laboratory between the *Groupe de Physique des Matériaux* within the University of Rouen Normandy and the *Department of Mechanical and Materials Engineering* within the University of Nebraska Lincoln. The work and results have been structured as following:

- The first chapter provides a definition and classification of the nanomaterials. Then it focuses on nanofibers which are the form investigated in this thesis as well as the electrospinning technique, varieties of setups and parameters impacting the process. Some of the emerging applications of electrospun nanofibers are also presented. Another part is dedicated to the characterization techniques of nanofibers together with their properties with a particular emphasis on their molecular orientation.

- The second chapter introduces the polymers studied and some of their main characteristics. It illustrates the structure of the electrospinning process used to produce nanofibers. The techniques used to study the structure of nanofibers are also briefly presented.

- The third chapter focuses on the polyacrylonitrile electrospun nanofibers where the signature of molecular orientation was tracked through two different aspects. The first one, investigated the glass transition temperature together with the degree of crystallinity. Then, Fast Scanning calorimetry was used in order to study the physical aging of electrospun nanofibers to understand and compare the structural relaxation kinetics of nanofiber mats with different average nanofiber diameters, and to determine the melting temperature of PAN nanofibers, a temperature that is not possible to obtain by standard differential scanning calorimetry.

- The fourth and last chapter, deals with polyamide 6 nanofiber mats with different average diameters, where the tunability of the crystalline structure of nanofibers was investigated by the estimation of the ratio of polymorphic phases using different techniques and the study of their melting behavior at low and high scanning rates.

References

[1] A. Barhoum *et al.*, “Review on Natural, Incidental, Bioinspired, and Engineered Nanomaterials: History, Definitions, Classifications, Synthesis, Properties, Market, Toxicities, Risks, and Regulations,” *Nanomaterials*, vol. 12, no. 2, p. 177, Jan. 2022, doi: 10.3390/nano12020177.

[2] F. J. Heiligtag and M. Niederberger, “The fascinating world of nanoparticle research,” *Materials Today*, vol. 16, no. 7–8, pp. 262–271, Jul. 2013, doi: 10.1016/j.mattod.2013.07.004.

[3] M. Aubert *et al.*, “Pleistocene cave art from Sulawesi, Indonesia,” *Nature*, vol. 514, no. 7521, pp. 223–227, Oct. 2014, doi: 10.1038/nature13422.

[4] A. K. Yetisen *et al.*, “Art on the Nanoscale and Beyond,” *Adv. Mater.*, vol. 28, no. 9, pp. 1724–1742, Mar. 2016, doi: 10.1002/adma.201502382.

[5] P. N. Sudha, K. Sangeetha, K. Vijayalakshmi, and A. Barhoum, “Nanomaterials history, classification, unique properties, production and market,” in *Emerging Applications of Nanoparticles and Architectural Nanostructures*, 2018, pp. 341–348

[6] J. Hulla, S. Sahu, and A. Hayes, “Nanotechnology: History and future,” *Hum Exp Toxicol*, vol. 34, no. 12, pp. 1318–1321, Dec. 2015, doi: 10.1177/0960327115603588.

[7] Kenry and C. T. Lim, “Nanofiber technology: current status and emerging developments,” *Progress in Polymer Science*, vol. 70, pp. 1–17, Jul. 2017, doi: 10.1016/j.progpolymsci.2017.03.002.

[8] V. Prakash Sharma, U. Sharma, M. Chattopadhyay, and V. N. Shukla, “Advance Applications of Nanomaterials: A Review,” *Materials Today: Proceedings*, vol. 5, no. 2, pp. 6376–6380, 2018, doi: 10.1016/j.matpr.2017.12.248.

[9] H. Feng *et al.*, “Core-shell nanomaterials: Applications in energy storage and conversion,” *Advances in Colloid and Interface Science*, vol. 267, pp. 26–46, May 2019, doi: 10.1016/j.cis.2019.03.001.

[10] W. Lee, K.-J. Kim, and D. G. Lee, “A novel mechanism for the antibacterial effect of silver nanoparticles on Escherichia coli,” *Biometals*, vol. 27, no. 6, pp. 1191–1201, Dec. 2014, doi: 10.1007/s10534-014-9782-z.

[11] D. Papkov *et al.*, “Extraordinary Improvement of the Graphitic Structure of Continuous Carbon Nanofibers Templated with Double Wall Carbon Nanotubes,” *ACS Nano*, vol. 7, no. 1, pp. 126–142, Jan. 2013, doi: 10.1021/nn303423x.

[12] M. S. Islam, B. C. Ang, A. Andriyana, and A. M. Afifi, “A review on fabrication of nanofibers via electrospinning and their applications,” *SN Appl. Sci.*, vol. 1, no. 10, p. 1248, Oct. 2019, doi: 10.1007/s42452-019-1288-4.

[13] D. Papkov, Y. Zou, M. N. Andalib, A. Goponenko, S. Z. D. Cheng, and Y. A. Dzenis, "Simultaneously Strong and Tough Ultrafine Continuous Nanofibers," *ACS Nano,* vol. 7, no. 4, pp. 3324–3331, Apr. 2013, doi: 10.1021/nn400028p.

[14] D. Papkov *et al.*, "Quantifying Polymer Chain Orientation in Strong and Tough Nanofibers with Low Crystallinity: Toward Next Generation Nanostructured Superfibers," *ACS Nano,* vol. 13, no. 5, pp. 4893–4927, May 2019, doi: 10.1021/acsnano.8b08725.

Chapter 1 State of the art of electrospun fibers and characterization of molecular orientation in nanofibers

1.1 Introduction to nanotechnology and electrospun nanofibers

For the last decades, nanotechnology have gained a growing interest of the scientific committee due to the compelling properties provided by nano-sized materials. Apart from their method of preparation or their chemical composition, the high surface to volume ratio of these materials is the main driving force for their development and characterization.

Nanomaterials may be defined as a material of which at least one external dimension is at the nanometric scale, that is approximately between one and several hundred nanometers. According to literature, two main categories of nanomaterials are distinguished; nano-objects and nanostructured materials [1].

Nano-objects: They include materials with one, two or three dimensions at the nanometric scale and may be classified as following:

- Nanoparticles: which designates materials with three external dimensions on the nanoscale. They can be spherical in size with a diameter of 1 to 50 nm, such as gold, palladium, or titanium nanoparticles…etc.
- Nanofibers, nanotubes or nanofilaments: which designates materials with two external dimensions on the nanoscale, and the third dimension significantly larger. Typically, it refers to longitudinal materials with a cross-section of several tens of nanometers and a length on the macroscale. A widely known example would be carbon nanotubes, polymer-based nanofibers...etc.
- Nanosheet or nanoplatelets: in which one external dimension is on the nanoscale and the other two dimensions are significantly larger, such as clay nanosheets…etc.

Nanostructured materials: They include materials with internal structure at the nanoscale. Several categories may be distinguished, among which;

- Aggregates and agglomerates of nano-objects: Within this category nano-objects may be either in individual form or an agglomeration of several particles that are significantly higher than 100 nm.
- Nanocomposites: The reinforcement part of this category may be composed totally or partially of nano-objects, that provide enhanced or specific properties of the nanometric dimension. These nano-objects can be incorporated into a matrix or a surface to modify or add a new functionality that may be magnetic, mechanical or thermal. An example of a nanocomposite can be polymers reinforced with carbon nanotubes that are used in sports equipment field to improve their mechanical behavior and reduce their weight.

- Nano-porous materials: These materials have nano-sized pores such as silica aerogels that have excellent thermal isolation properties [2] [3].

As mentioned above, nanofibers may be defined as a nanomaterial having nanoscaled dimensions in the cross-sectional direction, and macroscopic length according to the fiber axis. These structures are extremely thin, as 1000 times thinner than a human hair [4]. Thanks to their specific and unique morphology, nanofibers have emerged as the hotspot of several research areas. As a matter of fact, when the diameter of a fibrous material shrinks from several micrometers to several nanometers, amazing properties come to light such as tunable porosity, flexibility in surface functionalities and superior mechanical properties compared to bulk and other form of materials [5] [6]. The major impact of nanofibers is due to the huge variety of materials that can form them including natural and synthetic polymers, as well as metal-based materials.

The highly interesting features of nanofibers account for the development and the improvement of their manufacturing techniques. They may be classified into two types; top-down and bottom-up approaches. Top-down approach involves fabrication of nanostructures from a native structure with a large size by successive disintegration. In other words, a bulk material is broken-down into nano-sized structures, mainly by means of mechanical techniques such as cutting, refining and grinding [7]. For instance, cellulose nanofibers have been manufactured from sugarcane by enzymatic treatment of sugarcane fragments, oxidation and mechanical defibrillation [8]. Also, chitin nanofibrils were obtained from grounded and chemically treated crab shells [9]. On the other hand, in bottom-up approach small units like atoms, molecules or nanoparticles are used to fabricate nanofibers[10] [11]. Two examples using this approach are presented below, which are drawing and centrifugal jet spinning.

- **Drawing:** This technique allows the production of long individual nanofibers. It consists of placing a drop of polymer solution on a substrate. Then, by means of a micropipette a fiber is extracted at a specific rate, depending on the speed of solvent evaporation. *(Figure 1.1)* In spite of being simple and easy, this technique is time consuming and diameters of the obtained nanofibers cannot be controlled [12].
- **Centrifugal jet spinning:** This technique has the same basics as cotton candy fabrication. During this process, a jet of polymer solution or melt is generated from a rotating nozzle

under centrifugal force. The jet stretches, later, into thin nanofibres to be collected as a nanofiber web. [13]

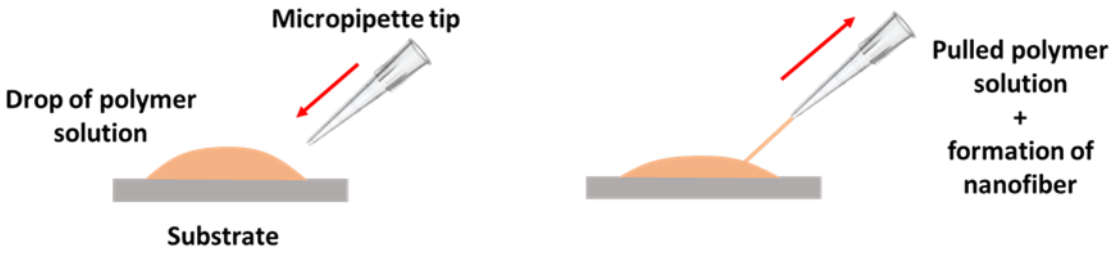

Figure 1.1 Illustration of the drawing process of nanofibers; on the left the micropipette tip is approaching the surface of the polymer drop and on the right the micropipette is pulling the polymer solution forming the nanofiber [12]

The main focus of the next part will be on another bottom-up technique that is widely used nowadays for nanofibers development which is electrospinning.

1.1.1 Electrospinning technique

It is one of the most widely adopted technique for nanofibers development, owing to its simple and low-cost set-up, along with a relatively high mass-production and adaptability with a large spectrum of polymers [4] [14]. An example of a basic electrospinning set-up, mostly used on the laboratory scale, is illustrated in *Figure 1.2* ;it consists of a source of high voltage, a syringe to which a polymer melt or solution will be fed, a syringe pump to control the polymer jet flow and a collector on which nanofibers will be deposited.

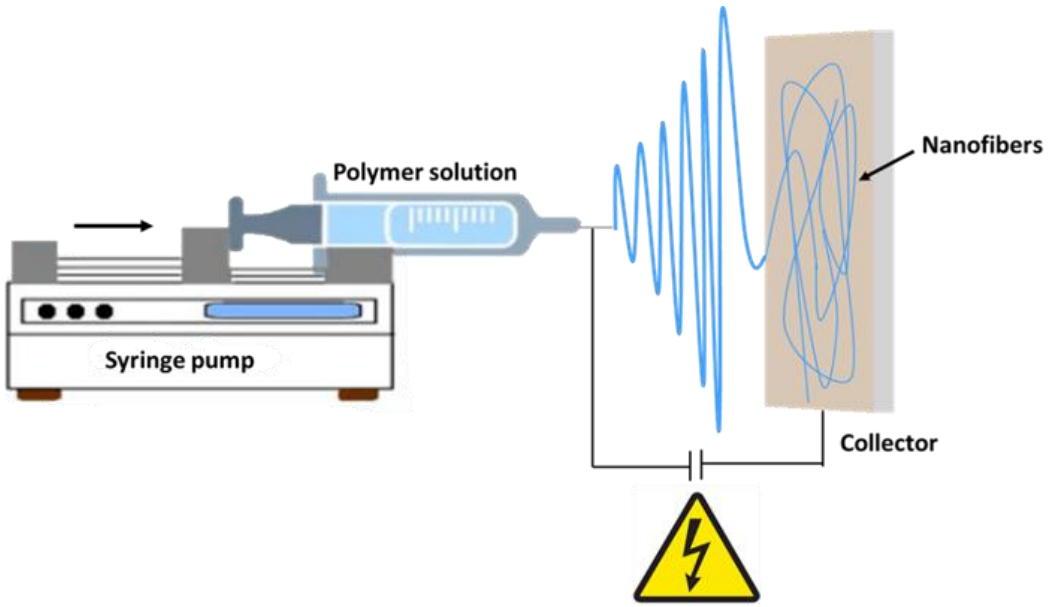

Figure 1.2 Illustration of a basic electrospinning setup

The process relies on electrostatics principle; it is the electrostatic repulsive force in a high electric field, created between the needle tip and the counter-electrode attached to the collector, that leads to nanofibers formation. More precisely, under this force a droplet of polymer solution is formed on the tip of the needle, the electric force becomes higher than the surface tension of the droplet and a jet of polymer is generated. The jet initially stretches into a straight line, then undergoes a whipping movement due to bending instabilities. As the solution jet reaches the counter-electrode, the solvent evaporates leading to the solidification of the jet that is collected on the target as nanofibers [14] [15].

Electrospinning is a versatile technique dating back to a few centuries ago. It started as a variant of electro-spraying which is also, based on the application of a high voltage to generate liquid jets. The main difference is the viscosity of the polymer jet that breaks into droplets during electro-spraying, while it remains continuous during electrospinning. [16]

The earliest work of what became electrospinning technology was realized by **William Gilbert** in 1600, during which he recorded the formation of a cone shaped water droplet in the presence of static electricity[14]. After years of research in order to understand this mechanism, several patents were filed to describe a prototype of an "electric spinning" setup until its commercialization by 1940 following the patents filed by **Formhals***(Figure 1.3)*[17]. Subsequently, the first applications of electrospun nanofiber mats have emerged with the development of air filters for aerosols and smoke-filters as gas masks [7].

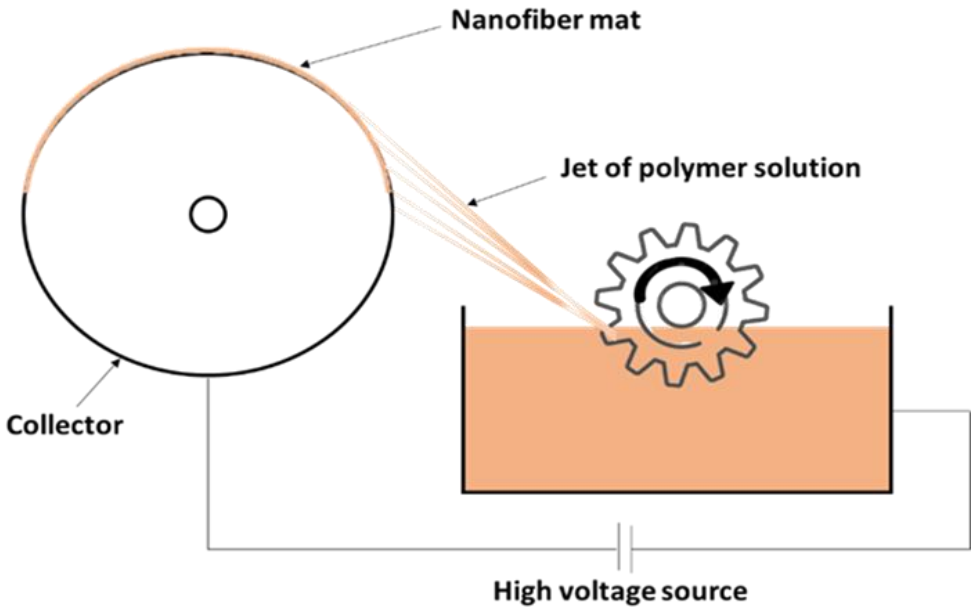

Figure 1.3 Illustration of the first electrospinning setup proposed by Formhals: it was used to manufacture synthetic nanofibers. Modified from[17]

Meanwhile, investigations to improve this technique were still carried-out. A theoretical approach was established by **Taylor** describing the spherical to conic shape change of the polymer solution droplet and its dependence on the strength of the applied electric field [18].

Later on, researches focused mainly on the study of the physical properties of the developed nanofibers, and by 1971 **Baumgarten** [19] succeeded to produce acrylic nanofilaments with diameters ranging from 500 to 1100 nm. He, also, determined in his work about polyacrylonitrile spun fibers the dependence of the fiber diameter on the solution properties, specifically the viscosity.

Ten years later, **Larrondo** and **Mandley** implemented a spinning technique for melt polymer, and succeeded to develop polypropylene and polyethylene-based fibers with relatively large diameters. In the same work, they stated that spun fibers diameters decreased when increasing the electric field voltage, which highlighted the impact of spinning condition on the physical properties of spun fibers [20]. Later on, investigations about electrospinning parameters and their impact on the stability of the polymer jet solution were carried out. It was found that for highly conductive polymer solutions, an increase in electric field generated spinning instabilities by forming multiple jets [21]. This finding proves the impact of the electric field on the physical properties of spun nanofibers such as the high distribution of their diameters. Despite these findings, the lack of characterization techniques suitable for submicron and nano-sized fibers induced a stagnancy in the development of this technique.

After a decade without any major breakthroughs in the field of electrostatic spinning, interest has arisen by the 1990s, following the work of **Reneker et al** [22] [23] that improved the spinning technique due to the increased accessibility to the characterization techniques, such as scanning electron microscopy (SEM). In their work, they studied the properties of a polyethylene oxide polymer solution by varying the polymer concentration and the voltage of the applied electric field. Consequently, they found that the diameter of the polymer jet at the tip of the needle decreased when increasing the needle/collector distance. Moreover, they determined a critical value of the polymer solution viscosity,4 Pa.s, beyond which the jet was too dense to form nanofibers [24].

Nowadays electrospinning became the technique of choice for obtaining continuous ultrathin fibers. Accordingly, the constant improving of electrospinning generated different types of spinning setups.

1.1.2 Types of electrospinning setups

To date, various electrospinning configurations have been developed to improve the properties of the resulting nanofibers and to further control their manufacturing parameters. Among these techniques the differences may be within the delivering system of the polymer melt/solution, in the shape and the position of the collector and its state, that is, stationary or moving.

The most basic and widespread type of electrospinning is the "needle setup", which was presented above in *Figure 1.2.* A hollow syringe needle is used as the spinneret, a conductive plate is used as collector and both systems are stationary. Due to its relatively low productivity, this configuration is best used on the laboratory scale for optimizing electrospinning parameters before large scale production, or for testing a new polymer material.

Therefore, to improve the productivity of nanofibers other configurations were developed such as multiple-needle electrospinning, consisting in the use of an array of several needles as its name indicates. In this configuration, needles can be organized in a straight line, circular or in elliptic arrangement through which the same or different polymer solutions may be pushed *(Figure 1.4)*. In spite of a very high voltage, the repulsion from adjacent jets is still an issue[25].

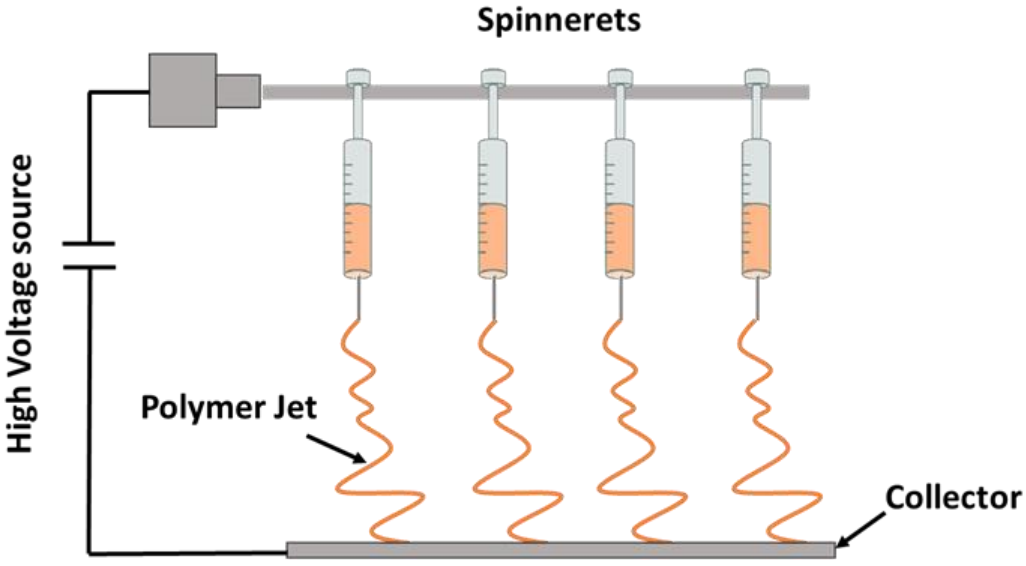

Figure 1.4 Illustration of a multiple-needle electrospinning setup.Modified from[25]

Needle-free or needleless electrospinning, present another straightforward way to increase the productivity of spun nanofibers, allowing industrial-scale production [26]. This configuration is based on open polymeric surface which simultaneously generates multiple jets under the influence of an electric field. Being next to each other, jets are formed all along the generating system of the spinning solution allowing a high and continuous mass-production of nanofibers.

Different configurations of the delivering system may exist such as a rotating cylinder immersed in a polymer solution, a translating plate associated to the container of the polymer solution or a rotary cone. *Figure 1.5* illustrates an example of a cylindrical spinneret used in needleless electrospinning [27].

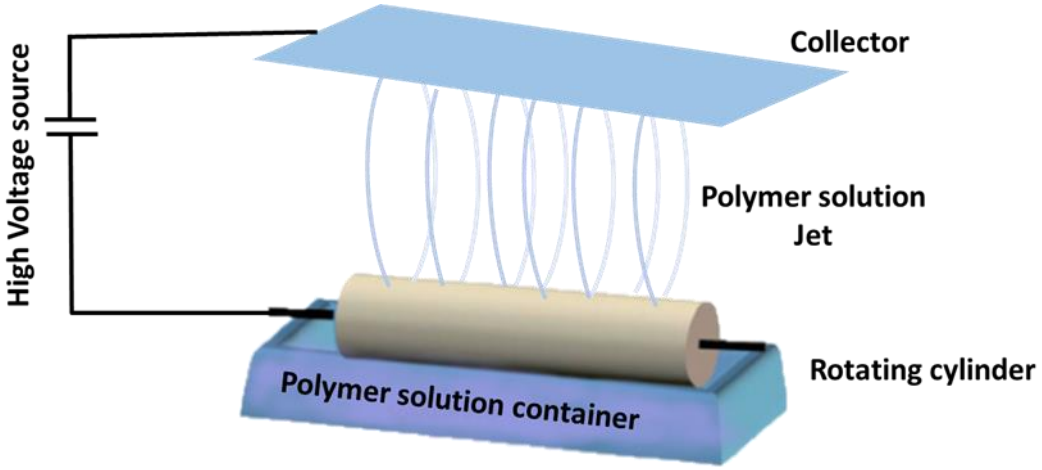

Figure 1.5 Illustration of a needleless electrospinning setup; the spinneret is a rotating cylinder.Modified from[26]

Further modifications of the basic electrospinning setups were applied in order to widen the application range of electrospun nanofibers in specific fields such as skeletal muscle regeneration, cell culture on nanofiber-based scaffolds or other applications requiring aligned nanofibers [28]. Previous studies found that changing the configuration of the collector can be an efficient route to obtain oriented nanofibers. The most common configuration to use, is a rotary collector such as a cylinder or a disk at a relatively high speed. During this process, nanofibers are mechanically drawn as they are deposited on the collector, hence being aligned along the periphery of the mandrel [29] [7]. In this matter, the impact of the rotating speed on nanofibers has been studied, and it was found that increasing the speed lead to the formation of thinner nanofibers. [30] Aligned nanofibers may, also, be obtained by a specific arrangement of stationary collector formed by two parts with aluminum or steel bar at the edges acting like a concentrator of the electric field, which leads to the stretching of the formed nanofibers, an example of these configurations is illustrated in *Figure 1.6* [29].

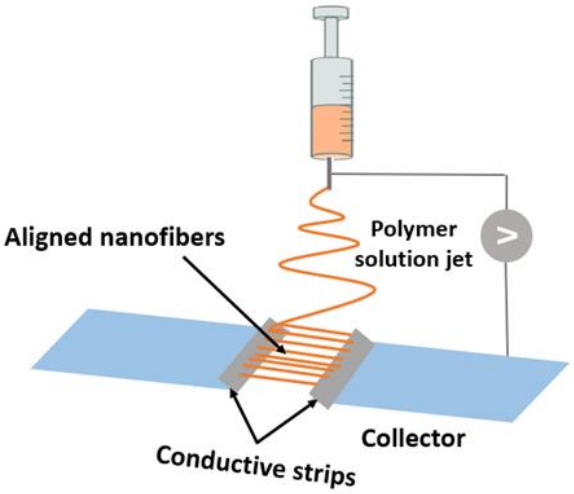

Figure 1.6 Illustration of an electrospinning setup with a modified configuration of the collector: two conductive strips are associated to both parts of the collector working as an electric field concentrator.Modified from [26]

Among the derivative techniques of electrospinning, coaxial and multiaxial configurations are emerging as a way to develop functional nanofibers from two or more different polymer solutions/melt simultaneously*(Figure 1.7)*.The process consists mainly in pumping two chemically different solutions, through a coaxial needle with a small capillary inside a larger one in coaxial geometry [25] [31]. In order to get the desired outcome, the polymer solutions should be immiscible, and the outer-solution should be spinnable to apply a shear stress on the inner-solution, that can be non-spinnable, when drawing the blended jet.

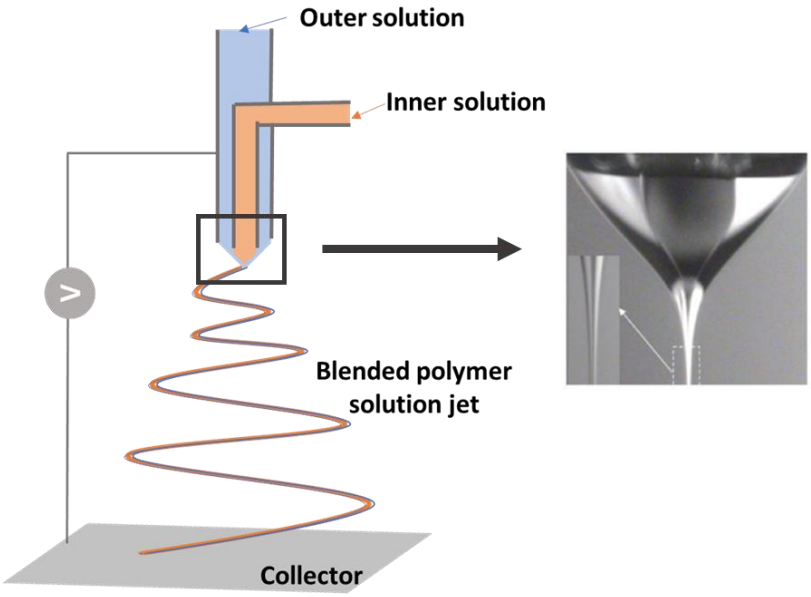

Figure 1.7 Illustration of a coaxial electrospinning setup with a detailed photo of the formed jet at the tip of the spinneret ; the inner solution forms the core of the nanofiber and the outer solution forms the shell[31]

The resulting nanofibers may have different cross-sectional shapes like a core-shell or hollow form. For hollow nanofibers or also referred to as nanotubes formation, the inner solution is removed after electrospinning either by selective dissolution or thermal degradation *(Figure 1.8)* [32].This configuration is mainly used for multidrug eluting systems with different release time to improve healing process [33] [34]. They can be also attractive for the fabrication of fluidic devices and optical waveguides [35].

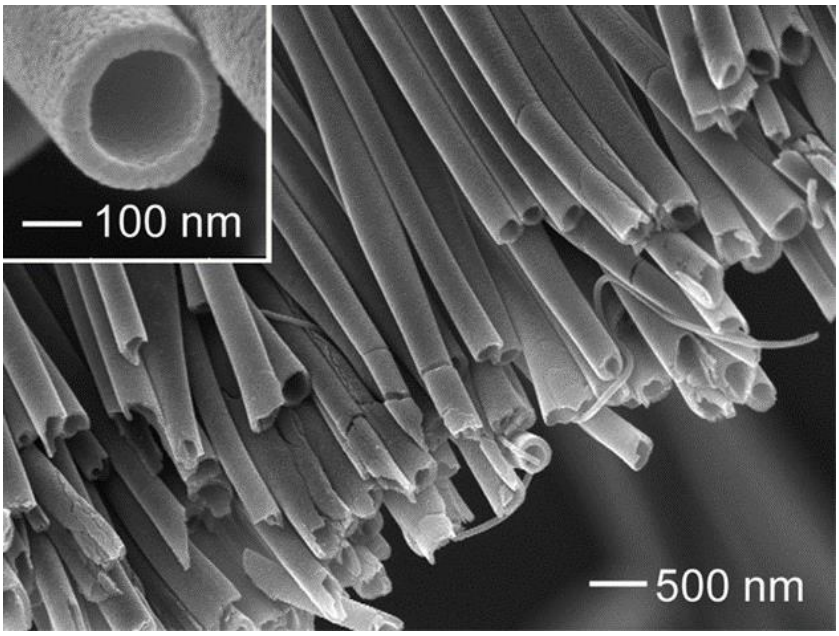

Figure 1.8 SEM images of hollow nanofibers obtained by coaxial electrospinning of Titanium isopropoxide Ti (OiPr)4 and poly (vinyl pyrrolidone) (PVP) as the outer solution and a heavy mineral oil as the inner-structure that has been removed later by immersing the fibers in octane[35]

1.1.3 Parameters of electrospinning

In order to be efficiently used in diverse applications, electrospun nanofibers must be continuous and collectable and should present specific criteria such as; a defect-free fiber surface and a uniform fiber diameter. As a matter of fact, electrospinning is governed by various parameters generally classified into three categories; the solution properties such as the concentration of the polymer, the polymer molecular weight, the processing parameters such as the applied voltage and environmental parameters. Each of these parameters significantly impacts the morphology and the characteristics of the obtained nanofibers.

Impact of polymer solution concentration

The formation of electrospun fibers is largely determined by the concentration of the polymer solution. During the electrospinning process, a balance should be established between the surface tension at the top of the spinneret and the viscosity of the polymer solution.

If the latter is too low, the surface tension dominates preventing the solution jet to be formed correctly and stretched till the collector. Indeed, a fully developed and continuous polymer jet cannot be formed and the solution is rather electro-sprayed which means that droplets are formed instead of nanofibers [22]. When increasing the solution concentration, a mixture of droplets or also referred to as beads, and nanofibers are formed. Then, further increase induces the increase of the distance between two beads and the modification of their shapes from spherical to spindle-like, till their disappearance which means the formation of bead-free nanofibers [36].

Thus, for each polymer/solvent pair, a range in which fibers may be spun efficiently is set by the intrinsic limits of the polymer solution. The lower limit is the concentration below which the macromolecular cohesion is weaker than the surface tension, leading to the formation of beads rather than continuous nanofibers. And, the upper limit is the concentration beyond which the macromolecular cohesion is too strong to be stretched and spun into nanofibers. Though, it may result in the formation of a micro-sized fibers [36].

The impact of solution concentration on nanofibers formation has been studied for a wide range of materials such as polyacrylonitrile, polylactic acid, silk…etc. [37] In this matter, **Deitzel et al.** [38] studied a polyethylene oxide solution having concentrations ranging from 4 to 10 wt%. They stated that 10 wt%-based nanofibers presented a larger average diameter, regular and cylindrical morphology, contrarily to 4 wt%-based nanofibers presenting defects and a non-uniform morphology. Similar results were found, when studying the impact of polymer solution concentration on ultrathin polyamide 6 (PA6) nanofibers. *Figure 1.9* presents SEM images of different nanofiber mats obtained upon electrospinning of 20 and 38 wt% of PA6 in formic acid and illustrates the appearance of beads for fibers obtained from 20 wt% polymer solution concentration *(Figure 1.9.A)* [39].

Impact of the molecular weight

Molecular weight influences the entanglement of polymer chains in solution, which impacts the rheological properties such as viscosity and surface tension. Typically, polymers to be electrospun present molecular weight high enough to reach spinnable polymer solution viscosities.

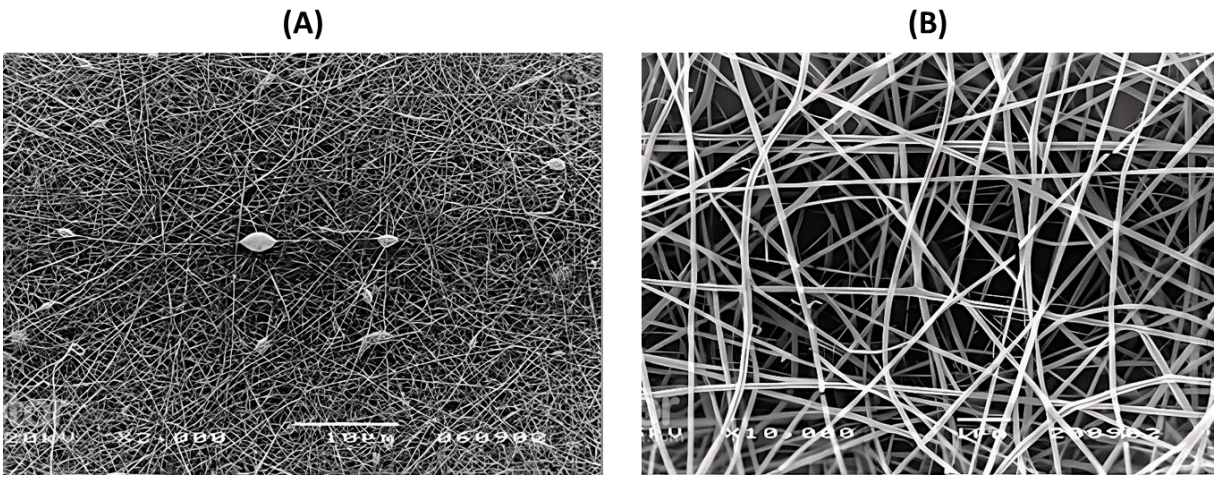

Figure 1.9 SEM images of nanofiber mats obtained from solutions of PA6 in formic acid with polymer concentration of (A) 24wt% [magnification = 2 000×, scale bar = 10 µm] and (B) 38 wt% [magnification = 10 000×, scale bar = 1 µm]. Modified from [39]

As a matter of fact, the intrinsic viscosity of a linear polymer is related to its molecular weight by the Mark-Houwink-Sakurada equation, presented below;

$$[\eta] = K \times M^{a} \quad (1)$$

Where *M* is the molecular weight *K* and *a* are constants and depend on the polymer, the solvent and the temperature [40]. It has been noted that a low molecular weight of a polymer leads to the formation of nanofibers with some defects such as the formation of beads. On the other hand, a high molecular weight will induce the formation of nanofibers with regular morphology but with relatively large diameters [41]. For a detailed investigation of the molecular weight effect, previous studies have defined specific polymer physics notions; the overlap concentration C* corresponding to the polymer concentration at which the viscosity of the solution changes abruptly, this value can be determined experimentally from the chain dimensions of the polymer and it depends on the molecular weight of the polymer. According to this value, three concentration regimes were determined; dilute for a concentration C < C*; during which the polymer chains act like isolated coils, semi-dilute for C > C*; during which an overlap of the coils and entanglement of chains occurs, and concentrated for C >> C*; for which polymer chains are highly entangled [40] [42]. This concept was found to be useful to study the impact of solution rheology on the morphology of electrospun nanofibers. In this matter, **McKee et al.** [43] studied nanofibers obtained from linear and branched polyesters in the semi-dilute regime. A critical entanglement concentration C_e was determined, above which defect-free fibers were obtained. This concentration value was considered to divide the semi-dilute regime into two sub-regimes; the semi-dilute unentangled and the semi-dilute entangled.

In the same context, **Gupta et al.** [40] investigated polymethyl methacrylate (PMMA) nanofibers with molecular weight values from 12470 – 365700 g/mol. Low molecular weight solution (12470 g/mol) in the semi-dilute regime resulted in deformed nanofibers with presence of beads. However, higher molecular weight values around 205000 g/mol resulted in the appearance of some beads in the unentangled and entangled semi-dilute regime but in uniform bead-free morphology for higher concentrations.

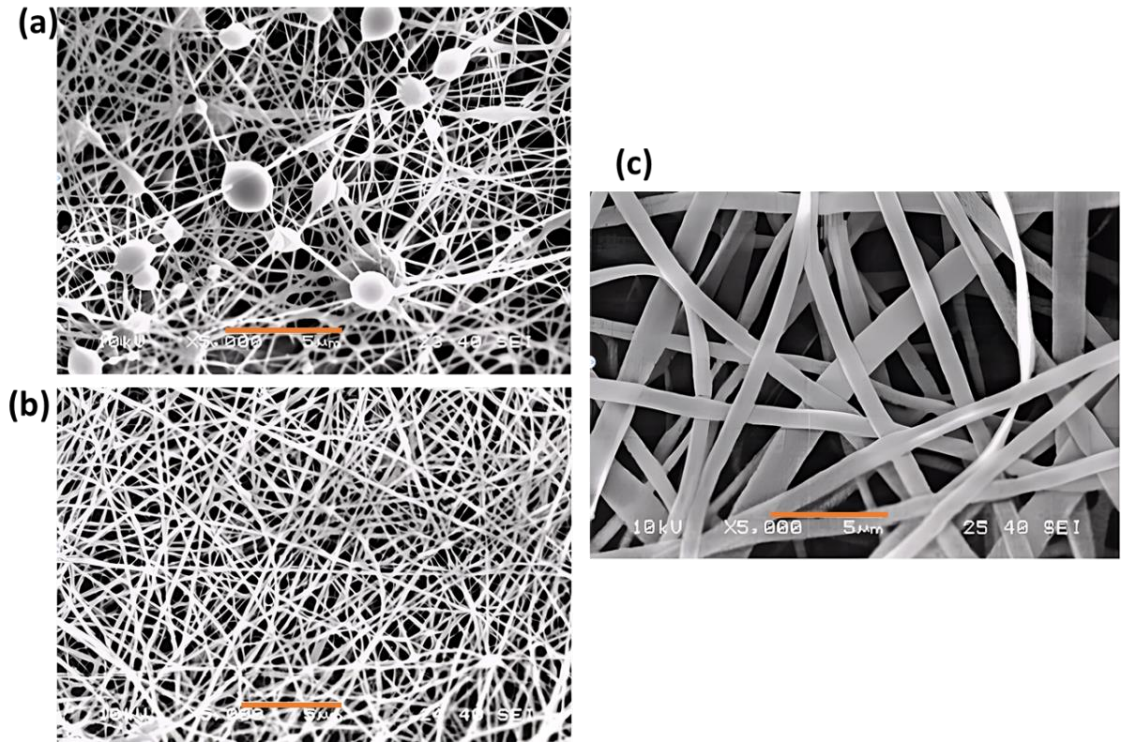

Figure 1.10 SEM images of the typical structure of electrospun PVA nanofibers for different molecular weights with (a) 9000-10000 g/mol (b) 13000-23000 g/mol (c) 31000-50000 g/mol. [magnification = 5000×, scale bar= 5μm]. Modified from [41]

Additionally, **Koski et al** [41] investigated polyvinyl alcohol (PVA) solution on nanofibers with molecular weights ranging from 9000 to 186000 g/mol. It was noticed that the average fiber diameter increased with increasing molecular weight and concentration, it varied from 250 nm till 2 μm. It was, also, stated that nanofibers with regular circular cross-section were spun for molecular weight values ranging from 13000 to 23000 g/mol *(Figure 1.10.b)*, and that flat

nanofibers with a ribbon-like cross section were formed for higher molecular weight values *(Figure 1.10.c).*

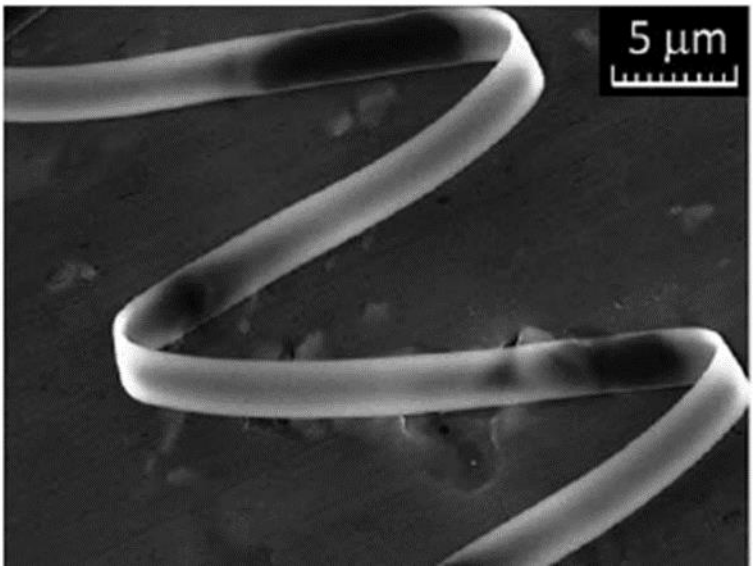

Figure 1.11 SEM image of PVP/AMT electrospun nanofiber. Modified from [44]

Figure 1.11 illustrates an example of a ribbon-like nanofiber. In this example, nanofibers are electrospun from polyvinylpyrrolidone/ammonium meta-tungstate (PVP/AMT) [44].

Impact of the applied voltage

As explained above, the concept of electrospinning is based on drawing polymer solution or melt jets under electrostatic forces. Therefore, the applied voltage during spinning is a crucial parameter to control. Practically, when a polymer solution is pumped into the syringe and an electric field is applied, a droplet is formed at the tip of the needle. When the electrostatic charges are higher than the surface tension of this droplet, it is deformed and stretched towards the counter electrode related to the collector. The electric force is, then, considered to impact the form of the drop and the stability of elongated jet, impacting the morphology of the resulting nanofibers[45]. For instance, the impact of the voltage has been studied on polyethylene oxide (PEO) nanofibers and it was noted that at 5.5 kV defect-free fibers were spun, while increasing the voltage above 9 kV, led to obtain nanofibers with a high density of beads[38].

Another influence of the voltage was revealed in the work of **Yuan et al.** [46] about bisphenol--A polysulfone (PSF), in which relatively high voltage values were applied; 10 kV, 15 kV and 20 kV. They found that nanofibers became more misaligned with the increase of the applied voltage. This was accorded to the increase of the polymer jet instability for relatively higher voltage.

Impact of the spinning distance

The spinning distance is defined as the distance between the tip of the spinneret and the collector. It is considered among the parameters influencing the resulting nanofibers diameters and morphology. In fact, it has been found that there is a minimum distance which means a minimum time required for the polymer jet to reach the collector so that the solvent can evaporate. For instance, **Ki et al**[47] investigated the impact of spinning distance of gelatin-based nanofibers. They stated that, by increasing the distance from 7.5 to 20 cm, the diameter of the obtained nanofibers presents a slight decrease along with the appearance of beads.

Impact of environmental conditions

Environmental conditions such as humidity and temperature can influence the electrospinning process and the collected fibers properties. The morphological and surface properties of nanofibers were found to change from smooth to wrinkled, ribbon-like or porous by varying the relative humidity while electrospinning [49]. Previous studies accorded this surface modification to the interaction of water, which is in most cases a nonsolvent, with the polymer jet. For instance, it was reported that polystyrene (PS) nanofibers electrospun in a high humidity environment presented a highly porous surface. This was explained by the miscibility of water and the solvent, in this case dimethylformamide (DMF). In fact, the relatively rapid diffusion of water within the polymer jet led to a liquid-liquid phase separation, taking place before the solidification of the polymer jet [48]. In a similar study, **Pai et al.** [50] reported that electrospinning at relative humidity values ≤ 15% resulted in roughness in the surface aspect of nanofibers.

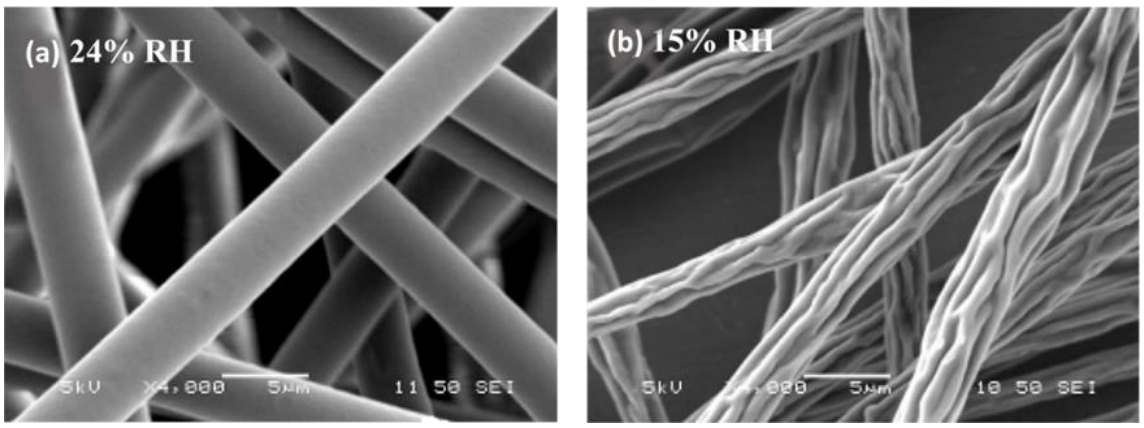

Figure 1.12 SEM images of polystyrene nanofibers from 30 wt% PS/DMF solution under (a) 24% (b) 15% of relative humidity. [magnification=4000×, scale= 5 µm][48]

For instance, *Figure 1.12* illustrates an example of this deformation that was also referred to as the formation of wrinkled nanofibers. It is believed that this aspect is related to the buckling of the external surface of the polymer jet under compressive radial stress, due to the rapid removal of the solvent from the core of the jet because of the relatively dry environment, along with a lateral contraction effect due to the stretching of the polymer jet.

1.2 Emerging applications of electrospun nanofibers

One of the most striking features of nanofibers is their exceptionally high surface to volume ratio and the tunability of their properties making them attractive candidates for several advanced applications. Nowadays, nanofibers can be made from a large spectrum of synthetic and natural polymers which enables a wider area for research about new possibilities of application.

Application in the medical field

The specific nano-sized cross-sectional continuous fiber morphology is one of the main reasons for its high applicability in the medical field. To date, enormous and progressive researches are being held in this area of applications. Several examples may be cited like; tissue engineering, wound healing, drug delivery and regenerative medicine [51] [52].For instance, for a material to be used for wound healing, it has to fulfill specific criteria such as a good physical barrier to protect the skin from bacterial penetration and acceleration of the re-epithelialization process [53]. Nanofiber mats gained interest in this application due to their nano to micro-sized, non-woven structure enabling them to mimic the human extracellular matrix (ECM). This non-woven structure promotes gas and liquid exchange with the environment and the possibility for numerous types of molecules to be incorporated in this structure. In this regard, previous studies have characterized the potential of electrospun polycaprolactone (PCL) mats containing biosynthesized silver nanoparticles (Ag), to be used as wound dressings. Silver is well known for its antimicrobial properties against several microorganisms and PCL is known for its application in biomedical field. The resulting material proved tensile properties comparable to that of a human skin, and promising antimicrobial property against two types of bacteria; E.coli and S.aureus [54]. The antimicrobial effect of PCL/Ag with different concentration of silver nanoparticles, is illustrated in *Figure 1.13*. The grey area around the small circular samples of PCL/Ag nanofiber mats are referred to as inhibitory zone of the bacteria.

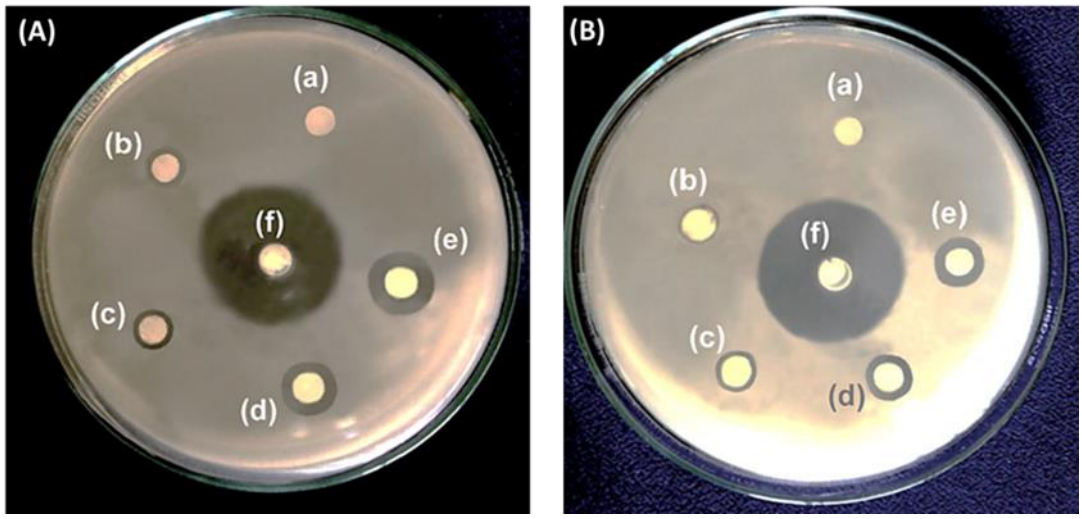

Figure 1.13 Plates showing the antimicrobial property of nanofiber mats on two bacteria (A) Staphylococcus aureus (B) Escherichia coli. (a) Neat PCL membrane (b) PCL/Ag nanocomposite membranes with 0.05% of Ag (c) with 0.25 wt% of Ag (d) 0.5 wt% (e) 1 wt% (f) Standard antibiotic disc of Ciprofloxacin used as positive control. The diameter of the inhibition zones (light grey area around the membranes) is larger when the concentration of Ag nanoparticles increases[54]

Wound dressings were, also, developed using different combinations of materials such as acrylonitrile nanofiber mats and nitric oxide particles. In vivo experiments were tried on mice and it showed a rapid healing process and a complete recovery [55]. More recently, nanofiber mats were investigated to improve the performance of protective masks, based on polyacrylonitrile (PAN) loaded by copper oxide particles. The resulting samples presented a good breathability that improved with the increase of copper oxide particles concentration from 0.25% till 1%, as well as good mechanical and antibacterial properties [56].

Additionally, nanofibers were found to present promising efficiency as drug delivery systems. The tunability of the porosity, the morphology and the composition of nanofibers facilitates the adjustment of drug release performance [57]. In this regard, electrospun nanofibers were used as carrier scaffolds for the controlled release of bioactive molecules for calvarial bone defects. The development of the scaffold was as following; nanoparticles of bovine serum albumin (BSM) loaded with a human bone morphogenic protein BMP-2 and chitosan, added to another protein dexamethasone (DEX) were electrospun along with poly(ε-caprolactone)-poly (ethylene glycol) (PCE) polymer solution. In vitro studies showed a preservation of the bioactivity of the proteins due to the incorporation in BSM. A release pattern was achieved in which most of the DEX was released in the original eight days and the BMP-2 release lasted up to 35 days. In vivo studies revealed high repair efficiency on a rat calvarial bone defect.

Hence, nanoparticles-loaded electrospun scaffold were considered to have promising applicability for bone repair in bone tissue engineering [58].

Application in reinforcement

The use of nanofibers in this field goes back to the fact that reinforcing a material with micro or macroscopic structures was found to lead, generally, to an increase in their brittleness [53]. Therefore, to overcome this inconvenience, nanofibers were used as good candidates for such fields due to the high surface to volume ratio granting better interfacial adhesion between fillers and matrices. In this matter, a previous study has investigated the mechanical properties of high-density polyethylene matrix reinforced by electrospun polyamide 66 nanofibers. The addition of a relatively small amount of electrospun reinforcement, have led to an increase in toughness, modulus and strength of the composite material which is extremely interesting for industrial applications [59]. In the same context, a new composite material was developed from recycled polyethylene terephthalate (PET) reinforced by polyacrylonitrile nanofibers (PAN), and characterization of the resulting composite stated an improvement in the compressive and flexural resistance and an increase of its barrier properties [60].

Application in Sound absorption

The impact of noise was revealed to induce very serious health issues. In order to improve sound barrier properties of the used materials, previous studies have proven the advantages of applying electrospun fibers. In fact, the continuous porous structure and high surface to volume ratio makes it perfect for the increase of the interaction between air and the material surface [57] [61]. Accordingly, nanofiber mats of polyacrylonitrile (PAN) and polyurethane (PU) were used to reinforce a commonly used combination for sound absorption which is composed of wool and polyester nonwovens. The acoustic properties of the resulting composite material were investigated, and it was stated that increasing the number and the weight per surface unit of nanofiber mat layers led to the increase of the effectiveness of sound proofing at both low and mid frequencies, contrarily to conventional materials [62].

1.3 Characterization of nanofibers

Nanofibers display a unique set of features and properties. These features include nano-sized cross-sectional dimension which makes analysis a difficult task. Despite several years of advanced research about nanofibers properties and potential of use in enormous applications, a clear understanding of the origin of their properties is still fragmentary because of the

complexity of characterizing such small-sized structures. However, an evolving interest in properly understanding the properties of nanofibers led to the application of several combination of characterization techniques and other newly emerging techniques, in order to overcome these challenges.

1.3.1 Methods of nanofibers characterization

Structural characterization

Physical properties of nanofibers are tightly related to their morphological aspects, such as the diameter, the uniformity and the defects existing within nanofibers, as well as the molecular conformation and composition. Therefore, evaluation of these aspects and their dependence on processing parameters seems crucial. Accordingly, several conventional and emerging techniques are being applied to investigate the structure of nanofibers for a better understanding and a wiser application of these materials [63].

Among these techniques, Scanning Electron Microscope (SEM) has provided relatively high-resolution images for the tested samples surfaces, giving that the magnification of an optical microscope is inadequate for characterizing nanofibers in the lower nanometer range. SEM is a suitable technique for conductive materials such as carbon nanofibers. Nevertheless, for non-conductive polymers an extra step needs to be realized, that is a coating with a thin layer of gold, which will damage the sample. Though, it remains one of the most widely used techniques to determine nanofibers diameters and identify the superficial defects [64]. An alternative to coating samples in SEM is to use environmental scanning electron microscopy (ESEM) [65]. This technique allows to examine samples with minimum specimen preparation prior to measurement, and to carry out imaging on wet samples as vapor is tolerated in the sample chamber [66].

Transmission electron microscopy (TEM) is another alternative for morphological characterization. It overcomes the limit of scanning electron microcopy, since it doesn't require coating of samples and allows the investigation of thin nanofibers with diameters smaller than 200 nm. It, also, enables investigation of nanofibrous materials with advanced structures such as bi-component nanofibers with core-shell structure [67]. Moreover, the beam of electrons transmitted through the sample varies according to the planar orientation of atoms, which reveals informations about the crystallographic arrangement and orientation within the studied material. For instance, TEM analysis was conducted to investigate the arrangement of multi

walled carbon nanotubes (MWNT) within electrospun nanofibers of poly(ethylene) oxide (PEO) [68].

Furthermore, Atomic Force Microscopy (AFM) has been used for its high-resolution probe microscope since it is a key-tool for nanoscale imaging and handling of materials at the nano-scale. Its micro-scaled cantilever with a pointed end is used to investigate materials surfaces. When the tip comes into contact with the surface, the cantilever is deformed by the forces between the material's surface and the tip, giving the possibility to assess several types of forces such as Van der Waals forces and other chemical bonding [63]. **Wang et al.** investigated the melting phenomenon of single PEO nanofibers by means of AFM which revealed a decrease of the melting temperature with decreasing nanofiber diameter [69].

Another important aspect of nanofibers that plays an increasingly prominent role in numerous applications such as drug delivery and filtration, is their porous morphology that can be obtained by adjusting electrospinning parameters like the relative humidity [49]. This aspect may be investigated by mercury porosimetry, a technique that is generally used as a standard procedure to determine pore size and distribution. Practically, mercury is introduced to a vacuum dried sample, then pressured to inter the pores within the tested materials [6]. An example of application of this technique is the investigation of the applicability of nanofibers of poly (D-L, lactide-co-glycolide) (PLGA) as a scaffold for tissue engineering. Results of mercury porosimetry allowed the estimation of pore size, volume and distribution, resulting in the fact that the formed pores are adequate for cell migration [70].

Chemical characterization

Fourier transform infrared spectroscopy (FTIR) is among the classically used technique for investigating the chemical composition of polymer nanofibers. Based on the interaction between the infrared radiation and the molecular bonds, a spectrum is obtained presenting absorption peaks with different intensities. The absorption peak intensity is related to the amount of the considered functional group within the material, and the frequency is related to the type of bond [71].

Along with the identification of molecular bonds, this technique may track the presence of residual solvent within nanofiber mats. A specific feature of this technique was particularly applied to study the macromolecular orientation within nanofibers, which is polarized FTIR; allowing the estimation of a dichroic ratio determined from orthogonal and parallel infrared

radiation to the fiber axis [72]. Other spectroscopic techniques are used for investigating the structure of nanofibers such as Raman spectroscopy and nuclear magnetic resonance (NMR).

Mechanical characterization

Nanofibers bring promising features in several fields that generally require high stress and strain levels and may lead to a deformation or a damage of these structures. Therefore, a number of methods for mechanical characterization were developed for both mat and single nanofibers.

Tensile testing is considered to be among the challenging techniques for mechanical behavior investigations of nanofibers, because it requires direct manipulation of the fibers. Previously, different setups and testing protocols were implemented to be suitable for testing nanofibrous samples. In an attempt to investigate the tensile behavior of single and mats of polycaprolactone (PCL) nanofibers, **Tan et al.** [73] used a Nano-tensile testing system. Due to the small sample size, some modifications were brought on the electrospinning setup, specifically the collector.

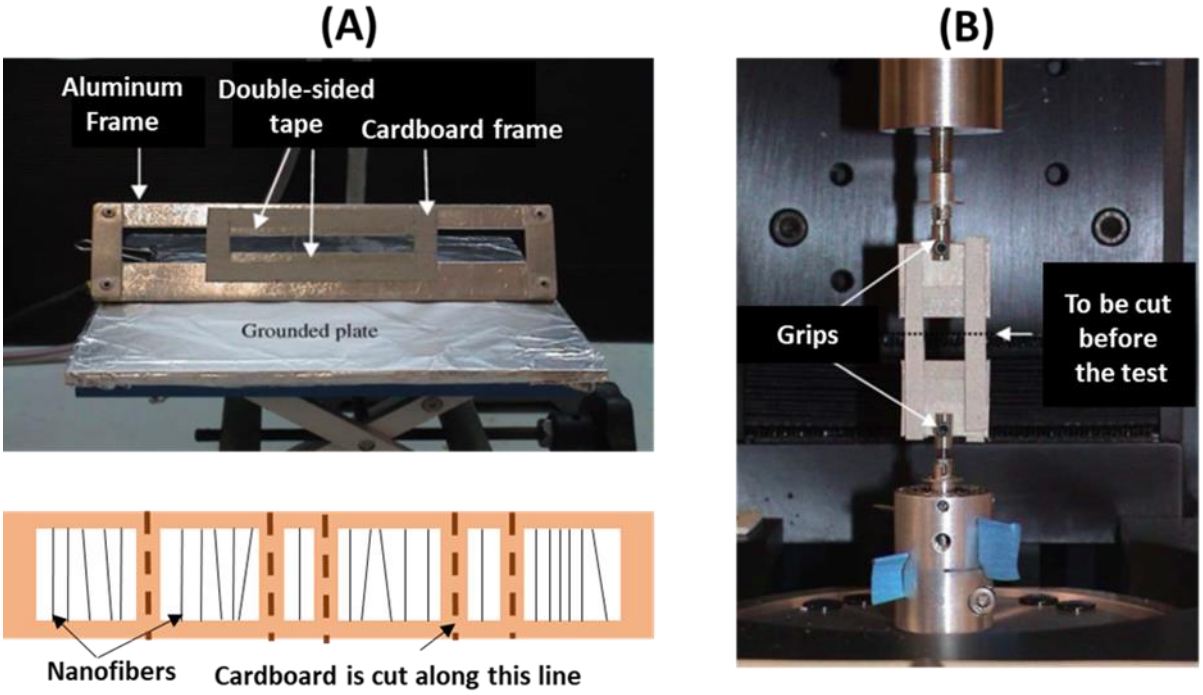

Figure 1.14 Nano-tensile testing system (A) the metallic frame used as a collector with an illustration of the partitioning of the cardboard for easier handling of nanofibers (B) the sample holder (cardboard) mounted on the tensile tester. Modified from[73]

As shown in *Figure 1.14*, a metallic frame was used as a collector to obtain aligned nanofibers, which is needed to avoid their bending or deformation when testing the mat. Another frame made of cardboard was glued on the metallic one using double-sided tape in order to facilitate the manipulation of nanofibers and avoid their slippage and altering. Results revealed high

extensibility of PCL nanofibers which is of an importance for the design of biodegradable scaffolds.

Further setups were developed for a better investigation of the mechanical behavior of individual nanofibers. Considering the nano-sized fibers, several approaches established a combination of AFM cantilever as the measuring load to carry out tests inside a scanning electron microscope (SEM) or a transmission electron microscope (TEM) [75].

For example, the setup illustrated in *Figure 1.15* allowed the investigation of the stress-strain behavior of PEO nanofibers with a diameter of 700 nm [74].

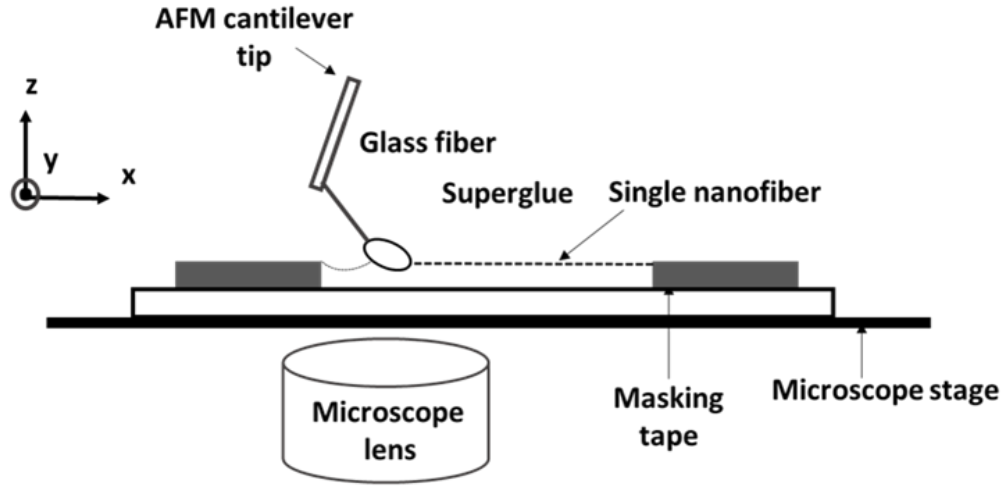

Figure 1.15 Illustration of a Nano tensile setup using AFM cantilever developed by Tan et al. Modified from [74]

The apparatus consists of a piezoresistive AFM cantilever, a microscope stage that serves as the actuator by applying the elongational deformation on the nanofiber and a camera to track the deformation of the nanofiber morphology during the test. Deflection of the cantilever tip results in a linear change of the resistance. Therefore, it is attached to a multimeter so that the resistance resulting from its deflection may be transformed into load measurements. A glass fiber is attached from one side to the tip and from the other side to the sample, facilitating the attachment of the fiber and allowing the use of the tip to test other samples.

Another setup was established by **Naraghi et al** [76] based on a microelectromechanical system (MEMS) with an integrated blade-spring load cell adjusted with an ion beam. Within this apparatus, the tested nanofiber is attached to the blade-spring load cell from one end. On the other end, the nanofiber is attached to a fix grip related to a tip-less AFM cantilever with epoxy adhesive. *(Figure 1.16).* In this work, the tested samples are PAN nanofibers with a diameter range of 300 to 600 nm. The displacement of the fiber is investigated through optical

microscopy that allows to assess the displacement of the fiber grip and the deflection of the beam supporting the load cell. Then, it is compared by digital image correlation to the unloaded configuration so that the stress and strain values can be determined. It was found that thinner nanofibers presented higher strength and lower ductility, unlike their thicker counterparts.

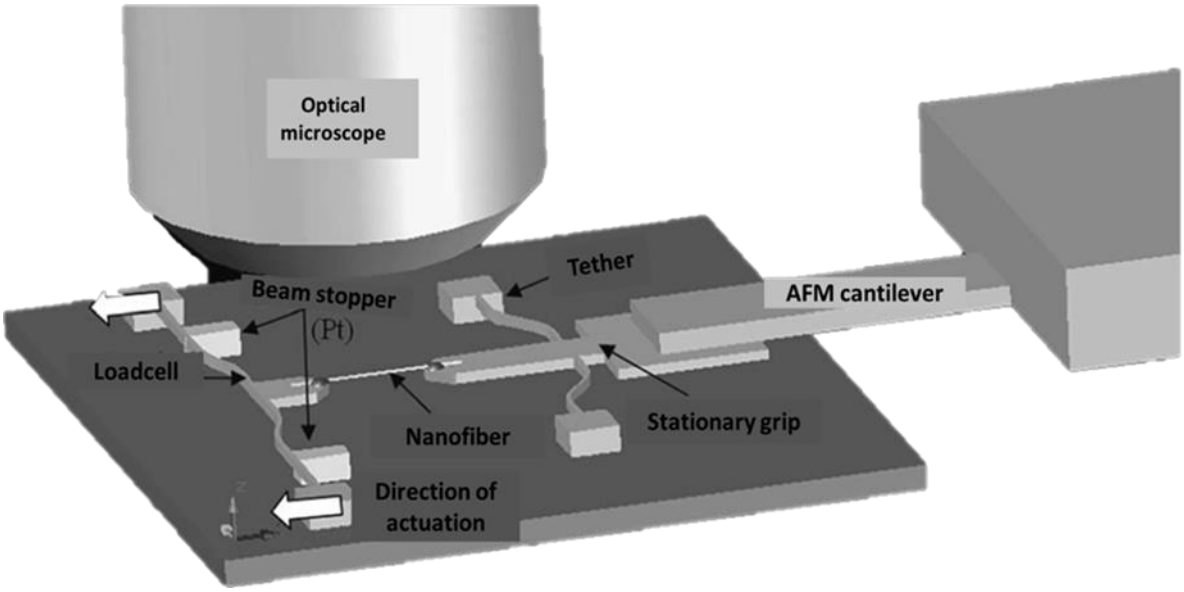

Figure 1.16 Test platform developed by Naraghi et a. Modified from [76]

A common outcome of these investigations is that nanofibers mechanical behavior is different from their bulk counterparts and depends on nanofibers characteristics. Correspondingly, nanofibers investigated in the above-mentioned studies showed an increase in strength and toughness with the decrease of their diameters, whereas thick nanofibers presented mechanical properties similar to the bulk material. This behavior has been attributed to the fact that electrospun fibers underwent high elongational deformation during the fabrication process leading to the macromolecular orientation within their polymer chain [64] [76] [77].

1.3.2 Characterization of molecular orientation within nanofibers

Molecular orientation within electrospun nanofibers is an intriguing characteristic that is frequently noted to have a major impact on their behavior, though its investigation remains challenging. With the development of different setups able to characterize single nanofibers, a number of studies have gained insight into the relationship between molecular orientation and nanofibers properties. This was achieved by tracking the signature of polymer chain orientation through the study of nanofibers mechanical properties, crystalline structure and thermal behavior, which will be treated in the following sections.

It is noteworthy that in the following part, the term “alignment” will designate the macroscopic arrangement of nanofibers within a mat and the term “orientation” will be used to describe the polymer chain macromolecular orientation within a single nanofiber.

1.3.2.1 Mechanical behavior of nanofibers

As mentioned in the previous section, several techniques have been implemented to investigate the mechanical behavior of nanofibers. Regarding nanofiber mats, their properties were found to depend on: the microstructure of individual nanofibers composing it, the porosity, the density of nanofibers within the studied mat as well as the alignment of nanofibers. As a matter of fact, it has been stated that the alignment of nanofibers helps improving Young modulus of the mat as it increases the homogenous stress distribution, when testing the sample according to the main direction of nanofibers [78]. It is the case of poly(butylene)terephthalate (PBT) nanofiber mats that have been electrospun using a rotating drum as the collector, to obtain aligned nanofibers. An increase of the strength and the modulus of the investigated nanofiber mats by a factor of 4 was noted, when the rotating velocity of the drum increased from 4 to 17.5 m/s [79]. Similar phenomenon has been stated for poly(L-lactide) (PLLA) nanofiber mats, when take-up velocity was found to have a major impact on both molecular orientation and alignment of nanofibers. Also, tensile strength determined by nano-indentation method was noted to be higher for aligned nanofibers comparing to randomly deposited nanofibers [80].

As stated in the aforementioned paragraph, the enhancement of equipment allowing the characterization on the nano-scale have led to an increasing interest in investigating individual nanofibers. Therefore, an extremely interesting aspect of single nanofibers behavior was discovered, which is the dependence of their mechanical behavior on their size. This was first stated by **Tan et al** [81] studying the physical properties of PLLA nanofibers by means of AFM imaging and three-point bending test. They noticed a drastic increase in Young modulus when nanofiber diameters were smaller than 350 nm *(Figure 1.17).*

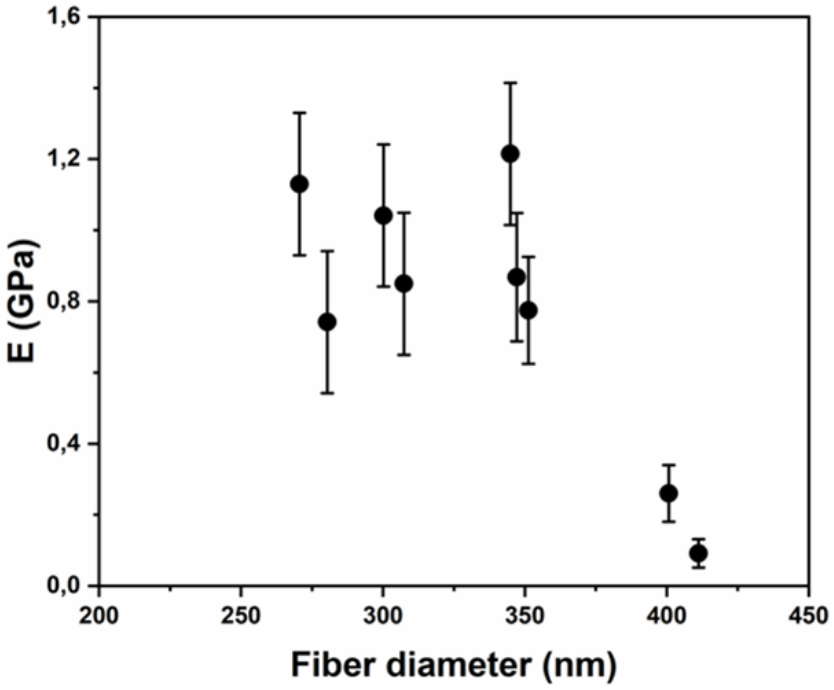

Figure 1.17 Variation of elastic modulus with nanofiber diameters of PLLA electrospun nanofibers. Modified from[81]

Further studies stated the same phenomenon, for poly (2-acrylamido-2-methyl-1-propanesulfonic acid), poly (AMPS), which is known for its poor mechanical properties in bulk. When electrospun, it showed an increase of Young modulus compared to its bulk counterpart and an exponential increase of this modulus with the decrease of nanofibers dimeter [79]. Moreover, different polymers were electrospun and the same observation was stated and the most common hypothesis of explanation is that the improvement of nanofibers behavior is related to a molecular orientation of thinner nanofibers.

Nevertheless, several studies tried to deepen the investigation to understand the origin of this behavior, by implementing different models and theories. Three main models were mostly reported in literature.

The first model was implemented by **Ji et al** [82], considering that during electrospinning, nanofibers form a thin external layer in which molecular chains are oriented due to the high stretching forces and surface tension in the outermost region of the fiber. They presumed that the degree of molecular orientation is related to the relative amount of monomers in contact with the surface compared to the amount of monomers within the sample. Therefore, as the fiber gets thinner molecular chains orient easier through the entire fiber. Besides, the polymer chains cover both surfaces when the nanofiber diameter decreases, so that the opposite sides of

the fiber are physically coupled, further strengthening the fiber. Contrarily, when the fiber thickens both surfaces are decorrelated and the amount of molecular chains in surface decreases compared to the inner fraction of molecular chains with a random coil conformation, leading to a bulk-like behavior *(Figure 1.18).*

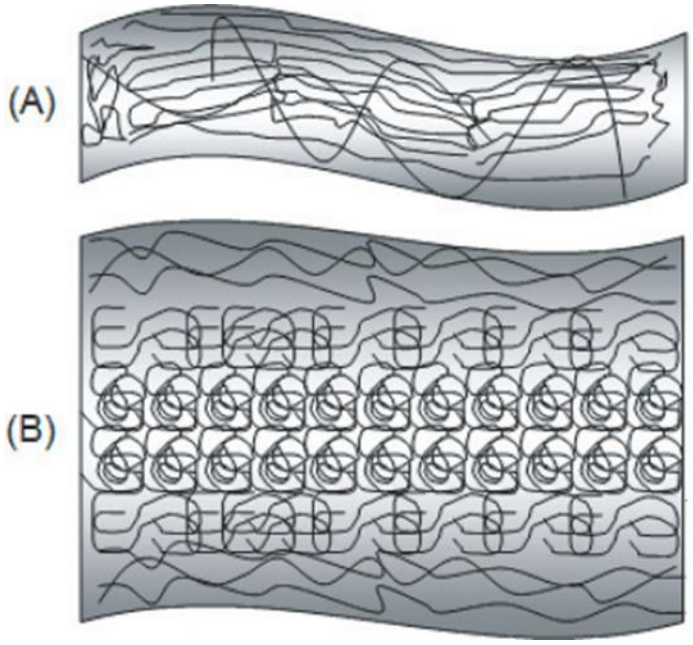

Figure 1.18 Model of the molecular chain orientation (A) Thin nanofibers with polymer chain oriented through the entire fiber (B) Thick nanofibers with oriented molecular chains on the surface extending to bulk-like random coils. Modified from [83]

Another model was later established considering the nanofiber to be formed by a "core-shell" configuration. This was noted to be related to electrospinning parameters, namely the concentration of polymer solution and the evaporation rate of the solvent [84]. As a matter of fact, it has been proposed that faster solvent evaporation takes place at the surface of the polymer jet, forming an external layer that is highly enriched in polymer compared to the core [79]. The difference between the outer and the inner parts during nanofibers formation, was attributed to a competition between the evaporation rate of the solvent and diffusion from the core which is rich in solvent to the shell in which the polymer concentration is higher. In other words, if the evaporation rate of the solvent is high, the surface thickens quickly acting like a barrier which hinders the solvent diffusion. The extreme case is that as the evaporation of the solvent progresses, the atmospheric pressure tends to deform the external layer till it collapses, leading to the formation of ribbon-like nanofibers *(Figure 1.19).*

Contrarily, for lower evaporation rates there will be no barrier preventing or delaying the diffusion of the solvent from the core to the outer surface. Hence when the solvent evaporates, cylindrical fibers are formed [85] [86] [87].

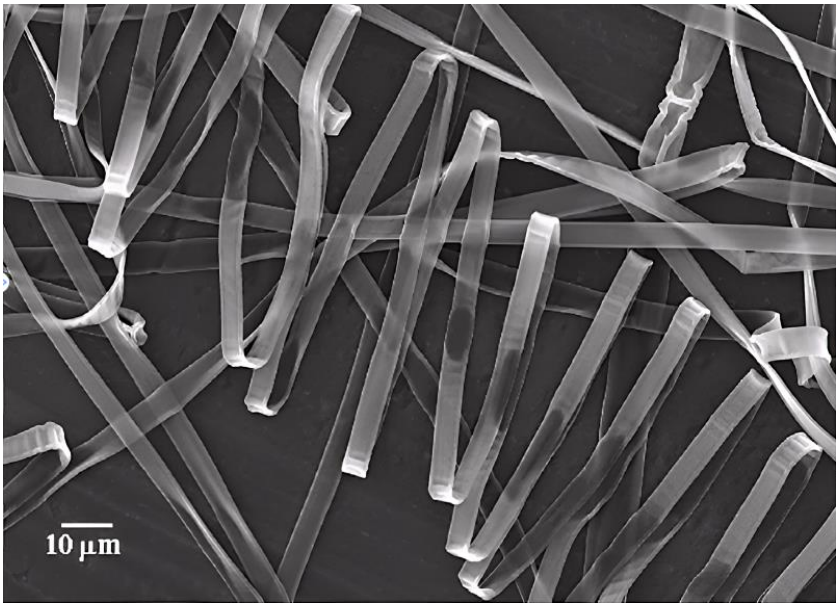

Figure 1.19 Flat ribbon electrospun from a solution of 10% poly (ether imide) in hexafluoro-2-propanol [87]

Further studies have investigated the kinetics of solvent evaporation and assumed that the residual solvent within nanofibers may induce post-processing modification of the configuration, like the relaxation of the orientation [79] [88].

Experimental support for the "core-shell" model was provided by the study of **Stachewicz et al**. [89] during which they investigated the mechanical behavior of polyvinyl-alcohol (PVA) single nanofibers. In this work, AFM imaging of the cross-section of PVA nanofibers that were prepared by Focused Ion Beam (FIB), has revealed the presence of a stiffer shell, the thickness of this shell was nearly constant when varying nanofibers diameters.

The Young modulus values of PVA nanofibers with varying diameters were quantified by AFM three-point bending and were found to increase as nanofibers diameter decreases *(Figure 1.20)*. This trend was explained by the fact that during electrospinning, the polymer jet undergoes high elongational deformation specifically at the surface of this jet due to a rapid solvent evaporation and a high electrical field leading to a higher shear stress at the surface of the jet. Therefore, PVA nanofibers were considered as composite structures formed by a shell region of oriented polymer chains and an isotropic core. Correspondingly, a "two-phase" model was implemented defining the Young modulus as a function of volume fraction of the core and the shell region.

It was reported that the elastic modulus of the shell region was higher than the modulus of the core region, and that the properties of the nanofibers are increasingly governed by the shell region when their diameter decreases [89].

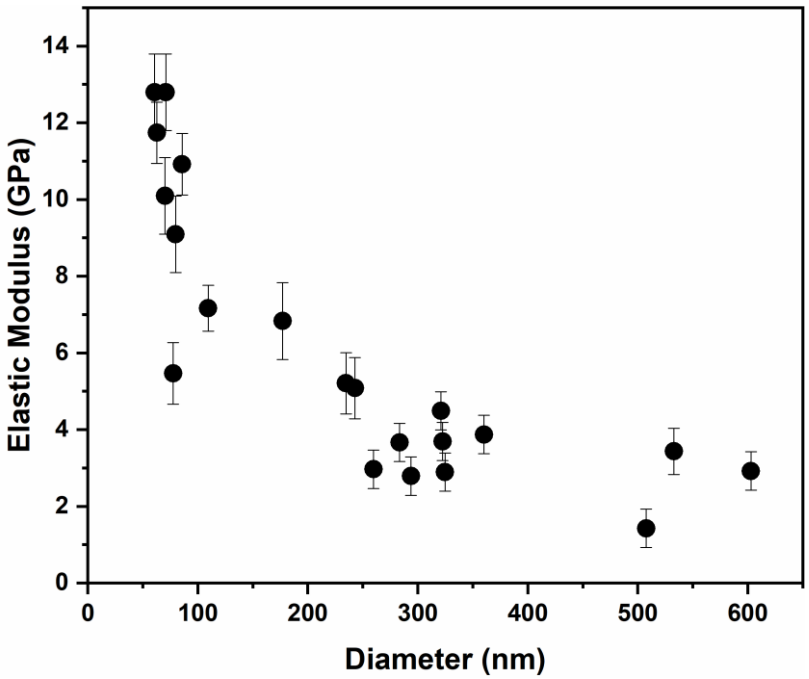

Figure 1.20 Variation of the elastic modulus as a function of electrospun PVA diameters. Modified from [89]

An alternative explanation of the size effect of nanofibers on their mechanical behavior was reported in another model, relating this phenomenon not only to a surface effect as mentioned in previous approaches, but to the formation of a supramolecular structure within the amorphous phase of the studied nanofibers. It is in their investigation about polyamide 6,6 (PA66) that **Arinstein et al.** [90] [91] studied these structures via elongation tests. It revealed an abrupt increase in Young modulus when nanofibers diameters decreased below 500 nm. However, their experimental results didn't present any abrupt change in the degree of crystallinity, neither orientation of the crystallites along the fiber axis nor the orientation of the macromolecules within the amorphous part of the fiber. Therefore, the approach suggested to explain this mechanical behavior, is that the amorphous phase contains anisotropic regions consisting of directional-correlated sub-chains that are partially oriented along the nanofiber axis. In order to introduce an efficient explanation and to be able to establish a mathematical model, these regions were schematically presented as "ellipsoid-like particles" *(Figure 1.21)*. It is the anisotropic "ellipsoid-like" regions that are considered as the structural element of the supramolecular structure of the amorphous phase. Accordingly, nanofibers are considered as composite materials formed by the above mentioned ordered regions surrounded by thin

amorphous polymer layers. When stretching the nanofiber along its axis, the ordered regions are assumed to undergo relative rotation that depends on the diameter of the studied nanofiber.

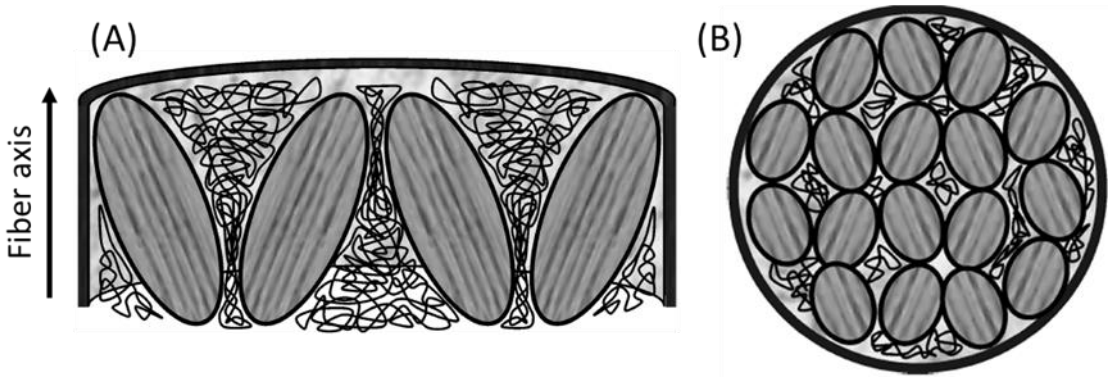

Figure 1.21 Schematic illustration of the internal structure of an electrospun nanofiber composed of ellipsoid-like ordered regions surrounded by thin amorphous layers (A) Longitudinal section of the nanofiber (B) Cross section of the nanofiber [90]

Further investigations related the improvement of mechanical behavior to the orientation within the amorphous phase. For instance, **Papkov et al.** [92] studied the mechanical behavior of PAN individual nanofibers using a nano-tensile testing machine, and noticed a simultaneous increase of the strength, toughness and modulus with the decrease of nanofibers diameters. Intriguingly, and in contrast with the previous observation of Arinstein et al, the improvement of the mechanical properties was accompanied by a decrease of crystallinity. They attributed this behavior to an enhancement of the molecular orientation due to the high elongation strains during electrospinning, and to the rapid solvent evaporation, hindering the crystallization process.

To summarize, the aforementioned models presented different approaches to how the molecular orientation of nanofibers impact their mechanical behavior and how it results from a complex combination of electrical; mechanical and mass-transfer phenomena that takes place when developing nanofibers.

1.3.2.2 Microstructure of nanofibers

Studies at the mat level

The electrospinning process allows the production of nanofibers on a millisecond scale revealing new features within the microstructure of the resulting nanofibers, such as a different crystallization behavior compared to bulk materials. As a matter of fact, the impact of the ultrafast solvent evaporation and high elongational deformation was compared to a rapid quenching process inducing, mostly, the formation of mesophase or polymorphic structure.

Few researches have investigated the impact of electrospinning on the formation of crystalline structure. One of the first studied polymers, in this matter, is polyamide 6, due to its polymorphic composition. Its structure was found to be governed mainly by two crystalline forms with different percentages according to the processing conditions; α crystals designated, normally, as the thermodynamic stable form and γ crystals designated as less stable thermodynamically or also metastable. [93] [94] When electrospun, PA6 nanofibers structure was noticed to modify, in a way that it is governed by γ-crystalline form. This was attributed to the rapid solidification of the polymer jet during electrospinning, leading to a rapid crystallization favoring the formation of γ crystals [95] [96]. In the same vein, **Giller et al** [97] studied the kinetics of solvent evaporation and its impact on the α/γ ratio by electrospinning into closed chamber, where they varied the concentration of the vapor solvent. They noticed a gradual increase of α crystals for a slow rate of solvent evaporation. Contrarily, a fast solvent evaporation led mainly to the formation of γ crystals. They accorded this phenomenon to the fact that solvent evaporation kinetics may be so fast that it overcomes the crystallization kinetics giving rise to a crystalline structure governed by γ crystals. Moreover, X-ray diffraction and polarized FTIR investigations of PA6 nanofibers with an average diameter of 200 nm have revealed a majority of γ form within its crystalline structure and have shown a preferential orientation of γ crystals along the fiber axis [96] [98].

Another example of the modification of the molecular structure arrangement of nanofibers was illustrated by a study on poly (vinylidene fluoride) (PVDF) which is known for its polymorphic structure that can reach till five different crystalline forms depending on the processing conditions. Three main forms can be mentioned which are; nonpolar α, polar γ obtained generally by melt crystallization and polar β obtained following a mechanical treatment such as drawing. In their study, **Yee et al.**[99] have electrospun PVDF nanofibers using a rotating mandrel as collector to obtain aligned nanofibers. The nanofibers microstructure was noticed to be governed by β crystals, and its spatial arrangement was reported to be extended and oriented along the fiber axis. During electrospinning, different rotation speeds were applied and no significant modification in the degree of orientation nor in the polymorphic behavior was noted. Therefore, the orientation of β crystals was explained by the forces applied by the electric field rather than the mechanical shear induced by the rotation speed of the collector.

The studies mentioned above have been realized on nanofiber mats, which means that the resulting informations relate to an average of a wide bundle consisting of different morphologies and probably some heterogeneities and defects leading to uncertainties and lack

of understanding of some phenomena. Therefore, a particular attention has been devoted to the characterization of individual nanofibers.

Studies at the single nanofiber scale

Selected Area Electron Diffraction (SAED) is among the emerging techniques for single nanofibers investigation. One of the first studies realized by this technique, investigated electrospun PA6 nanofibers with a diameter of 50 nm for a fiber length of 600 nm. Results revealed the presence of orientational order along the fiber axis, though with regions more oriented than others along the tested segment of the nanofibers. Such heterogeneity was expected considering the instabilities that the polymer jet undergoes during electrospinning [95]. Similar investigations have been realized on single nanofibers of polyethylene (PE) obtained by high-temperature electrospinning. Processing parameters were varied in a way to have a wide range of nanofiber diameters from 150 nm till several micrometers and different morphologies; circular and ribbon-like. SAED experiments showed different molecular arrangement according to nanofibers diameters; for diameters thicker than 1µm nanofibers were isotropic and for diameters ranging from 400nm till 1µm a preferential orientation was detected. High degree of orientation was noted for nanofibers thinner than 400 nm [100].

Nevertheless, few studies couldn't reveal highly efficient informations about molecular orientation by means of SAED. For instance, in their work about individual PAN nanofibers, **Papkov et al** [101] explained that SAED results exhibited weak and diffuse ring from which an effective signature of orientation wasn't possible to detect. This might be explained by the fact that SAED is restricted to the analysis of crystalline phase and was reported to be effective mostly for polymers with relative high degree of crystallinity. It is also due to the fact that electrospinning process hinders the crystallization because of the rapid solidification of the polymer jet and to the fact that the properties of nanofibers are expected to depend strongly on the orientation of the amorphous phase [101] [79].

Another technique was found to be useful for single nanofibers microstructure investigations which is the confocal Raman spectroscopy. This technique is expected to reveal information about molecular orientation in both crystalline and amorphous phases [79]. It has been reported that **Bellan et al.** [102] were the first to suggest the use of this technique for the investigation of individual PA6 nanofibers with diameters around 280 nm. Observations were realized in different spots on the same nanofiber, and the resulting spectra showed significant molecular orientation but with different levels, which was accounted for the inhomogeneity of the

electrospun fiber. The degree of orientation was quantified using orientation function designated as "Hermann's function". In spite of quantitative characterization of molecular orientation, this technique was limited by the quality of the spectra leading sometimes to anomalous values of orientation.

In the same context, individual nanofibers of poly (ethylene terephthalate) (PET) with diameters down to 500 nm were investigated. Raman spectra with a good signal-to-noise ratio were recorded and quantitative information about the crystallinity and chain conformations were obtained. It was noticed that tested nanofibers presented a high orientation level with a relatively low crystallinity, and some orientation aspects were attributed to the presence of a highly anisotropic mesophase [103]. This study highlighted the possibility of a high degree of orientation even within a nanocrystalline polymer.

Further advances in nano-sized investigations led to the emergence of other techniques that may allow deeper characterization of structural conformation and orientation within nanofibers. An example of a rising technique is infrared spectroscopy coupled with a photothermal detection by an AFM tip (AFM-IR). It involves irradiating a spot or region of the sample by a tunable IR laser light and measuring the resulting photothermal expansion of the sample with a tip of AFM, allowing a higher spatial resolution and more precise investigations of nanofibers [104].

Gong et al. [105] have proceeded with this technique in their study of nanofibers with diameters ranging from 270-500 nm, electrospun from poly[(R)-3- hydroxybutyrate-co-(R)-3-hydroxyhexanoate] (PHBHx) which is a polymorphous copolymer well known for its high potential of use in the medical field. Investigations with AFM-IR proved a modification within the crystalline composition of the nanofibers which is expressed by the appearance of a new polymorphic form when electrospinning aligned nanofibers, designated as strain-induced β-form. Also, it allowed to study the impact of the collector used during electrospinning on the molecular orientation of the resulting structure, and to determine the orientation degree within a nanofiber which couldn't be possible by standard FTIR, because of the smearing within the spectra resulting from the averaging over a distribution of several nanofibers.

This technique was also applied for several other electrospun nanofibers such as polyacrylonitrile (PAN) and poly (vinylidene fluoride) (PVDF) [106]. *Figure 1.22.A* illustrates an AFM image of PVDF nanofiber with a diameter of 475nm. Infrared spectra perpendicular and parallel to the fiber axis were recorded at the green spot and showed preferential polymer chains orientation along the fiber axis. Results of the same experiment on a wider range of

diameters revealed an increase of the molecular orientation, along the fiber axis, with the decrease of nanofibers diameters, through the determination of the dichroic ratio allowing the quantification of molecular orientation *(Figure 1.22.B).*

Furthermore, AFM equipped with a heating chamber was applied for investigating the thermal properties of single nanofibers and their evolution as a function of nanofibers diameters.

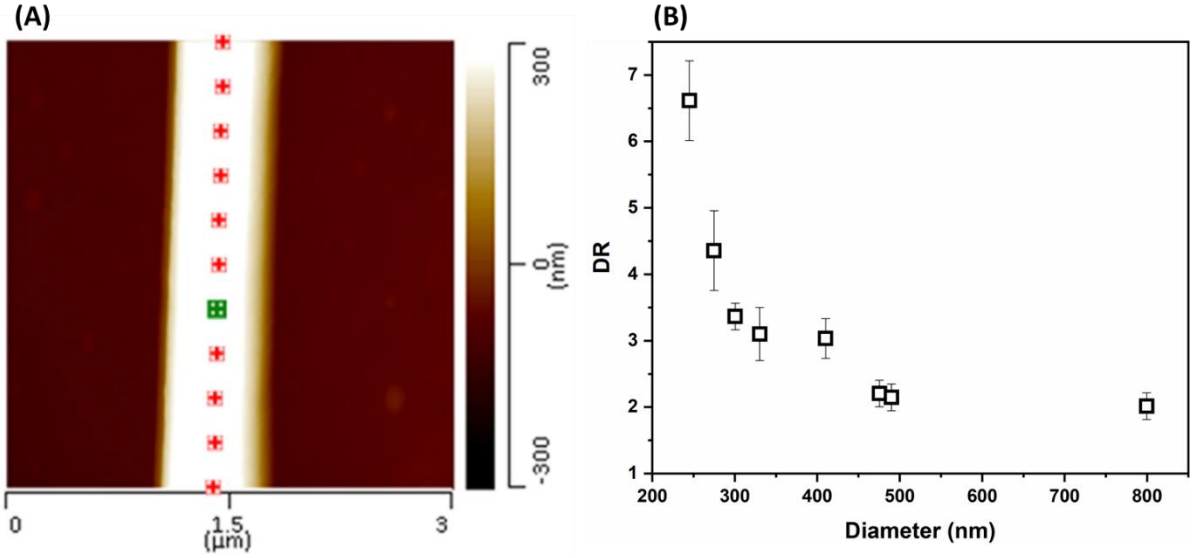

Figure 1.22 AFM-IR results on PVDF single nanofibers (A) AFM image (B) IR dichroic ratio determined from polarized AFM-IR along individual fiber of uniform diameter at different locations marked in (A). Modified from [106]

Using this apparatus, **Wang et al.** [69] were able to determine the melting temperature of single PEO nanofibers and found a decrease of this value when decreasing nanofibers diameters, that was more pronounced for diameters lower than 300 nm. The same observation was noted for the corresponding nanofiber mats after analysis with a differential scanning calorimeter (DSC). Also, the crystallinity degree, quantified by DSC measurements, was found to decrease when decreasing nanofibers diameters. The experimental results found in this work fitted a model developed previously based on Gibbs-Thompson equation *(Figure 1.23)*[107].

Their hypothesis to explain the above described behavior, is that the variation of the melting temperature (T_m) of nanofibres is determined by two competing mechanisms. The first one is related to the decrease of T_m with decreasing nanofibers diameters due to the presence of polymer chains with higher mobility at the surface of the fiber, comparing to the ones in the inner part of the fiber, and the increase of its fraction when the fiber gets thinner. The second mechanism is related to the increase of T_m for thinner nanofibers due to a higher degree of

orientation of the polymer chains in the fiber. In this case, the enhanced polymer chain mobility at the surface overcomes the orientation effect.

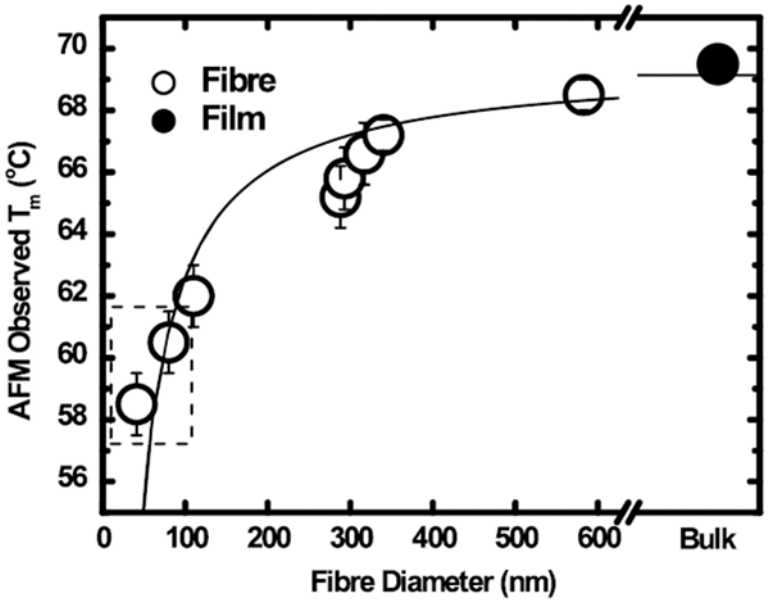

Figure 1.23 Plot of the melting temperature (Tm) as a function of PEO nanofibers diameters determined by AFM with the melting temperature of PEO film. The black curve presents the model used in this study [69]

Similar results were found for nanofibers electrospun from poly (ethylene-co-vinyl acetate) (PEVA) copolymers when determining their melting temperature by means of shear modulation force microscopy (SMFM) equipped with a heating chamber purged with nitrogen [108]. This technique allows the measurement of the lateral deflection amplitude of the cantilever, from which the shear modulus of the nanofiber is determined. When heating, the modulus decreases resulting with a large increase of the deflection. The discontinuity in the deflection is indicative of the nanofiber melting.

The decrease of melting temperature with decreasing nanofibers diameter was explained according to a hypothesis that relates this phenomenon to the difference of entanglement density of polymer chains between thin and thick nanofibers. The explanation is based on the electrospinning process during which the polymer jet undergoes high elongational stretching combined with fast solvent evaporation, leading to the formation of polymer chains in a non-equilibrium state. The regain of equilibrium state is expected to be hindered, resulting in additional entropy that would increase as the concentration of the polymer solution decreases which means as thinner nanofibers are formed, leading to a decrease of the melting temperature [109].

Contrarily, different trend was reported when investigating single PVDF nanofibers whose melting temperature was noticed to increase when decreasing nanofibers diameter *(Figure 1.24)*. Local thermal analysis (LTA) technique was used in this study, allowing to determine the melting temperature at a precise spot of the nanofiber via a high resolution heating AFM probe [110]. Melting temperatures around 220-230°C were obtained for nanofibers with diameters ≤ 200 nm which is notably higher than that of a bulk PVDF that was reported to be around 170°C.

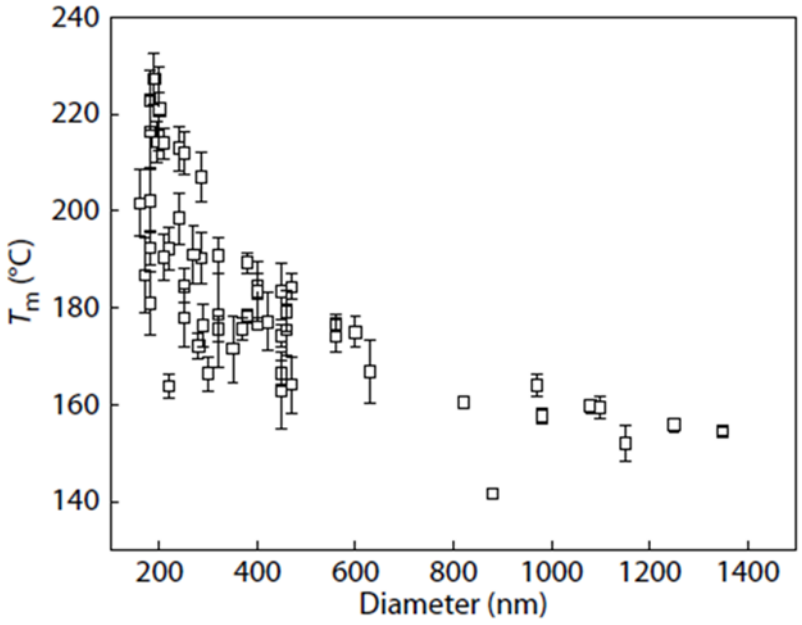

Figure 1.24 Plot of the melting temperatures Tm of single PVDF nanofibers as a function of their diameters [110]

The theory presented in this work relates the increase of melting temperature to a higher molecular orientation within thinner nanofibers resulting from a higher impact of the elongational forces and rapid solvent evaporation. Consequently, this higher polymer chains orientation would facilitate, according to the authors, the crystallization resulting int the formation of bigger and more perfect crystals, which leads to higher melting temperature [110].

The effect of molecular orientation was further explained when investigating a nanofiber presenting imperfections designated as “beads” that are accounted in literature to the instability of the jet of polymer solution [22]. The dichroic ratio determined by AFM-IR and the melting temperature determined by local thermal analysis showed similar patterns. At the center of the beaded area, the value of the dichroic ratio indicated no preferential molecular orientation and lower melting temperature were determined at the same spot. However, in the straight parts of the fiber, away from the beaded area, melting temperature increases as well as the dichroic ratio indicating a preferential orientation along the fiber axis, confirming the hypothesis that the

melting behavior of nanofibers is governed by molecular orientation of polymer chains within these nanofibers *(Figure 1.25).*

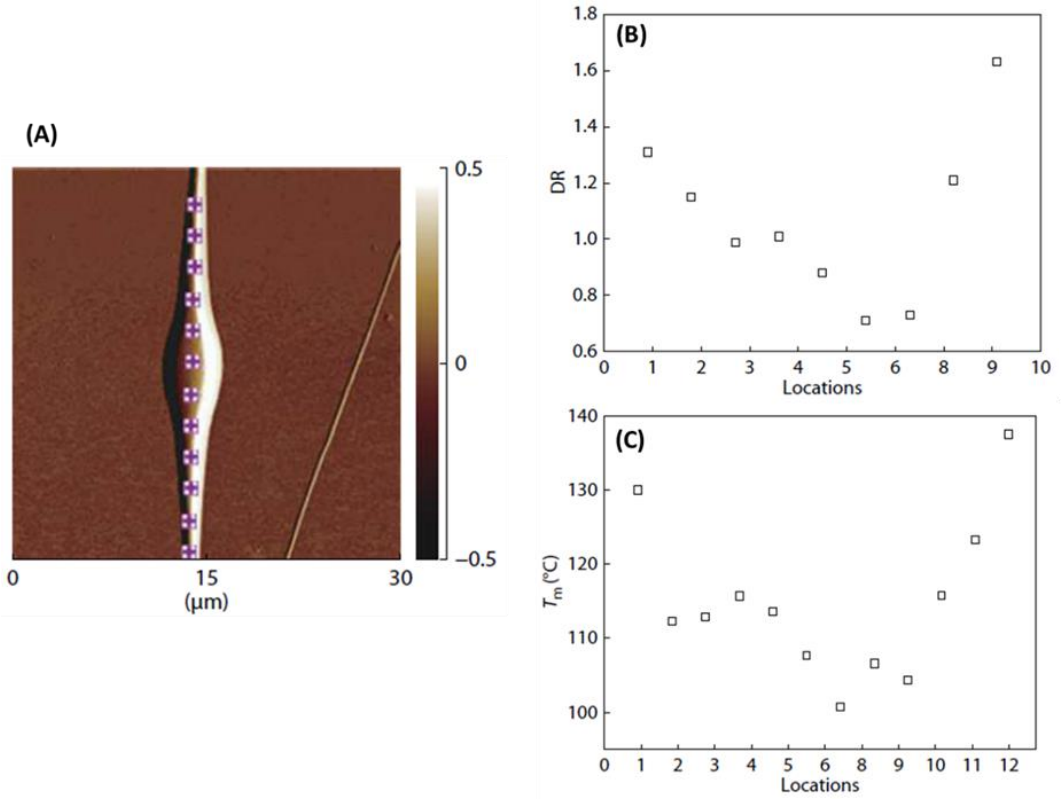

Figure 1.25 (A) AFM image of beaded PVDF nanofiber. The purple marks correspond to the spots at which melting temperature and AFM-IR were investigated (B) Dichroic ratio determined by AFM-IR for the investigated spots (C) Melting temperature of the investigated spots [110]

The inconsistencies of the above-mentioned results about the microstructure of nanofibers emphasize the hypothesis that electrospun nanofibers mechanical and thermal properties are defined by several competing mechanisms that depend on the studied polymer and the electrospinning parameters. It is, though, worthy to note, that molecular orientation is considered as one of the driving forces of the particular behavior of nanofibers [79].

Accordingly, molecular orientation within nanofibers remains a subject for progressing research considering its high impact, not only on the mechanical properties of the resulting fibers, but also on specific applications requiring this peculiarity. For instance, highly oriented nanofibers were found to be extremely interesting for certain tissue engineering scaffolds to guide cell growth with a desired anisotropy, and also for applying electric stimuli to control the adhesion of certain cell types by blending electrospun conductive materials with polymers [111].

1.4 Conclusion

Nanofibers development has a history of centuries of discoveries and results. It is due to the impressive dual of nano-macro structure providing a simple way to bridge scales, that nanofibers are readily applicable for a large range of macroscopic applications. Notable examples including sustainable applications in water treatment and agriculture as nano-bio composites, in food packaging and in the field of renewable energy. [112] [113]

In this chapter, the history of the formation of nanofibrous materials was assessed with a focus on the mostly used techniques nowadays which is electrospinning, as well as its governing parameters that impact significantly the structural and morphological properties of nanofibers. Emerging techniques and challenges of characterizing these nano-sized structures have been also assessed. A specific aspect of nanofibers has been presented, which is the high degree of polymer chain orientation compared to the bulk of the same material, that is expected to be related to the high elongational deformation and rapid solidification of the polymer jet during electrospinning. It is a compelling feature that is found to govern several characteristics of the resulting material such as its mechanical behavior and applicability in functional fields. Despite its interest, the understanding of this aspect is still fragmentary and a subject for controversy.

1.5 References

[1] B. D. Malhotra and Md. A. Ali, "Nanomaterials in Biosensors," in Nanomaterials for Biosensors, Elsevier, 2018, pp. 1–74. doi: 10.1016/B978-0-323-44923-6.00001-7.

[2] "Nanomatériaux, Nanoparticules." Institut Nationale de Recherche Scientifique INRS. [Online]. Available: www.inrs.fr/risques/nanomateriaux

[3] P. J. Brown and K. A. Stevens, Nanofibers and nanotechnology in textiles. Boca Raton (Fla.): CRC press, 2007.

[4] A. Greiner and J. H. Wendorff, "Electrospinning: A Fascinating Method for the Preparation of Ultrathin Fibers," Angew. Chem. Int. Ed., vol. 46, no. 30, pp. 5670–5703, Jul. 2007, doi: 10.1002/anie.200604646.

[5] H. Matsumoto and A. Tanioka, "Functionality in Electrospun Nanofibrous Membranes Based on Fiber's Size, Surface Area, and Molecular Orientation," Membranes, vol. 1, no. 3, pp. 249–264, Aug. 2011, doi: 10.3390/membranes1030249.

[6] F. K. Ko and Y. Wan, Introduction to nanofiber materials. Cambridge, United Kingdom ; New York: Cambridge University Press, 2014.

[7] A. Barhoum, K. Pal, H. Rahier, H. Uludag, I. S. Kim, and M. Bechelany, "Nanofibers as new-generation materials: From spinning and nano-spinning fabrication techniques to emerging applications," Appl. Mater. Today, vol. 17, pp. 1–35, Dec. 2019, doi: 10.1016/j.apmt.2019.06.015.

[8] S. R. Djafari Petroudy et al., "Recent Advances in Cellulose Nanofibers Preparation through Energy-Efficient Approaches: A Review," Energies, vol. 14, no. 20, p. 6792, Oct. 2021, doi: 10.3390/en14206792.

[9] R. N. Wijesena, N. Tissera, Y. Y. Kannangara, Y. Lin, G. A. J. Amaratunga, and K. M. N. de Silva, "A method for top down preparation of chitosan nanoparticles and nanofibers," Carbohydr. Polym., vol. 117, pp. 731–738, Mar. 2015, doi: 10.1016/j.carbpol.2014.10.055.

[10] H.-S. Liao, J. Lin, Y. Liu, P. Huang, A. Jin, and X. Chen, "Self-assembly mechanisms of nanofibers from peptide amphiphiles in solution and on substrate surfaces," Nanoscale, vol. 8, no. 31, pp. 14814–14820, 2016, doi: 10.1039/C6NR04672J.

[11] P. Iqbal, J. A. Preece, and P. M. Mendes, "Nanotechnology: The 'Top-Down' and 'Bottom-Up' Approaches," in Supramolecular Chemistry, P. A. Gale and J. W. Steed, Eds. Chichester, UK: John Wiley & Sons, Ltd, 2012, p. smc195. doi: 10.1002/9780470661345.smc195.

[12] S. Ramakrishna, Ed., An introduction to electrospinning and nanofibers. Hackensack, NJ: World Scientific, 2005.

[13] Kenry and C. T. Lim, "Nanofiber technology: current status and emerging developments," Prog. Polym. Sci., vol. 70, pp. 1–17, Jul. 2017, doi: 10.1016/j.progpolymsci.2017.03.002.

[14] J. Xue, T. Wu, Y. Dai, and Y. Xia, “Electrospinning and Electrospun Nanofibers: Methods, Materials, and Applications,” Chem. Rev., vol. 119, no. 8, pp. 5298–5415, Apr. 2019, doi: 10.1021/acs.chemrev.8b00593.

[15] M. S. Islam, B. C. Ang, A. Andriyana, and A. M. Afifi, “A review on fabrication of nanofibers via electrospinning and their applications,” SN Appl. Sci., vol. 1, no. 10, p. 1248, Oct. 2019, doi: 10.1007/s42452-019-1288-4.

[16] T. Subbiah, G. S. Bhat, R. W. Tock, S. Parameswaran, and S. S. Ramkumar, “Electrospinning of nanofibers,” J. Appl. Polym. Sci., vol. 96, no. 2, pp. 557–569, Apr. 2005, doi: 10.1002/app.21481.

[17] A. Formhals, “Artificial thread and method of producion same,” 2187306

[18] G. Taylor, “Electrically driven jets,” Proceeding R. Soc., vol. 313, p. 29, 1969.

[19] P. K. Baumgarten, “Electrostatic spinning of acrylic microfibers,” J. Colloid Interface Sci., vol. 36, no. 1, pp. 71–79, May 1971, doi: 10.1016/0021-9797(71)90241-4.

[20] L. Larrondo and R. St. John Manley, “Electrostatic fiber spinning from polymer melts. II. Examination of the flow field in an electrically driven jet,” J. Polym. Sci. Polym. Phys. Ed., vol. 19, no. 6, pp. 921–932, Jun. 1981, doi: 10.1002/pol.1981.180190602.

[21] I. Hayati, A. I. Bailey, and Th. F. Tadros, “Investigations into the mechanisms of electrohydrodynamic spraying of liquids,” J. Colloid Interface Sci., vol. 117, no. 1, pp. 205–221, May 1987, doi: 10.1016/0021-9797(87)90185-8.

[22] H. Fong, I. Chun, and D. H. Reneker, “Beaded nanofibers formed during electrospinning,” Polymer, vol. 40, no. 16, pp. 4585–4592, Jul. 1999, doi: 10.1016/S0032-3861(99)00068-3.

[23] X. Fang and D. H. Reneker, “DNA fibers by electrospinning,” J. Macromol. Sci. Part B, vol. 36, no. 2, pp. 169–173, Mar. 1997, doi: 10.1080/00222349708220422.

[24] H. Reneker and J. Doshi, “Electrospinning Process and Applications of Electrospun Fibers,” presented at the Industry Applications Conference Twenty Eighth IAS Annual Meeting, Toronto, Oct. 1993, p. 6.

[25] H. A. Begum, “Nanofiber, Electrospinning, Needleless electrospinning,” Int. J. Text. Sci., p. 8, 2017.

[26] O. Jirsak and S. Petrik, “Recent advances in nanofibre technology: needleless electrospinning,” Int. J. Nanotechnol., vol. 9, no. 8–9, p. 836, 2012, doi: 10.1504/IJNT.2012.046756.

[27] H. Niu and T. Lin, “Fiber Generators in Needleless Electrospinning,” J. Nanomater., vol. 2012, pp. 1–13, 2012, doi: 10.1155/2012/725950.

[28] B. K. Gu, S. J. Park, and C.-H. Kim, "Beneficial effect of aligned nanofiber scaffolds with electrical conductivity for the directional guide of cells," J. Biomater. Sci. Polym. Ed., vol. 29, no. 7–9, pp. 1053–1065, Jun. 2018, doi: 10.1080/09205063.2017.1364097.

[29] Y.-Z. Long, X. Yan, X.-X. Wang, J. Zhang, and M. Yu, "Electrospinning : the setup and procedure," in Electrospinning: Nanofabrication and Applications, Elsevier, 2019, pp. 21–52. doi: 10.1016/B978-0-323-51270-1.00002-9.

[30] A. Becker, H. Zernetsch, M. Mueller, and B. Glasmacher, "A novel coaxial nozzle for in-process adjustment of electrospun scaffolds' fiber diameter: Electrospun mats and their dependence on process parameters," Curr. Dir. Biomed. Eng., vol. 1, no. 1, pp. 104–107, Sep. 2015, doi: 10.1515/cdbme-2015-0027.

[31] I. G. Loscertales, A. Barrero, I. Guerrero, R. Cortijo, M. Marquez, and A. M. Gañán-Calvo, "Micro/Nano Encapsulation via Electrified Coaxial Liquid Jets," Science, vol. 295, no. 5560, pp. 1695–1698, Mar. 2002, doi: 10.1126/science.1067595.

[32] N. Wang and Y. Zhao, "Coaxial Electrospinning," in Electrospinning: Nanofabrication and Applications, Elsevier, 2019, pp. 125–200. doi: 10.1016/B978-0-323-51270-1.00005-4.

[33] S. Homaeigohar, Y. Davoudpour, Y. Habibi, and M. Elbahri, "The Electrospun Ceramic Hollow Nanofibers," Nanomaterials, vol. 7, no. 11, p. 383, Nov. 2017, doi: 10.3390/nano7110383.

[34] R. Sahay, V. Thavasi, and S. Ramakrishna, "Design Modifications in Electrospinning Setup for Advanced Applications," J. Nanomater., vol. 2011, pp. 1–17, 2011, doi: 10.1155/2011/317673.

[35] D. Li and Y. Xia, "Direct Fabrication of Composite and Ceramic Hollow Nanofibers by Electrospinning," Nano Lett., vol. 4, no. 5, pp. 933–938, May 2004, doi: 10.1021/nl049590f.

[36] R. Khajavi and M. Abbasipour, "Controlling nanofiber morphology by the electrospinning process," in Electrospun Nanofibers, Elsevier, 2017, pp. 109–123. doi: 10.1016/B978-0-08-100907-9.00005-2.

[37] S. V. Fridrikh, J. H. Yu, M. P. Brenner, and G. C. Rutledge, "Controlling the Fiber Diameter during Electrospinning," Phys. Rev. Lett., vol. 90, no. 14, p. 144502, Apr. 2003, doi: 10.1103/PhysRevLett.90.144502.

[38] J. M. Deitzel, J. Kleinmeyer, D. Harris, and N. C. Beck Tan, "The effect of processing variables on the morphology of electrospun nanofibers and textiles," Polymer, vol. 42, no. 1, pp. 261–272, Jan. 2001, doi: 10.1016/S0032-3861(00)00250-0.

[39] C. Mit-uppatham, M. Nithitanakul, and P. Supaphol, "Ultrafine Electrospun Polyamide-6 Fibers: Effect of Solution Conditions on Morphology and Average Fiber Diameter," Macromol. Chem. Phys., vol. 205, no. 17, pp. 2327–2338, Nov. 2004, doi: 10.1002/macp.200400225.

[40] P. Gupta, C. Elkins, T. E. Long, and G. L. Wilkes, "Electrospinning of linear homopolymers of poly(methyl methacrylate): exploring relationships between fiber formation, viscosity, molecular weight and concentration in a good solvent," Polymer, vol. 46, no. 13, pp. 4799–4810, Jun. 2005, doi: 10.1016/j.polymer.2005.04.021.

[41] A. Koski, K. Yim, and S. Shivkumar, "Effect of molecular weight on fibrous PVA produced by electrospinning," Mater. Lett., vol. 58, no. 3–4, pp. 493–497, Jan. 2004, doi: 10.1016/S0167-577X(03)00532-9.

[42] C. Salas, "Solution electrospinning of nanofibers," in Electrospun Nanofibers, Elsevier, 2017, pp. 73–108. doi: 10.1016/B978-0-08-100907-9.00004-0.

[43] M. G. McKee, G. L. Wilkes, Ralph. H. Colby, and T. E. Long, "Correlations of Solution Rheology with Electrospun Fiber Formation of Linear and Branched Polyesters," Macromolecules, vol. 37, no. 5, pp. 1760–1767, Mar. 2004, doi: 10.1021/ma035689h.

[44] A. Stanishevsky et al., "Ribbon-like and spontaneously folded structures of tungsten oxide nanofibers fabricated via electrospinning," RSC Adv., vol. 5, no. 85, pp. 69534–69542, 2015, doi: 10.1039/C5RA11884K.

[45] A. L. Yarin, B. Pourdeyhimi, and S. Ramakrishna, Fundamentals and Applications of Micro- and Nanofibers, 1st ed. Cambridge University Press, 2014. doi: 10.1017/CBO9781107446830.

[46] X. Yuan, Y. Zhang, C. Dong, and J. Sheng, "Morphology of ultrafine polysulfone fibers prepared by electrospinning," Polym. Int., vol. 53, no. 11, pp. 1704–1710, Nov. 2004, doi: 10.1002/pi.1538.

[47] C. S. Ki, D. H. Baek, K. D. Gang, K. H. Lee, I. C. Um, and Y. H. Park, "Characterization of gelatin nanofiber prepared from gelatin–formic acid solution," Polymer, vol. 46, no. 14, pp. 5094–5102, Jun. 2005, doi: 10.1016/j.polymer.2005.04.040.

[48] P. Lu and Y. Xia, "Maneuvering the Internal Porosity and Surface Morphology of Electrospun Polystyrene Yarns by Controlling the Solvent and Relative Humidity," Langmuir, vol. 29, no. 23, pp. 7070–7078, Jun. 2013, doi: 10.1021/la400747y.

[49] P. K. Szewczyk and U. Stachewicz, "The impact of relative humidity on electrospun polymer fibers: From structural changes to fiber morphology," Adv. Colloid Interface Sci., vol. 286, p. 102315, Dec. 2020, doi: 10.1016/j.cis.2020.102315.

[50] C.-L. Pai, M. C. Boyce, and G. C. Rutledge, "Morphology of Porous and Wrinkled Fibers of Polystyrene Electrospun from Dimethylformamide," Macromolecules, vol. 42, no. 6, pp. 2102–2114, Mar. 2009, doi: 10.1021/ma802529h.

[51] T. J. Sill and H. A. von Recum, "Electrospinning: Applications in drug delivery and tissue engineering," Biomaterials, vol. 29, no. 13, pp. 1989–2006, May 2008, doi: 10.1016/j.biomaterials.2008.01.011.

[52] R. Rasouli, A. Barhoum, M. Bechelany, and A. Dufresne, "Nanofibers for Biomedical and Healthcare Applications," Macromol. Biosci., vol. 19, no. 2, p. 1800256, Feb. 2019, doi: 10.1002/mabi.201800256.

[53] A. Greiner and J. H. Wendorff, "Electrospinning: A Fascinating Method for the Preparation of Ultrathin Fibers," Angew. Chem. Int. Ed., vol. 46, no. 30, pp. 5670–5703, Jul. 2007, doi: 10.1002/anie.200604646.

[54] R. Augustine, N. Kalarikkal, and S. Thomas, "Electrospun PCL membranes incorporated with biosynthesized silver nanoparticles as antibacterial wound dressings," Appl. Nanosci., vol. 6, no. 3, pp. 337–344, Mar. 2016, doi: 10.1007/s13204-015-0439-1.

[55] A. Lowe, J. Bills, R. Verma, L. Lavery, K. Davis, and K. J. Balkus, "Electrospun nitric oxide releasing bandage with enhanced wound healing," Acta Biomater., vol. 13, pp. 121–130, Feb. 2015, doi: 10.1016/j.actbio.2014.11.032.

[56] M. Hashmi, S. Ullah, and I. S. Kim, "Copper oxide (CuO) loaded polyacrylonitrile (PAN) nanofiber membranes for antimicrobial breath mask applications," Curr. Res. Biotechnol., vol. 1, pp. 1–10, Nov. 2019, doi: 10.1016/j.crbiot.2019.07.001.

[57] J. Ding et al., "Electrospun polymer biomaterials," Prog. Polym. Sci., vol. 90, pp. 1–34, Mar. 2019, doi: 10.1016/j.progpolymsci.2019.01.002.

[58] L. Li, G. Zhou, Y. Wang, G. Yang, S. Ding, and S. Zhou, "Controlled dual delivery of BMP-2 and dexamethasone by nanoparticle-embedded electrospun nanofibers for the efficient repair of critical-sized rat calvarial defect," Biomaterials, vol. 37, pp. 218–229, Jan. 2015, doi: 10.1016/j.biomaterials.2014.10.015.

[59] B. Lu, G. Zheng, K. Dai, C. Liu, J. Chen, and C. Shen, "Enhanced mechanical properties of polyethylene composites with low content of electrospun nylon-66 nanofibers," Mater. Lett., vol. 140, pp. 131–134, Feb. 2015, doi: 10.1016/j.matlet.2014.10.151.

[60] M. J. Chinchillas-Chinchillas et al., "A new application of recycled-PET/PAN composite nanofibers to cement–based materials," J. Clean. Prod., vol. 252, p. 119827, Apr. 2020, doi: 10.1016/j.jclepro.2019.119827.

[61] J. Mohrova and K. Kalinova, "Different Structures of PVA Nanofibrous Membrane for Sound Absorption Application," J. Nanomater., vol. 2012, pp. 1–4, 2012, doi: 10.1155/2012/643043.

[62] A. Rabbi, H. Bahrambeygi, A. M. Shoushtari, and K. Nasouri, "Incorporation of Nanofiber Layers in Nonwoven Materials for Improving Their Acoustic Properties," J. Eng. Fibers Fabr., vol. 8, no. 4, p. 155892501300800, Dec. 2013, doi: 10.1177/155892501300800412.

[63] F. K. Ko and Y. Wan, Introduction to Nanofiber Materials, 1st ed. Cambridge University Press, 2014. doi: 10.1017/CBO9781139021333.

[64] E. P. S. Tan and C. T. Lim, "Mechanical characterization of nanofibers – A review," Compos. Sci. Technol., vol. 66, no. 9, pp. 1102–1111, Jul. 2006, doi: 10.1016/j.compscitech.2005.10.003.

[65] A. Meléndez, K. Morales, I. Ramos, E. Campo, and J. J. Santiago-Avilés, "Synthesis and characterization of electrospun gallium nitride nanofibers," presented at the SPIE NanoScience + Engineering, San Diego, CA, Aug. 2009, p. 740210. doi: 10.1117/12.825368.

[66] A. Mayeen, L. K. Shaji, A. K. Nair, and N. Kalarikkal, "Morphological Characterization of Nanomaterials," in Characterization of Nanomaterials, Elsevier, 2018, pp. 335–364. doi: 10.1016/B978-0-08-101973-3.00012-2.

[67] S. Megelski, J. S. Stephens, D. B. Chase, and J. F. Rabolt, "Micro- and Nanostructured Surface Morphology on Electrospun Polymer Fibers," Macromolecules, vol. 35, no. 22, pp. 8456–8466, Oct. 2002, doi: 10.1021/ma020444a.

[68] S. D. McCullen, D. R. Stevens, W. A. Roberts, S. S. Ojha, L. I. Clarke, and R. E. Gorga, "Morphological, Electrical, and Mechanical Characterization of Electrospun Nanofiber Mats Containing Multiwalled Carbon Nanotubes," Macromolecules, vol. 40, no. 4, pp. 997–1003, Feb. 2007, doi: 10.1021/ma061735c.

[69] W. Wang and A. H. Barber, "Diameter-dependent melting behaviour in electrospun polymer fibres," Nanotechnology, vol. 21, no. 22, p. 225701, Jun. 2010, doi: 10.1088/0957-4484/21/22/225701.

[70] W.-J. Li, C. T. Laurencin, E. J. Caterson, R. S. Tuan, and F. K. Ko, "Electrospun nanofibrous structure: A novel scaffold for tissue engineering," J. Biomed. Mater. Res., vol. 60, no. 4, pp. 613–621, Jun. 2002, doi: 10.1002/jbm.10167.

[71] F. K. Ko and Y. Wan, Introduction to Nanofiber Materials, 1st ed. Cambridge University Press, 2014. doi: 10.1017/CBO9781139021333.

[72] B. Jasse and J. L. Koenig, "Orientational Measurements in Polymers Using Vibrational Spectroscopy," J. Macromol. Sci. Part C Polym. Rev., vol. 17, no. 1, pp. 61–135, Jan. 1979, doi: 10.1080/00222357908080905.

[73] E. P. S. Tan, S. Y. Ng, and C. T. Lim, "Tensile testing of a single ultrafine polymeric fiber," Biomaterials, vol. 26, no. 13, pp. 1453–1456, May 2005, doi: 10.1016/j.biomaterials.2004.05.021.

[74] E. P. S. Tan, C. N. Goh, C. H. Sow, and C. T. Lim, "Tensile test of a single nanofiber using an atomic force microscope tip," Appl. Phys. Lett., vol. 86, no. 7, p. 073115, 2005, doi: 10.1063/1.1862337.

[75] E. Zussman, D. Rittel, and A. L. Yarin, "Failure modes of electrospun nanofibers," Appl. Phys. Lett., vol. 82, no. 22, pp. 3958–3960, Jun. 2003, doi: 10.1063/1.1579125.

[76] M. Naraghi, I. Chasiotis, H. Kahn, Y. Wen, and Y. Dzenis, "Novel method for mechanical characterization of polymeric nanofibers," Rev. Sci. Instrum., vol. 78, no. 8, p. 085108, Aug. 2007, doi: 10.1063/1.2771092.

[77] S. Lu, Z. Guo, W. Ding, and R. S. Ruoff, "Analysis of a microelectromechanical system testing stage for tensile loading of nanostructures," Rev. Sci. Instrum., vol. 77, no. 5, p. 056103, May 2006, doi: 10.1063/1.2198789.

[78] S. F. Fennessey and R. J. Farris, "Fabrication of aligned and molecularly oriented electrospun polyacrylonitrile nanofibers and the mechanical behavior of their twisted yarns," Polymer, vol. 45, no. 12, pp. 4217–4225, May 2004, doi: 10.1016/j.polymer.2004.04.001.

[79] M. Richard-Lacroix and C. Pellerin, "Molecular Orientation in Electrospun Fibers: From Mats to Single Fibers," Macromolecules, vol. 46, no. 24, pp. 9473–9493, Dec. 2013, doi: 10.1021/ma401681m.

[80] R. Inai, M. Kotaki, and S. Ramakrishna, "Structure and properties of electrospun PLLA single nanofibres," Nanotechnology, vol. 16, no. 2, pp. 208–213, Feb. 2005, doi: 10.1088/0957-4484/16/2/005.

[81] E. P. S. Tan and C. T. Lim, "Physical properties of a single polymeric nanofiber," Appl. Phys. Lett., vol. 84, no. 9, pp. 1603–1606, Mar. 2004.

[82] Y. Ji, B. Li, S. Ge, J. C. Sokolov, and M. H. Rafailovich, "Structure and Nanomechanical Characterization of Electrospun PS/Clay Nanocomposite Fibers," Langmuir, vol. 22, no. 3, pp. 1321–1328, Jan. 2006, doi: 10.1021/la0525022.

[83] Y. Ji et al., "Confinement-induced super strong PS/MWNT composite nanofibers," EPL Europhys. Lett., vol. 84, no. 5, p. 56002, Dec. 2008, doi: 10.1209/0295-5075/84/56002.

[84] D. H. Reneker and A. L. Yarin, "Electrospinning jets and polymer nanofibers," Polymer, vol. 49, no. 10, pp. 2387–2425, May 2008, doi: 10.1016/j.polymer.2008.02.002.

[85] A. J. Guenthner, S. Khombhongse, W. Liu, P. Dayal, D. H. Reneker, and T. Kyu, "Dynamics of Hollow Nanofiber Formation During Solidification Subjected to Solvent Evaporation," Macromol. Theory Simul., vol. 15, no. 1, pp. 87–93, Jan. 2006, doi: 10.1002/mats.200500034.

[86] L. Wang, C.-L. Pai, M. C. Boyce, and G. C. Rutledge, "Wrinkled surface topographies of electrospun polymer fibers," Appl. Phys. Lett., vol. 94, no. 15, p. 151916, Apr. 2009, doi: 10.1063/1.3118526.

[87] S. Koombhongse, W. Liu, and D. H. Reneker, "Flat polymer ribbons and other shapes by electrospinning," J. Polym. Sci. Part B Polym. Phys., vol. 39, no. 21, pp. 2598–2606, Nov. 2001, doi: 10.1002/polb.10015.

[88] A. Arinstein and E. Zussman, "Postprocesses in tubular electrospun nanofibers," Phys. Rev. E, vol. 76, no. 5, p. 056303, Nov. 2007, doi: 10.1103/PhysRevE.76.056303.

[89] U. Stachewicz, R. J. Bailey, W. Wang, and A. H. Barber, "Size dependent mechanical properties of electrospun polymer fibers from a composite structure," Polymer, vol. 53, no. 22, pp. 5132–5137, Oct. 2012, doi: 10.1016/j.polymer.2012.08.064.

[90] A. Arinstein, M. Burman, O. Gendelman, and E. Zussman, "Effect of supramolecular structure on polymer nanofibre elasticity," Nat. Nanotechnol., vol. 2, no. 1, pp. 59–62, Jan. 2007, doi: 10.1038/nnano.2006.172.

[91] A. Arinstein, "Confinement mechanism of electrospun polymer nanofiber reinforcement," J. Polym. Sci. Part B Polym. Phys., vol. 51, no. 9, pp. 756–763, May 2013, doi: 10.1002/polb.23246.

[92] D. Papkov, Y. Zou, M. N. Andalib, A. Goponenko, S. Z. D. Cheng, and Y. A. Dzenis, "Simultaneously Strong and Tough Ultrafine Continuous Nanofibers," ACS Nano, vol. 7, no. 4, pp. 3324–3331, Apr. 2013, doi: 10.1021/nn400028p.

[93] N.S.Murthy, "Metastable crystalline phases in nylon 6," Polymer, vol. 10, no. 32, pp. 301–305, Jan. 1991.

[94] D. R. Holmes, C. W. Bunn, and D. J. Smith, "The crystal structure of polycaproamide: Nylon 6," J. Polym. Sci., vol. 17, no. 84, pp. 159–177, Jun. 1955, doi: 10.1002/pol.1955.120178401.

[95] R. Dersch, T. Liu, A. K. Schaper, A. Greiner, and J. H. Wendorff, "Electrospun nanofibers: Internal structure and intrinsic orientation," J. Polym. Sci. Part Polym. Chem., vol. 41, no. 4, pp. 545–553, Feb. 2003, doi: 10.1002/pola.10609.

[96] Y. Liu et al., "Crystalline Morphology and Polymorphic Phase Transitions in Electrospun Nylon-6 Nanofibers," Macromolecules, vol. 40, no. 17, pp. 6283–6290, Aug. 2007, doi: 10.1021/ma070039p.

[97] C. B. Giller, D. B. Chase, J. F. Rabolt, and C. M. Snively, "Effect of solvent evaporation rate on the crystalline state of electrospun Nylon 6," Polymer, vol. 51, no. 18, pp. 4225–4230, Aug. 2010, doi: 10.1016/j.polymer.2010.06.057.

[98] K.-H. Lee, K.-W. Kim, A. Pesapane, H.-Y. Kim, and J. F. Rabolt, "Polarized FT-IR Study of Macroscopically Oriented Electrospun Nylon-6 Nanofibers," Macromolecules, vol. 41, no. 4, pp. 1494–1498, Feb. 2008, doi: 10.1021/ma701927w.

[99] W. A. Yee, M. Kotaki, Y. Liu, and X. Lu, "Morphology, polymorphism behavior and molecular orientation of electrospun poly(vinylidene fluoride) fibers," Polymer, vol. 48, no. 2, pp. 512–521, Jan. 2007, doi: 10.1016/j.polymer.2006.11.036.

[100] T. Yoshioka, R. Dersch, M. Tsuji, and A. K. Schaper, "Orientation analysis of individual electrospun PE nanofibers by transmission electron microscopy," Polymer, vol. 51, no. 11, pp. 2383–2389, May 2010, doi: 10.1016/j.polymer.2010.03.031.

[101] D. Papkov et al., "Quantifying Polymer Chain Orientation in Strong and Tough Nanofibers with Low Crystallinity: Toward Next Generation Nanostructured Superfibers," ACS Nano, vol. 13, no. 5, pp. 4893–4927, May 2019, doi: 10.1021/acsnano.8b08725.

[102] L. M. Bellan and H. G. Craighead, "Molecular orientation in individual electrospun nanofibers measured via polarized Raman spectroscopy," Polymer, vol. 49, no. 13–14, pp. 3125–3129, Jun. 2008, doi: 10.1016/j.polymer.2008.04.061.

[103] M. Richard-Lacroix and C. Pellerin, "Orientation and Structure of Single Electrospun Nanofibers of Poly(ethylene terephthalate) by Confocal Raman Spectroscopy," Macromolecules, vol. 45, no. 4, pp. 1946–1953, Feb. 2012, doi: 10.1021/ma202749d.

[104] A. Dazzi, C. B. Prater, Q. Hu, D. B. Chase, J. F. Rabolt, and C. Marcott, "AFM–IR: Combining Atomic Force Microscopy and Infrared Spectroscopy for Nanoscale Chemical Characterization," Appl. Spectrosc., vol. 66, no. 12, pp. 1365–1384, Dec. 2012, doi: 10.1366/12-06804.

[105] L. Gong et al., "Discovery of β-Form Crystal Structure in Electrospun Poly[(R)-3-hydroxybutyrate- co -(R)-3-hydroxyhexanoate] (PHBHx) Nanofibers: From Fiber Mats to Single Fibers," Macromolecules, vol. 48, no. 17, pp. 6197–6205, Sep. 2015, doi: 10.1021/acs.macromol.5b00638.

[106] Z. Wang, B. Sun, X. Lu, C. Wang, and Z. Su, "Molecular Orientation in Individual Electrospun Nanofibers Studied by Polarized AFM–IR," Macromolecules, vol. 52, no. 24, pp. 9639–9645, Dec. 2019, doi: 10.1021/acs.macromol.9b01778.

[107] Q. Jiang, C. C. Yang, and J. C. Li, "Size-Dependent Melting Temperature of Polymers," Macromol. Theory Simul., vol. 12, no. 1, pp. 57–60, Feb. 2003, doi: 10.1002/mats.200390003.

[108] Y. Liu et al., "Electrospinning of poly(ethylene- co -vinyl acetate)/clay nanocomposite fibers: Electrospinning of PEVA /Clay Nanocomposite Fibers," J. Polym. Sci. Part B Polym. Phys., vol. 47, no. 24, pp. 2501–2508, Dec. 2009, doi: 10.1002/polb.21877.

[109] A. Arinstein, Y. Liu, M. Rafailovich, and E. Zussman, "Shifting of the melting point for semi-crystalline polymer nanofibers," EPL Europhys. Lett., vol. 93, no. 4, p. 46001, Feb. 2011, doi: 10.1209/0295-5075/93/46001.

[110] Z.-Q. Wang, Z.-X. Zhong, Y.-Y. Ma, X.-F. Lu, C. Wang, and Z.-H. Su, "Melting Temperature of Individual Electrospun Poly(vinylidene fluoride) Fibers Studied by AFM-based Local Thermal Analysis," Chin. J. Polym. Sci., vol. 39, no. 2, pp. 219–227, Sep. 2020, doi: 10.1007/s10118-020-2476-9.

[111] M.-C. Chen, Y.-C. Sun, and Y.-H. Chen, "Electrically conductive nanofibers with highly oriented structures and their potential application in skeletal muscle tissue engineering," Acta Biomater., vol. 9, no. 3, pp. 5562–5572, Mar. 2013, doi: 10.1016/j.actbio.2012.10.024.

[112] K. Badgar, N. Abdalla, H. El-Ramady, and J. Prokisch, "Sustainable Applications of Nanofibers in Agriculture and Water Treatment: A Review," Sustainability, vol. 14, no. 1, p. 464, Jan. 2022, doi: 10.3390/su14010464.

[113] J. D. Schiffman and C. L. Schauer, “A Review: Electrospinning of Biopolymer Nanofibers and their Applications,” Polym. Rev., vol. 48, no. 2, pp. 317–352, May 2008, doi: 10.1080/15583720802022182.

Chapter 2 Experimental section

2.1 Materials and manufacturing technique

In this study, nanofibers developed from two different polymers: polyamide 6 (PA6) and polyacrylonitrile (PAN) were investigated. In the following part, a brief overview of the electrospinning setup and both polymers will be presented along with their manufacturing parameters. Then, the nanofibers characterization techniques used in this work will be reported.

It is noteworthy that all samples have been developed by the partners of this project, in the Department of Mechanical and Materials Engineering within the University of Nebraska Lincoln in USA.

2.1.1 Electrospinning setup

As mentioned in the first chapter, electrospinning is considered as a simple technique for producing nanofibres with diameters on the nanometer scale [1]. Different setups of this technique were developed. In the case of this work, a basic horizontal setup was used. It consists of a needle with a syringe as the emitting source of the polymer solution, a stationary plate covered with aluminum foil as collector and a high-voltage source *(Figure 2.1).*

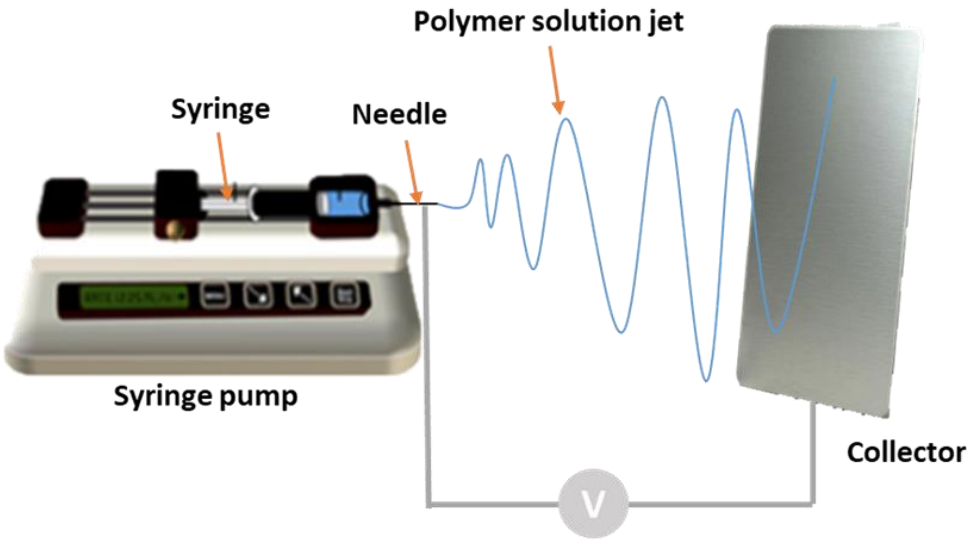

Figure 2.1 Schematic illustration of the electrospinning setup used in this work

2.1.2 Polyacrylonitrile (PAN)

Polyacrylonitrile is a linear polymer with the molecular formula $[C_3H_3N]_n$ (*Figure 2.2).* It may be formed either by free radical polymerization of acrylonitrile or by copolymerization. Monomers like vinyl acetate and methyl acrylate are mostly used for this purpose[2]. The crystalline structure of polyacrylonitrile is subject for controversy, it was considered in

literature to be a “laterally ordered” structure or also a para-crystalline structure with an hexagonal conformation [3] [4].

This polymer is well known for its thermal stability, high melting temperature and its great carbon yield ; more than 50% of the original mass can be transformed into carbon [5][6]. These interesting properties are related to the particular chemical structure of PAN composed of strong intermolecular forces, hydrogen bonding and the presence of the -CΞN adjacent groups that restricts the bond rotation leading to a stiff chain [7]. As a matter of fact, polyacrylonitrile is considered the most widely used polymer as a precursor for carbon fibers. It has been proved that the resulting fibers present higher mechanical and structural properties than those developed from other precursors such as pitch. [8] [9]

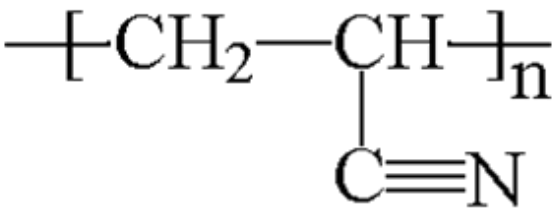

Figure 2.2 Molecular formula of polyacrylonitrile

In order to obtain PAN-based carbon fibers, a heating process with three main steps is generally followed. Starting by an oxidative stabilization so that the fibers maintain their properties while undergoing the second step which is carbonization and then graphitization. The former involves heating fibers at a temperature range of 180-600°C and keeping them under tension through the entire process. For the fibers to be stabilized, they are subject to several steps including oxidation, dehydrogenation and aromatization, during which the molecular chain endures major modifications. For instance, the formation of a back-bone containing oxygen which helps creating activation centers for cyclization, the conversion of triple carbon nitrogen bond-CΞN into a double bond -C=N, and the formation of aromatic rings [2] [5]. The obtained structure is further heated at a temperature range of 800-3000°C to be carbonized in inert environment, a step at which non-carbon elements are removed and a highly cross-linked structure is formed [2] *(Figure 2.3).*

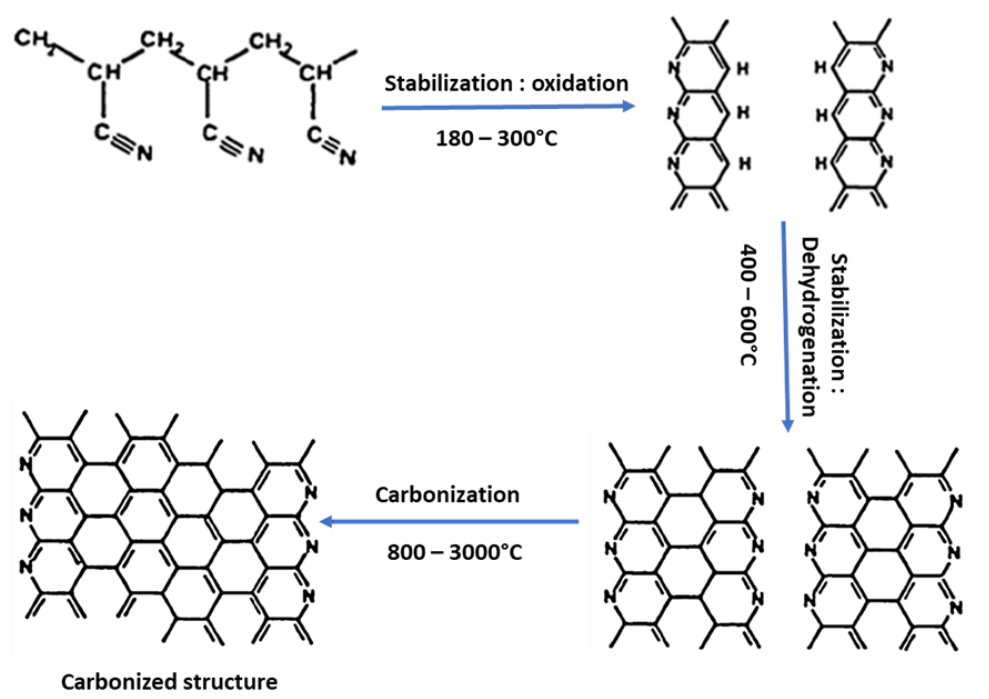

Figure 2.3 Illustration of some steps of the process of converting PAN fiber into carbonized structure. Modified from [2]

PAN nanofibers are of interest in this study for their high surface-to-volume ratio and their promising mechanical properties that outcome those of bulk materials. As a matter of fact, the mechanical behavior of single PAN nanofibers was investigated and it was reported that the modulus, toughness and strength increase simultaneously with the decrease of nanofibers diameters, a behavior that cannot be provided in case of bulk polyacrylonitrile[10]. Moreover, the growing research have led to the application of PAN nanofiber mats in a wide range of fields, among which the manufacturing of electrochemical, photoelectric and fluorescent sensors. For example, electrochemical sensors formed by PAN-based nanocomposites have revealed high sensitivity and high stability [11].

In this work, PAN nanofibers were obtained by dissolving PAN, purchased from Pfaltz and Bauer, Inc® having an average molecular weight of M_w = 150 000 g/mol, in N,N-dimethylformamide (DMF) purchased from Sigma-Aldrich® . The electrospinning parameters were chosen as following; a working distance (needle-tip to collector distance) of 20 cm, an applied voltage of 12 kV, a feed rate of 0.06 mL/h and a 20-gauge needle with a 1 mL syringe was used. Nanofibers were electrospun from three different solution with 8, 10 and 12wt% of polyacrylonitrile in DMF resulting with an average nanofiber diameter of 237, 482 and 800 nm,

respectively. SEM images and diameter distribution of the obtained nanofiber mats are illustrated in *(Figure 2.4)*.

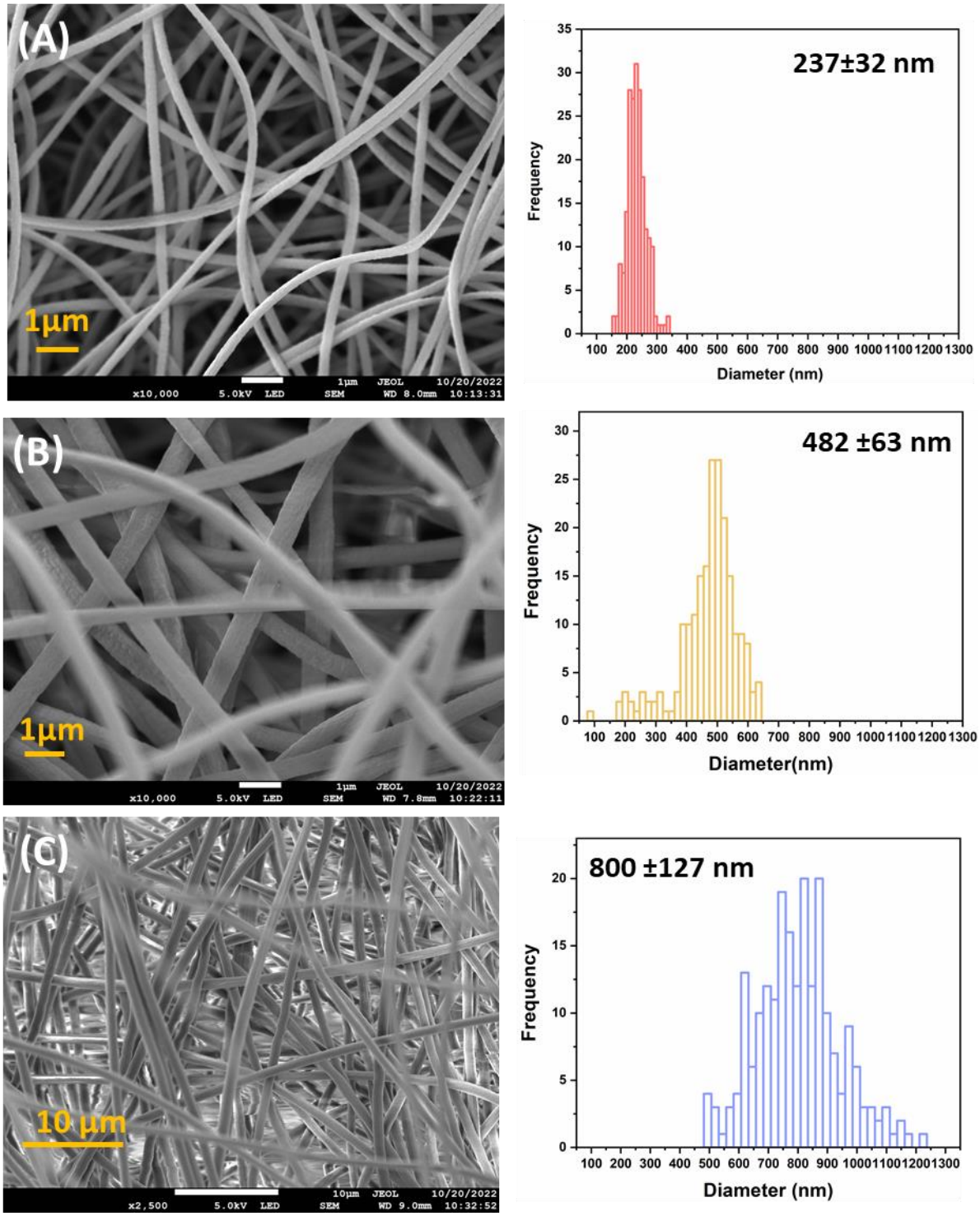

Figure 2.4 SEM images of the electrospun PAN nanofiber mats with different average nanofiber diameter with the corresponding diameter distribution (A) 237 nm [magnification = 10 000×, scale bar = 1 µm] (B) 482 nm [magnification = 10 000×, scale bar = 1 µm] (C) 800 nm [magnification= 25 00×, scale bar = 1 µm]

2.1.3 Polyamide 6 (PA6)

Polyamide 6, also designated as nylon 6, is a semi-crystalline thermoplastic polymer obtained by anionic polymerization of ε-caprolactame. *Figure 2.5* illustrates its chemical formula. It is an aliphatic polymer whose microstructure is governed by strong interchain interaction resulting from hydrogen bonds formed between amide groups of adjacent chains and dipole-dipole interactions[12] [13].

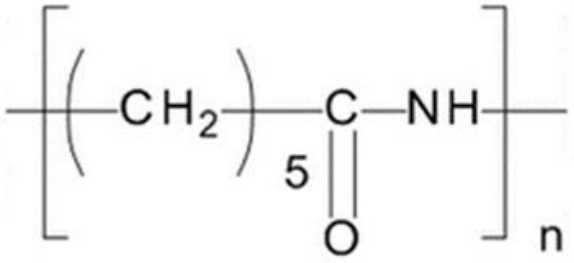

Figure 2.5 Illustration of the chemical formula of polyamide 6 (PA6)

Polyamide 6 is well known for its polymorphic structure, that is the formation of different crystalline forms depending on the crystallization conditions. Previous studies have revealed at least four different crystalline forms, but it has been suggested, later, that PA6 can be considered to be formed mainly by two forms which are α and γ forms. [14] The main difference lies in the molecular arrangement. It was reported that hydrogen bonds are formed between anti-parallel chains within the α crystalline form and between parallel chains within the γ crystalline form *(Figure 2.6)* [13] [15].

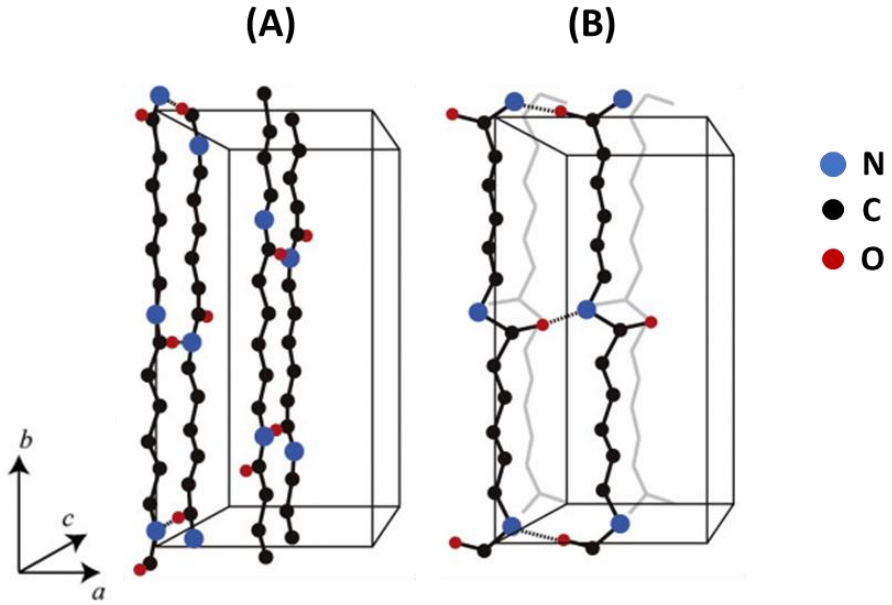

Figure 2.6 Schematic illustration of PA6 crystalline fomrs (A) α crystalline form (B) γ crystalline form [16]

Nylon 6 is widely used in engineering applications for its high chemical stability, mechanical properties and high performance/cost-effective ratio[13]. The nanofibrous structure of PA6 has been studied extensively and several researches have proven its applicability in several fields. In combination with polystyrene (PS), PA6 nanofibers have performed efficiently as superhydrophobic membranes for water repellency, self-cleaning and contamination prevention applications[17]. They have also shown appreciable performance for water waste and air filtration as well as micro-sized particles separation [18] [19]

Moreover, polyamide 6 nanofiber mats have been used in some biomedical applications. For instance, PA6 /lecithin and PA6/Chitosan based composites were used as scaffolds for cell culture and found to be suitable for cell development. An example of human osteoblast cells implementation revealed growth and good interconnectivity of the cells which led to potential use of these composites in tissue and bone regeneration applications [20].

In this work, PA6 nanofiber mats were electrospun from PA6 (Sigma-Aldrich®, USA, M_w = 10 000 g/mol) solutions in formic acid (Sigma-Aldrich®, USA) in a 1 mL syringe using a 22-27-gauge needles and a feed rates of 0.6-2 mL/h. The applied voltage during electrospinning is 16.5 kV. Fibers were collected on a stationary target at a distance of 20 cm from the spinneret. The samples were electrospun from 12, 20 and 28 wt% of PA6 in formic acid, resulting with average nanofiber diameters of 60, 133 and 325 nm respectively. SEM images of the electrospun nanofiber mats and the corresponding diameter distribution are shown in *Figure 2.7*

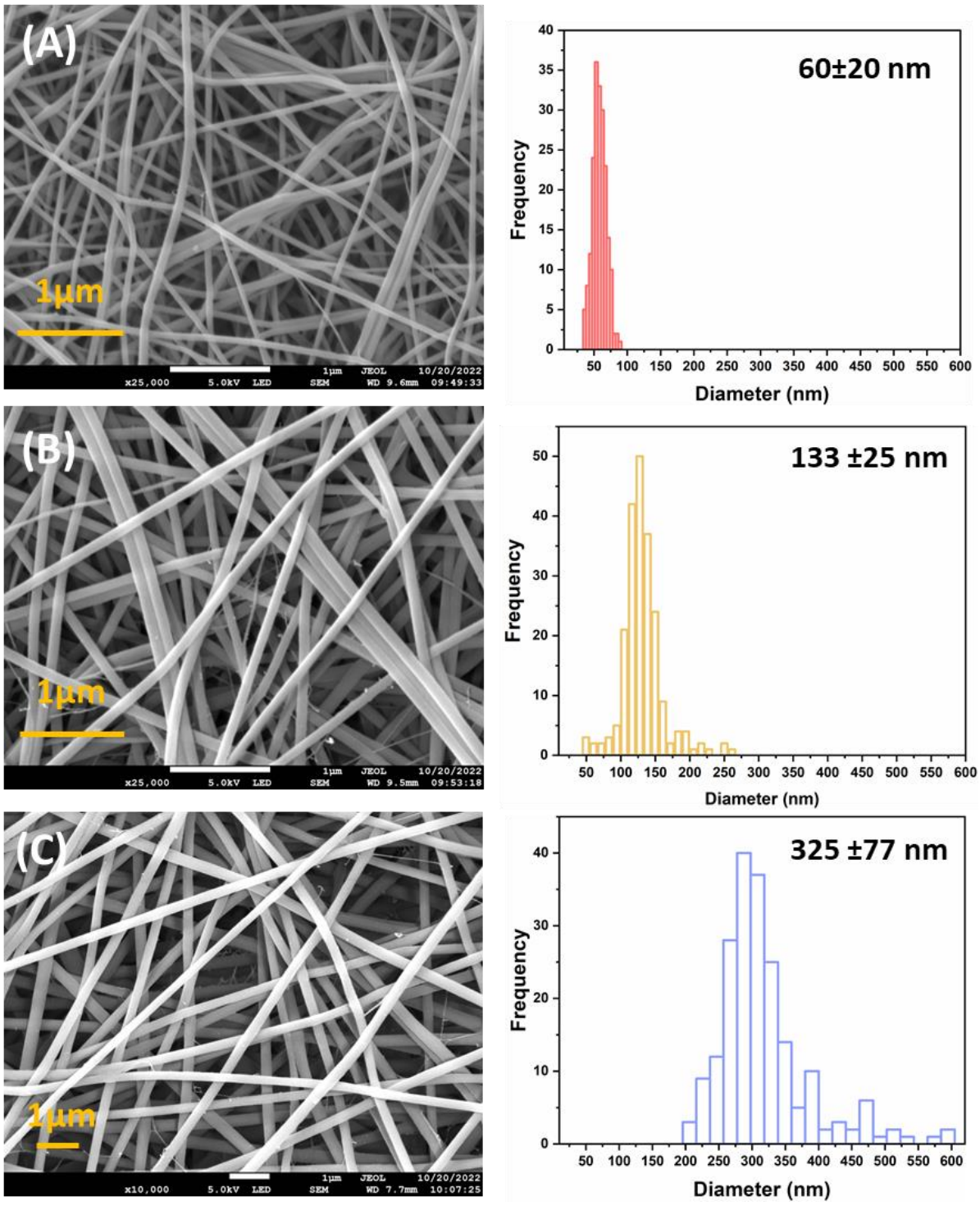

Figure 2.7 SEM images of polyamide 6 nanofiber mats with different average nanofiber diameter (A) 60 nm [magnification = 25 000×, scale bar = 1 µm] (B) 133 nm [magnification = 25 000×, scale bar = 1 µm] (C) 325 nm [magnification = 10 000×, scale bar = 1 µm]

2.2 Characterization methods

A set of characterization methods were used in this study to investigate different aspects of nanofiber mats. Techniques investigating the crystalline structure and its potential modification depending on the size of the nanofiber, were used. Chemical composition was also assessed, as well as thermal properties, allowing a deeper understanding of the possible structural anisotropy within nanofibers with regards to the variation of electrospinning parameters.

2.2.1 Thermogravimetric analysis (TGA)

Thermogravimetric analysis is a quantitative analytical technique that allows the study of thermal stability of a material by measuring the weight of a sample as a function of temperature or time. The sample is typically heated according to a customized protocol which may be isothermal or non-isothermal. During this process, a weight loss occurs due to several phenomena such as evaporation of volatile constituents or thermal decomposition. [21]

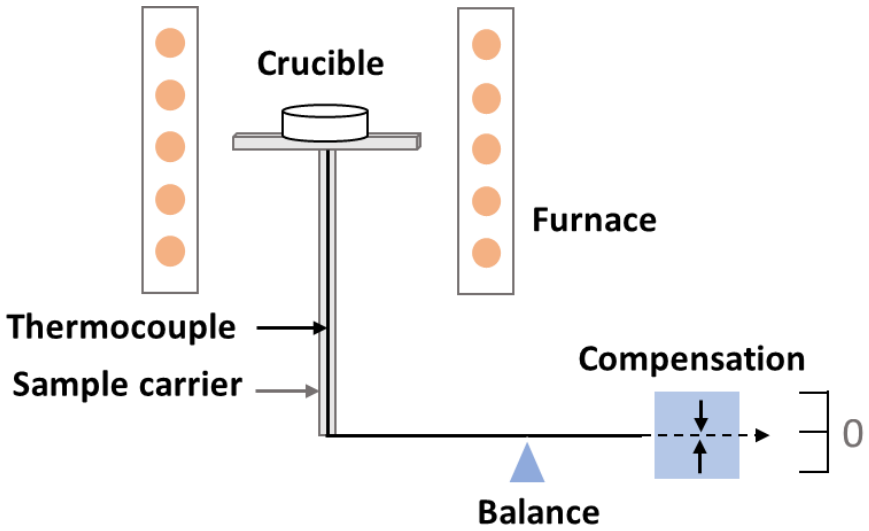

Figure 2.8 Schematic Iillustration of a thermogravimeter

In this work, experiments were carried out using a Netzsch TG 209 thermogravimeter. This apparatus consists of a micro-balance connected to an alumina crucible inside a furnace with a temperature programmer and controller thermo-balance *(Figure 2.8)* [22]. Samples were cut and put in the crucible, then heated at 20 K/min till 800°C, after a calibration run with the same protocol and an empty crucible.

2.2.2 Modulated-Temperature Differential Scanning Calorimetry (MT-DSC)

Differential scanning calorimetry is a technique that allows a quantitative and qualitative assessment of thermal events related to a phase transformation such as crystallization and melting, or a structural evolution of a material, such as physical aging. The principle of a heat flux DSC instrument consists in quantifying the difference in the amount of heat required to increase the temperature of a sample and a reference. *(Figure 2.9)* Accordingly, the apparatus determines the associated heat flow as a function of time and temperature.

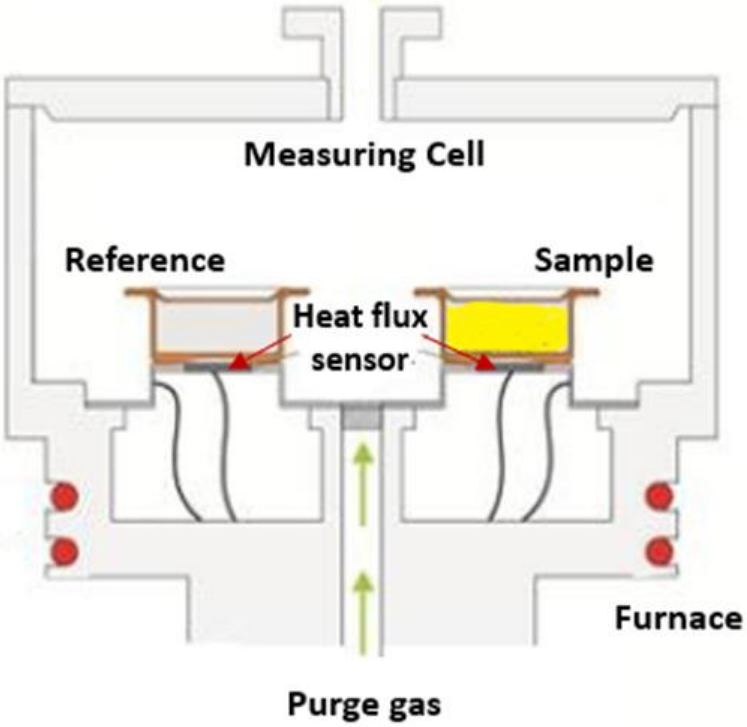

Figure 2.9 Schematic illustration of a heat-flux DSC

As mentioned before, during DSC measurements, the studied material may undergo several events like glass transition/evaporation or recrystallization/melting. These events may occur at the same temperature range leading to an overlapping of thermal phenomena that cannot be distinguished. As a matter of fact, within this kind of DSC the imposed temperature program is either isotherm or has linear variation of the temperature with time which may be expressed as following;

$$T = T_i + \beta t \qquad (1)$$

Where T is the temperature at the time t and T_i the initial temperature and β the scanning rate. The resulting heat flow measured by a standard DSC was stated to be determined as following [23];

$$\phi = \frac{dQ}{dt} = C^* \beta + f(t,T) \quad (2)$$

Where *f (t, T)* represents the part of heat flow related to the kinetic events, also stated as "non-reversing heat flow ϕ_{NR}". The other contribution is related to thermodynamic events, referred to as "reversing heat flow ϕ_R" and can be stated as the product of the complex heat capacity and the scanning rate *C*β.*

In the case of Modulated-temperature DSC (MT-DSC), **Reading et al.** [24] proposed the idea of superimposing a sinusoidal modulation on the linear ramp as a way to dissociate the thermal signal related to kinetic events from the one related to thermodynamic events.

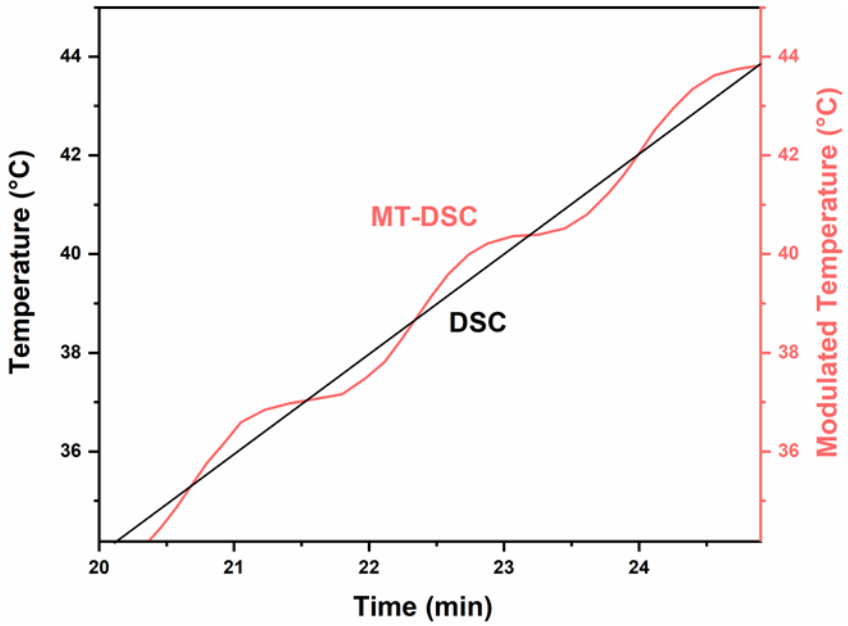

Figure 2.10 Illustration of a sinusoidal oscillation superimposed to a linear heating ramp.Modified from [23]

An illustration of this principle is presented in *Figure 2.10* and further explained with the following equation [25];

$$T = T_i + \beta t + A\,sin(\omega t) \quad (3)$$

In which A is the amplitude of the sinusoidal oscillation, ω is the angular frequency with $p = 2\pi/\omega$ is the period. So, the modulated heat flow can be presented as;

$$\phi = \frac{dQ}{dt} = C^*(\beta + A\omega\,cos(\omega t)) \quad (4)$$

Where C^* is the complex heat capacity and it can be defined as;

$$C^* = \frac{A_{HF}}{A_\beta} = \frac{\omega A C^*}{\omega A} \quad (5)$$

Where A_{HF} and A_β are the modulation amplitudes of the heat flow and the scanning rate respectively. Thermodynamic events are related to the vibrational and translational motions of the molecules within the sample. These motions are very fast and can easily follow slights modulations of the sample temperature. Contrarily, kinetic events are not able to follow these temperature variations. The reversing heat flow φ_R and the non-reversing heat flow φ_{NR} may be estimated by the following equation [25];

$$\phi_R = C^*\beta = \frac{A_{HF}}{A_\beta}\beta \quad (6)$$

$$\phi_{NR} = \phi - \phi_R = C^* A\omega \cos(\omega t) \quad (7)$$

Experimentally, a phase lag φ is measured between the heating modulation and the "total heat flow", which is the global response of the calorimeter. Considering this phase lag, two components of the apparent heat capacity C*, the “reversing heat capacity” C′ and the “non-reversing heat capacity” C′′, respectively related to the reversing heat flow ϕ_R and the non-reversing heat flow ϕ_{NR} , can be distinguished. These two components are calculated as indicated in the equation below;

$$C' = |C^*| \cos\phi \quad (8)$$

$$C'' = |C^*| \sin\phi \quad (9)$$

In the framework of this study, the used calorimeter is a DSC Q2000 (TA instruments) with a nitrogen gas flow of 50 mL/min. A full calibration procedure in temperature and energy with several steps was carried out; starting with the baseline run by heating an empty cell over the same temperature range that will be used for the sample’s experiments, then running two sapphire disks to obtain Tzero cell resistance and capacitance values. Afterwards, a calibration step is carried out with a standard indium at the same heating rate of the subsequent experiment, evaluating the melting endothermic peak. A final run with sapphire is realized for specific heat capacity calibration through the calculation of the cell constant calibration K_{Cp}. This factor corrects the apparent heat capacity of the sample, it is averaged on the investigated temperature range and calculated from the theoretical and experimental heat capacity values. As for the

sample preparations, nanofiber mats were cut, folded then encapsulated in Tzero DSC aluminum alloy pans.

Two modulation modes were used for experimentations; the “Heat only” because it enables a better investigation of the melting behavior without risk of recrystallization, or distortion of the modulation response because of a negative instantaneous heating rate. The parameters chosen for this mode are; an amplitude of ±0.318 K, a period of 60 s and a heating rate of 2 K/min. The second temperature-modulation mode used in this work is the “Heat cool” for a better investigation of the glass transition due to a large amplitude of modulation temperature, and the modulation parameters are; an amplitude of ±2.5 K, a period of 100 s and a heating rate of 1 K/min.

2.2.3 Fast Scanning Calorimetry (FSC / Flash DSC)

Ongoing investigations to improve the thermal analysis of materials have led to the development of the Fast Scanning Calorimetry. This technique allows very high scanning rates applied on very small samples which delays or totally inhibit kinetic thermal events, enabling the investigation of the kinetics of fast transformations. It is a power-compensated DSC apparatus, in which the sample and the reference are placed in separated furnaces. A linear temperature ramp is applied to both the sample and the reference. Because of the thermal events occurring to the sample, a different power is required to keep the sample and the reference at the same temperature; this difference is measured and converted to a heat flow signal [26] [27].

In this study, FSC measurements were realized using a Flash DSC 1 apparatus from Mettler Toledo equipped with Huber TC100 IntraCooler. The experiments were carried out using a power-compensation MultiSTAR UFS1 twin-chip sensor, based on MEMS technology, consisting of two sides; reference and sample working as two independent furnaces. The chip sensor is mounted on a stable ceramic with electrical connections. *(Figure 2.11)* The temperature resolution is determined by the time constant of the sensor which is about 1 millisecond, about thousand times less than a standard DSC. The heat flow is measured through sixteen thermocouples, eight for each side. They are arranged symmetrically in the form of a star around the measurement area on the sample and reference sides of the sensor. The measurement area of the chip is made of a silicon nitride and silicon dioxide coated with a thin layer of aluminum in order to provide homogeneous temperature distribution across the sensor [26].

.

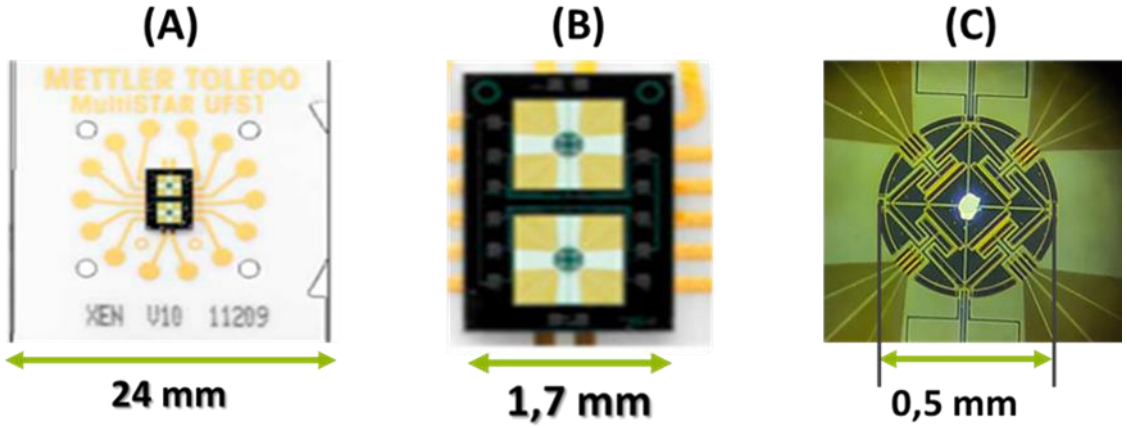

Figure 2.11 (A) MultiSTAR UFS1 ceramic sensor chip (B) MEMS chip containing two compartments, the upper one corresponds to the sample and the lower one to the reference (C) The upper part of the MEMS chip with a sample placed on the sensitive area of the sensor

Prior to use, each empty sensor chip is calibrated following the recommendations of the manufacturer. In our case, before putting the sample on the sensitive area of the sensor, a droplet of silicone oil was used to improve the thermal contact between the sample and the sensor. Experiments were performed under a 20mL/min nitrogen flow gas.

In order to estimate the mass of the sample, several procedures were proposed. In our case, depending on the tested material, two procedures were followed. For polyamide 6, samples were melt-quenched to their amorphous state at a scanning rate of 1500 K/s and the mass value is determined by comparing the heat flow at glass transition $\Delta h\,(FSC)$ determined by FSC and the heat capacity step at glass transition of a fully amorphous material that can be found in literature $\Delta C_p^\circ = 0.47\ J/(g.K)$ [28], according to the following equation;

$$m = \frac{\Delta h(FSC)}{\beta(FSC) * \Delta C^\circ{}_p} \qquad (10)$$

With β(FSC) the heating rate in FSC.

For PAN nanofiber mats, samples were heated till melting at scanning rates ranging from 1500 K/s and 3000 K/s. Then, the sample mass was determined by comparing the heat flow at glass transition from FSC measurement $\Delta h(FSC)$ to the heat capacity step at glass transition determined by MT-DSC $\Delta C_p\,(MT\text{-}DSC)$, according to the following equation [29].

$$m = \frac{\Delta h(FSC)}{\beta(FSC) * \Delta C_p(MTDSC)} \quad (11)$$

During FSC measurement, a delay of the heat transfer between the sample and the sensor takes place because of the high scanning rates and the geometry of the sample, leading to a shift of the temperature. Hence, the measured thermal events appear to happen at higher temperatures. This temperature gradient is referred to as the thermal lag. Its correction has been widely discussed in literature and realized by the melting of an indium piece placed on the top of the sample[30] [31]. More recently, **Schawe et al** [32] proposed another method with two thermal corrections, dynamic and static for more accurate results. The dynamic thermal lag ΔT_D was calculated as the half distance between the heating and cooling at the same scanning rate. The static thermal lag ΔT_S is determined as the third of the distance between the onset of the melting temperatures of two indium pieces, one placed on the reference and the other placed on the top of the sample.

2.2.4 Wide angle X-ray diffraction (WAXD)

X-ray diffraction is an analytical technique used to determine the spatial organization of atoms or molecules in ordered structures. It is mainly used to characterize and quantify the crystalline phase in semi-crystalline microstructures. The principle of WAXD is based on the bombarding of a sample with an X-ray beam and the measuring of intensity related to the diffracted rays as a function of the scattered angle 2θ. Regular or irregular arrangements of atoms or molecules lead X-rays to diffract or scatter, respectively, into many specific directions after elastic interactions with electronic clouds from the sample. *(Figure 2.12)* As a consequence, high intensity diffraction peaks or low intensity halos may be recorded.

The crystalline domains of a sample are detected through the presence of diffraction peaks, which are generally analyzed with the Bragg's law: [33]

$$n\lambda = 2d\ sin(\theta) \quad (12)$$

Where *n* is an integer referred to as the order of diffraction, λ is the wavelength of the incident X-ray beam, *d* is the space between diffracting planes in the crystalline lattice and θ is the angle between the incident and the scattered rays.

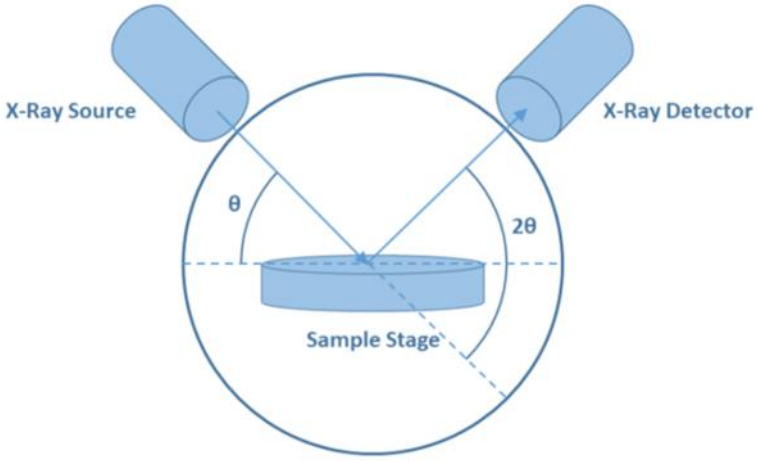

Figure 2.12 Schematic illustration of a Wide-angle X-ray diffraction apparatus in a θ :2θ configuration (reflection mode)

In this work, measurements were performed on a Malvern Panalytical Empyrean X-ray diffractometer. The generator was setup on 35 kV and 40 mA and a copper Cu K_α radiation (λ=0.154 nm) was used. Two types of measurements were realized, room temperature and with temperature variation. In the first case, XRD spectra were registered from 5 to 50° with a step size of 0.02°/s.

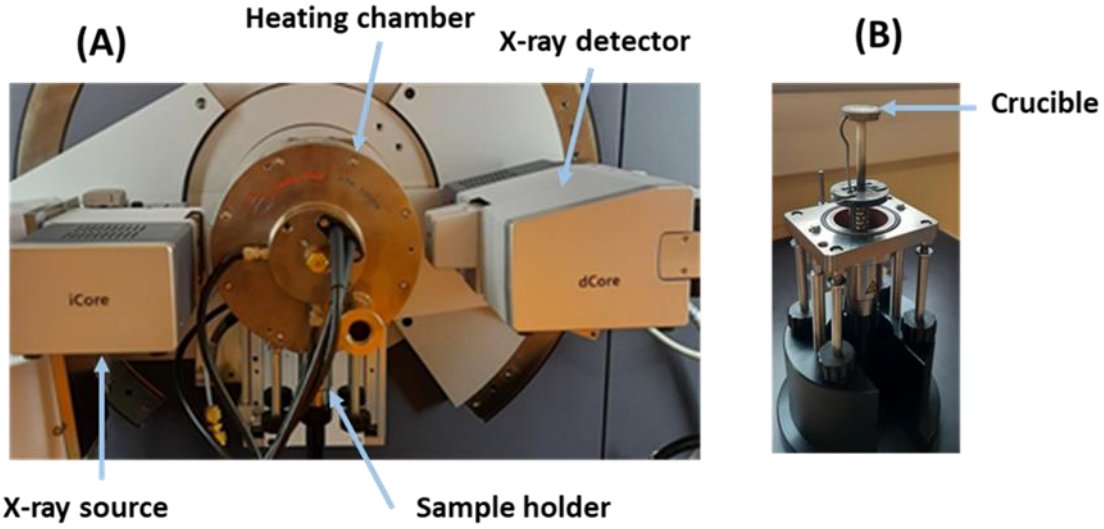

Figure 2.13 Panalytical X-ray Diffractometer (A) With HTK 1200N heating chamber and the sample held inside the chamber (B) The sample holder

For measurement with temperature variation, an HTK 1200N high temperature oven-chamber was used under vacuum. (*Figure 2.13)* The heating range was from 25°C till melting at a heating rate of 2K/min and an XRD scan was registered each 10°C. This protocol was used to study PA6 nanofiber mats.

2.2.5 Fourier Transform Infrared Spectroscopy (FTIR)

FTIR is a non-destructive technique used mainly for the investigation of chemical composition of materials, based on the determination of the interaction between an IR radiation and the chosen sample to study. It enables qualitative and quantitative investigation by measuring the frequencies at which the sample absorbs the IR radiation and also the intensities of these absorptions. [34] The infrared region of the electromagnetic spectrum extends from the visible to the microwave, and can be divided into ;

- Near (NIR, υ=10 000 – 4000 cm^{-1})
- Middle (MIR, υ= 4000 – 200 cm^{-1})
- Far (FIR, υ= 200 – 10 cm^{-1})

The principle of the FTIR is as following; a sample is irradiated by infrared light and the reflected or transmitted light is measured. The investigation of the amount of absorbed light by the molecules is wavelength dependent and it is due to the vibrations of molecules. As a matter of fact, the energy associated with vibrations of interatomic bonds within a molecule is close to that of infrared light, so that molecules absorb infrared light and vibrate. The vibrations that can be induced by infrared light are limited to those involving a change in dipole moment. For instance, infrared absorption does not occur if the vibrations of bonds between atoms cancel each other. The result of an FTIR analysis is illustrated as a spectrum of transmittance or absorbance intensities as a function of wavenumber (cm^{-1}).

In the framework of our study, a Thermo Fischer Scientific Nicolet iS10 FTIR spectrometer was used with an attenuated total reflectance (ATR) accessory. Spectra were registered on a wavenumber range of 400-4000 cm^{-1}, a resolution of 4 cm^{-1} and a scan number of 250.

The principle of the ATR-FTIR is as following; the infrared light is introduced to a suitable prism at an angle exceeding the critical angle for internal reflection, developing, therefore, a special type of electromagnetic irradiation referred to as “evanescent wave” at the reflecting surface. Interaction of this evanescent wave with the sample determines ATR spectrum recording [35].

2.2.6 Scanning Electron Microscopy (SEM)

SEM is a widely used technique to investigate the surface features of a material. Its resolution is noted to be 1000 times higher than a light microscope. As its name suggests, this apparatus is based on a finely focused beam of electrons to produce image of a sample placed in a vacuum chamber. More specifically, an incident beam is accelerated through an anode, condenser lenses and objective lens to interact with the sample surface, leading to the emission of electrons such as secondary electrons, back-scattered electrons and X-rays. *(Figure 2.14)* [36].

In this work, a JOEL 7900F scanning electron microscope was used. Samples were coated with a platinum thin layer for 4 minutes before undergoing the microscope.

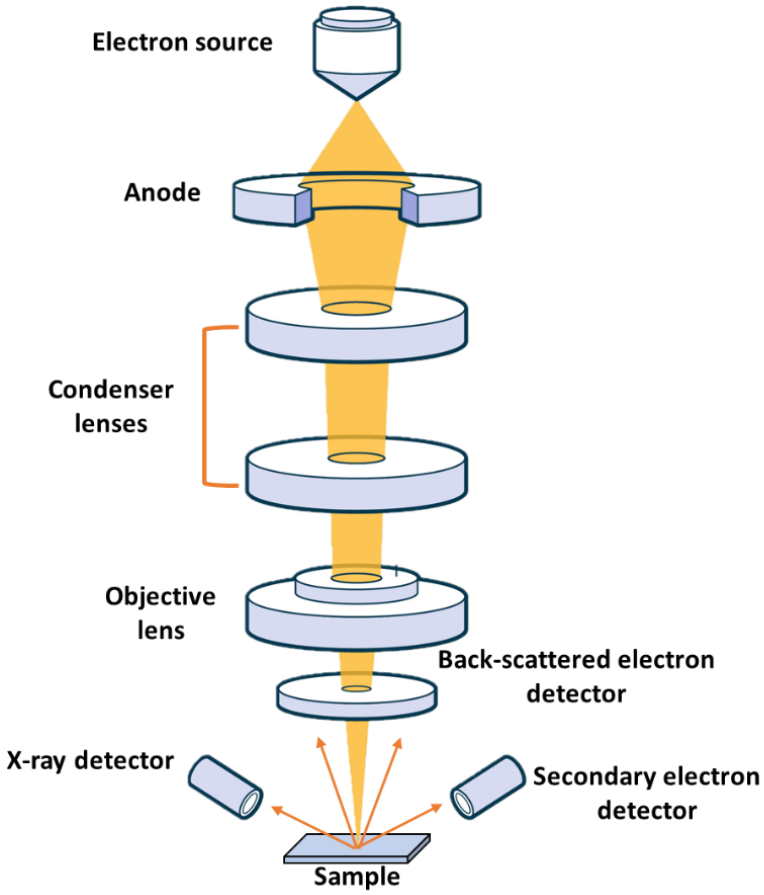

Figure 2.14 Schematic illustration of scanning electron microscope [37]

2.3 References

[1] M. L.F. Nascimento, E. S. Araujo, E. R. Cordeiro, A. H.P. de Oliveira, and H. P. de Oliveira, "A Literature Investigation about Electrospinning and Nanofibers: Historical Trends, Current Status and Future Challenges," *Recent Pat. Nanotechnol.*, vol. 9, no. 2, pp. 76–85, Aug. 2015, doi: 10.2174/1872210509021508191515 32.

[2] S. K. Nataraj, K. S. Yang, and T. M. Aminabhavi, "Polyacrylonitrile-based nanofibers—A state-of-the-art review," *Prog. Polym. Sci.*, vol. 37, no. 3, pp. 487–513, Mar. 2012, doi: 10.1016/j.progpolymsci.2011.07.001.

[3] S. Dalton, F. Heatley, and P. M. Budd, "Thermal stabilization of polyacrylonitrile fibres," *Polymer*, vol. 40, no. 20, pp. 5531–5543, Sep. 1999, doi: 10.1016/S0032-3861(98)00778-2.

[4] B. G. Colvin and P. Storr, "The crystal structure of polyacrylonitrile," *Eur. Polym. J.*, vol. 10, no. 4, pp. 337–340, Apr. 1974, doi: 10.1016/0014-3057(74)90147-5.

[5] M. S. A. Rahaman, A. F. Ismail, and A. Mustafa, "A review of heat treatment on polyacrylonitrile fiber," *Polym. Degrad. Stab.*, vol. 92, no. 8, pp. 1421–1432, Aug. 2007, doi: 10.1016/j.polymdegradstab.2007.03.023.

[6] X.-P. Hu, "The molecular structure of polyacrylonitrile fibers," p. 8.

[7] Y.-J. Bai, C.-G. Wang, N. Lun, Y.-X. Wang, M.-J. Yu, and B. Zhu, "HRTEM microstructures of PAN precursor fibers," p. 6, 2006.

[8] S. M. Saufi and A. F. Ismail, "Development and characterization of polyacrylonitrile (PAN) based carbon hollow fiber membrane," vol. 24, p. 12, 2002.

[9] D. Li, C. Lu, J. Hao, and H. Wang, "A comparative analysis of polyacrylonitrile-based carbon fibers: (I) Microstructures," *New Carbon Mater.*, vol. 35, no. 6, pp. 793–801, Dec. 2020, doi: 10.1016/S1872-5805(20)60527-3.

[10] D. Papkov, Y. Zou, M. N. Andalib, A. Goponenko, S. Z. D. Cheng, and Y. A. Dzenis, "Simultaneously Strong and Tough Ultrafine Continuous Nanofibers," *ACS Nano*, vol. 7, no. 4, pp. 3324–3331, Apr. 2013, doi: 10.1021/nn400028p.

[11] A. Babakhanian *et al.*, "A fabricated electro-spun sensor based on Lake Red C pigments doped into PAN (polyacrylonitrile) nano-fibers for electrochemical detection of Aflatoxin B1 in poultry feed and serum samples," *The Analyst*, vol. 140, no. 22, pp. 7761–7767, 2015, doi: 10.1039/C5AN01602A.

[12] P. Matthies and W. F. Seydl, "History and Development of Nylon 6," in *High Performance Polymers: Their Origin and Development*, R. B. Seymour and G. S. Kirshenbaum, Eds. Dordrecht: Springer Netherlands, 1986, pp. 39–53. doi: 10.1007/978-94-011-7073-4_4.

[13] N. S. Murthy, "Hydrogen bonding, mobility, and structural transitions in aliphatic polyamides," *J. Polym. Sci. Part B Polym. Phys.*, vol. 44, no. 13, pp. 1763–1782, Jul. 2006, doi: 10.1002/polb.20833.

[14] D. R. Holmes, C. W. Bunn, and D. J. Smith, "The crystal structure of polycaproamide: Nylon 6," *J. Polym. Sci.*, vol. 17, no. 84, pp. 159–177, Jun. 1955, doi: 10.1002/pol.1955.120178401.

[15] N.S.Murthy, "Metastable crystalline phases in nylon 6," *Polymer*, vol. 10, no. 32, pp. 301–305, Jan. 1991.

[16] H. Suzuki, S. Ishii, C. Otani, and H. Hoshina, "Low-frequency vibrations of polyamide-6 as a function of temperature and thermal history investigated by terahertz absorption spectroscopy," *Eur. Polym. J.*, vol. 67, pp. 284–291, Jun. 2015, doi: 10.1016/j.eurpolymj.2015.04.009.

[17] X. Li, B. Ding, J. Lin, J. Yu, and G. Sun, "Enhanced Mechanical Properties of Superhydrophobic Microfibrous Polystyrene Mats via Polyamide 6 Nanofibers," *J. Phys. Chem. C*, vol. 113, no. 47, pp. 20452–20457, Nov. 2009, doi: 10.1021/jp9076933.

[18] F. Yalcinkaya, B. Yalcinkaya, and J. Hruza, "Electrospun Polyamide-6 Nanofiber Hybrid Membranes for Wastewater Treatment," *Fibers Polym.*, vol. 20, no. 1, pp. 93–99, Jan. 2019, doi: 10.1007/s12221-019-8820-4.

[19] A. M. Anjeh, "Preparation, Characterization and Properties of a Novel Electrospun Polyamide-6/ Chitosan/Graphene Oxide Composite Nanofiber," *J. Polym. Environ.*, p. 15, 2022.

[20] R. Nirmala, R. Navamathavan, S.-J. Park, and H. Y. Kim, "Recent Progress on the Fabrication of Ultrafine Polyamide-6 Based Nanofibers Via Electrospinning: A Topical Review," *Nano-Micro Lett.*, vol. 6, no. 2, pp. 89–107, Apr. 2014, doi: 10.1007/BF03353773.

[21] C. De Blasio, "Thermogravimetric Analysis (TGA)," in *Fundamentals of Biofuels Engineering and Technology*, Cham: Springer International Publishing, 2019, pp. 91–102. doi: 10.1007/978-3-030-11599-9_7.

[22] J. D. Menczel and R. B. Prime, Eds., *Thermal analysis of polymers: fundamentals and applications*. Hoboken, N.J: John Wiley, 2009.

[23] E. Verdonck, K. Schaap, and L. C. Thomas, "A discussion of the principles and applications of Modulated Temperature DSC (MTDSC)," *Int. J. Pharm.*, vol. 192, no. 1, pp. 3–20, Dec. 1999, doi: 10.1016/S0378-5173(99)00267-7.

[24] M. Reading, B. K.Hahn, and B. S.Crowe, "Method and apparatus for modulated differential analysis," 5,224,775, 1993

[25] M. Reading and D. J.Hourston, *Modulated-Temperature Differential Scanning Calorimetry Theoretical and practical applications in polymer characterisation*. Netherlands: Springer, 2006.

[26] C. Schick and V. Mathot, Eds., *Fast Scanning Calorimetry*. Cham: Springer International Publishing, 2016. doi: 10.1007/978-3-319-31329-0.

[27] V. Mathot *et al.*, "The Flash DSC 1, a power compensation twin-type, chip-based fast scanning calorimeter (FSC): First findings on polymers," *Thermochim. Acta*, vol. 522, no. 1–2, pp. 36–45, Aug. 2011, doi: 10.1016/j.tca.2011.02.031.

[28] B. Wunderlich, "The ATHAS database on heat capacities of polymers," *Pure Appl. Chem.*, vol. 67, no. 6, pp. 1019–1026, Jan. 1995, doi: 10.1351/pac199567061019.

[29] P. Cebe *et al.*, "Heat of fusion of polymer crystals by fast scanning calorimetry," *Polymer*, vol. 126, pp. 240–247, Sep. 2017, doi: 10.1016/j.polymer.2017.08.042.

[30] J. E. K. Schawe, "Influence of processing conditions on polymer crystallization measured by fast scanning DSC," p. 9.

[31] N. Shamim, Y. P. Koh, S. L. Simon, and G. B. McKenna, "Glass transition temperature of thin polycarbonate films measured by flash differential scanning calorimetry," *J. Polym. Sci. Part B Polym. Phys.*, vol. 52, no. 22, pp. 1462–1468, Nov. 2014, doi: 10.1002/polb.23583.

[32] J. E. K. Schawe, "Measurement of the thermal glass transition of polystyrene in a cooling rate range of more than six decades," *Thermochim. Acta*, vol. 603, pp. 128–134, Mar. 2015, doi: 10.1016/j.tca.2014.05.025.

[33] W. H. Bragg and W. L. Bragg, "The reflection of X-rays by crystals," *Proc. R. Soc. Lond. Ser. Contain. Pap. Math. Phys. Character*, vol. 88, no. 605, pp. 428–438, Jul. 1913, doi: 10.1098/rspa.1913.0040.

[34] R. A. Spragg, "IR Spectrometers," in *Encyclopedia of Spectroscopy and Spectrometry*, Elsevier., 1999, pp. 1048–1057.

[35] C. M. Simonescu, "Application of FTIR Spectroscopy in Environmental Studies," in *Advanced Aspects of Spectroscopy*, InTech., Croatia, 2012, p. 36.

[36] A. Mayeen, L. K. Shaji, A. K. Nair, and N. Kalarikkal, "Morphological Characterization of Nanomaterials," in *Characterization of Nanomaterials*, Elsevier, 2018, pp. 335–364. doi: 10.1016/B978-0-08-101973-3.00012-2.

[37] N. Gleichmann, "SEM vs TEM," *Technology Networks*, Feb. 2020. https://www.technologynetworks.com/analysis/articles/sem-vs-tem-331262

Chapter 3 Structural characterization and physical aging in environmentally aged electrospun polyacrylonitrile nanofiber mats: role of the nanofiber size

3.1 Molecular orientation within PAN nanofibers: previous studies

3.1.1 Scope of the study

Polyacrylonitrile (PAN) is amongst the most used precursors for producing high performance carbon fibers owing to its properties. The chemistry of PAN is of a specific interest for its thermal stability due to its very high melting temperature and for yielding great amount of carbon [1]. A growing interest in improving the performance of carbon fibers, have led to the investigation of another class of this material, that is nanofibers. In case of application as reinforcement of composite materials, it is believed that reducing fibers diameters, improves their interactions with matrix, increases the shear strength and helps reducing the size and number of defects that may be present in the structure. Accordingly, Arshad et al[2] investigated carbon nanofibers obtained from PAN electrospun fibers, with diameters varying from 150-500 nm, and reported that the average tensile strength of a single PAN-based carbon nanofiber was three times higher than previously studied carbon fibers. In the same vein, Papkov et al [3] revealed a simultaneous improvement of the toughness, modulus and strength of PAN nanofibers along with decreasing nanofibers diameters. This outstanding behavior was attributed to a low degree of crystallinity along with molecular orientation, both resulting from nanofibers fabrication process.

For a better understanding of the origin and control of the above described peculiar behavior, Araujo et al[4] have studied the signature of molecular orientation within PAN nanofibers with average diameters varying from 232-785 nm, by combining calorimetric analysis (MT-DSC) and dielectric relaxation spectroscopy (DRS). MT-DSC analysis of these samples allowed the determination of the corresponding glass transition temperature (T_g) along with the heat capacity step at T_g. By decreasing nanofibers average diameters, a broadening of the glass transition was noticed and an increase of its mid-point values, along with an increase in the heat capacity step at T_g. Knowing from previous work that PAN nanofibers possess relatively low crystallinity, the increase in glass transition temperature was designated as a signature of a constrained amorphous phase. Moreover, DRS analysis provided informations about the signature of α-relaxation, which is the dielectric signature of the glass transition. It showed at temperatures higher than that of calorimetric glass transition (the one detected by MT-DSC), precisely 20°C above T_g, that nanofibers with different average diameters presented the same behavior. Being at temperatures well below the melting of PAN nanofibers, this change could not be caused by the disappearance of the crystalline phase. It was rather attributed to the slackening of the initially oriented molecular chains, when crossing the glass transition.

The results mentioned so far, illustrate the impact of nanofibers diameters variation on the molecular dynamics around glass transition. This was explained by a constrained amorphous phase with an increased chain rigidity for the thinnest nanofibers, being a signature of higher molecular orientation when decreasing nanofibers diameters. However, whether the orientation is maintained during storage remains to be investigated. This information would be of particular interest for applications that require a long-lasting durability. For this purpose, the nanofiber mats were stored under ambient conditions during three years after their fabrication. Subsequently, structural characterization was performed and the orientation was investigated using molecular dynamic studies.

It is noteworthy that the above-mentioned investigations were realized on relatively high mass of PAN nanofiber mats, that is a large amount of randomly macroscopically aligned fibers and higher porosity within nanofibers, that may lead to relatively high uncertainties. Additionally, it was noted, by means of DRS, that by heating above the glass transition temperature the orientation effect vanishes and samples with different average diameters present the same behavior. Ideally, the impact of aging during storage should be tracked from the structural relaxation process occurring in the glassy state, since it is more representative of realistic conditions. This could be performed by studying the impact of the nanofiber size on the physical aging kinetics. However, such study is generally incomplete when using a standard DSC, or even, modulated temperature DSC. Indeed, the calorimetric investigation of physical aging involves two heating scans: the first one for the aged material and the second scan recording the response of the rejuvenated one. Unfortunately, on a first heating to temperatures above glass transition, a slackening of the orientation will take place (which is the case for the above-mentioned study) and on a subsequent heating there will be no sign of orientation within the studied samples. In other terms, the second scan will not contain the expected information regarding oriented and rejuvenated material but information regarding rejuvenated and unoriented material.

Aiming to overcome these limits, nano-sized samples will be tested in our work to be more suitable for investigating nanofibrous structures, by means of Fast Scanning Calorimetry that allows the study of sample weights as low as 10 ng and having dimensions smaller than 0.5 mm. As mentioned in the previous chapter, this technique enables the widening of the scanning rate range to thousands of kelvins per seconds. This will help avoiding irreversible kinetic events during the study of structural recovery around glass transition temperature. Therefore, a study of the physical aging kinetics of PAN nanofiber mats was realized, in this work, in order

to track, more closely, the polymer chain orientation signature within the amorphous phase of electrospun polymer solution.

In the following part, a brief definition of the physical aging phenomenon and related concepts used for the interpretation of the collected data will be presented.

3.1.2 Concept of physical aging

Physical aging is a reversible phenomenon that describes the time and temperature dependence of a polymer's amorphous phase behavior below its glass transition [5] It is widely known to occur within glassy materials due to their out-of-equilibrium state, induced by their formation process.

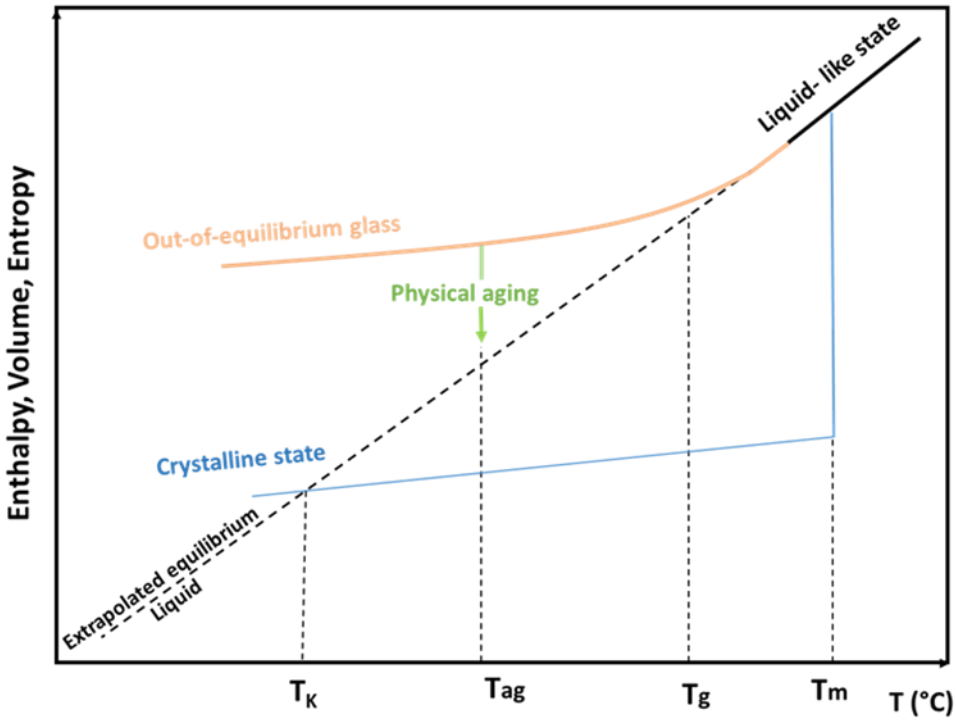

Figure 3.1 Illustration of the temperature dependence of thermodynamic properties of glass forming liquid and the time dependent properties of a glassy out-of-equilibrium material in order to regain equilibrium state: T_k Kauzmann temperature, T_{ag} is the aging temperature, T_g the glass transition temperature and T_m the melting temperature

As illustrated in *Figure 3.1,* the process involves generally cooling down the material from its molten state at very high rates, avoiding its crystallization. Thus, the molecular movements slow down to an extent that the relaxation time is way higher than that available by the imposed cooling rate. The resulting "frozen in" state of this material leads to the deviation from the equilibrium line and to undergo the glass transition [6]. Being in an out-of-equilibrium state, the glassy material displays an excessive amount of thermodynamic entities that will be reduced slowly to approach a new metastable equilibrium state corresponding to the extrapolation of thermodynamic quantities of the liquid-like state. This is known as physical aging phenomenon triggered by structural relaxation [7] [8] [9]. The same figure presents the first-order transition through which the crystalline state of the system reaches the liquid-like state, on increasing the temperature. This is accompanied by an instant increase of the thermodynamic properties at T_m, the melting temperature. Upon cooling, the entropy difference between the liquid-like and the solid states decreases. The Kauzmann temperature is designed as the temperature at which this difference equals zero [8]. In our work, this notion won't be further referred to.

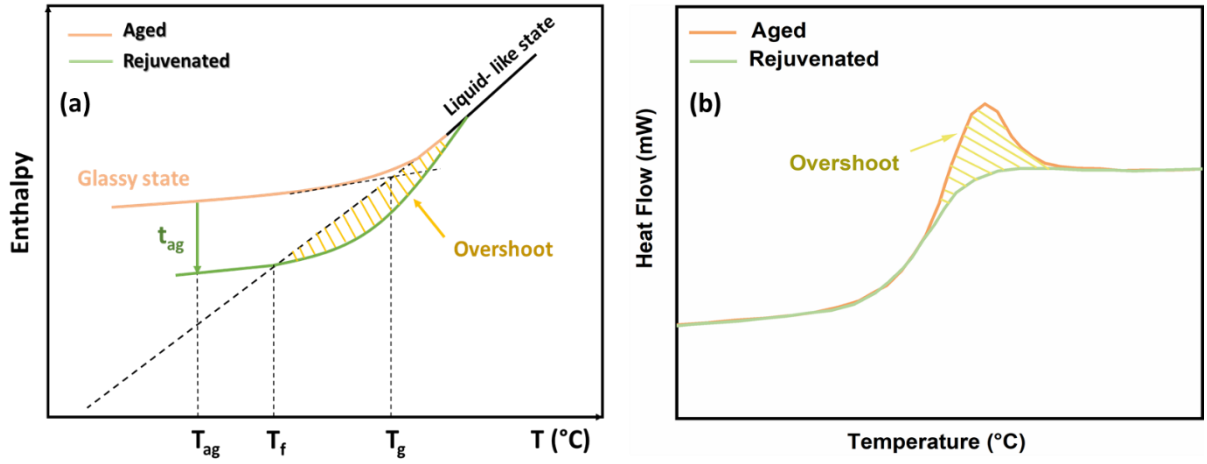

Figure 3.2 Schematic representation of (a) the temperature dependence of the enthalpy of a glassy material upon aging (b) heat flow of an aged and rejuvenated glassy material. T_{ag}: aging temperature, T_g: glass transition temperature and T_f: fictive temperature

The physical aging can be investigated using several techniques, by observing the evolution of the aged system's macroscopic properties or thermodynamic quantities such as enthalpy in the case of calorimetric analysis. As explained above, the out-of-equilibrium glassy system reaches a lower energetic state while decreasing its excess of enthalpy. Being in this state was found to delay the recovery of the equilibrium upon a subsequent heating. This delay is presented in *Figure 3.2.a* by the hatched area. Therefore, when an isothermal heat treatment is applied on a glass, the response during a subsequent heating is illustrated by an overshoot of enthalpy

superimposed to the glass transition *(Figure 3.2.b).* This is related to the amount of energy released to regain equilibrium.

The enthalpy recovery of an aged system at a defined temperature (T_{ag}) and duration (t_{ag}) is determined by the integration of the difference between the scans of an aged and a rejuvenated sample, according to the following equation [10];

$$\Delta H(T_{ag}, t_{ag}) = \int_{T_1}^{T_2} \left[C_p^{ag}(T) - C_p^{r}(T)\right].dT \quad (1)$$

With $C_p^{ag}(T)$ and $C_p^{r}(T)$ present respectively the heat capacity of the aged and the rejuvenated glass and T_1, T_2 are two arbitrary temperature values slightly above and beyond the glass transition temperature, for which the heat capacity of aged and rejuvenated systems is identical. The total enthalpy loss ΔH_∞ , defined as the enthalpy lost when the structural relaxation is fully accomplished, depends on the aging temperature T_{ag}, the glass transition temperature T_g and the heat capacity step at glass transition ΔC_p. It is estimated by the following equation;

$$\Delta H_\infty = \Delta C_p \times \left(T_g - T_{ag}\right) \quad (2)$$

3.1.3 Concept of fictive temperature

The structural relaxation phenomenon may be investigated through the fictive temperature T_f concept. It is defined as the temperature at which the properties of the studied material, undergoing the structural relaxation, would be at equilibrium [11]. Under zero aging time, the fictive temperature is equal to the glass transition temperature. This temperature is expected to come closer to T_{ag} as the aging time increases. Therefore, studying the fictive temperature as a function of aging time may provide informations about the structural relaxation kinetics. The value of fictive temperature is estimated from calorimetric investigations by the matching area method *(Figure 3.3)* according to the following equation [12] ;

$$\int_f^{T_2} \left(C_{p,l} - C_{p,g}\right)dt = \int_{T_1}^{T_2} \left(C_p - C_{p,g}\right)dt \quad (3)$$

Where T_1 and T_2 are arbitrary temperatures above and beyond the glass transition, in a way that $C_p = C_{p,g}$ at T_1 and $C_p = C_{p,l}$ at T_2. C_p is the heat capacity of the sample, $C_{p,g}$ and $C_{p,l}$ corresponds respectively to the extrapolation of the heat capacity lines of the liquid and glassy state of the

sample. Following the evolution of the fictive temperature with time is thus an alternative way to depict the structural relaxation. In our study, the calculation of the enthalpy recovery has been preferred though.

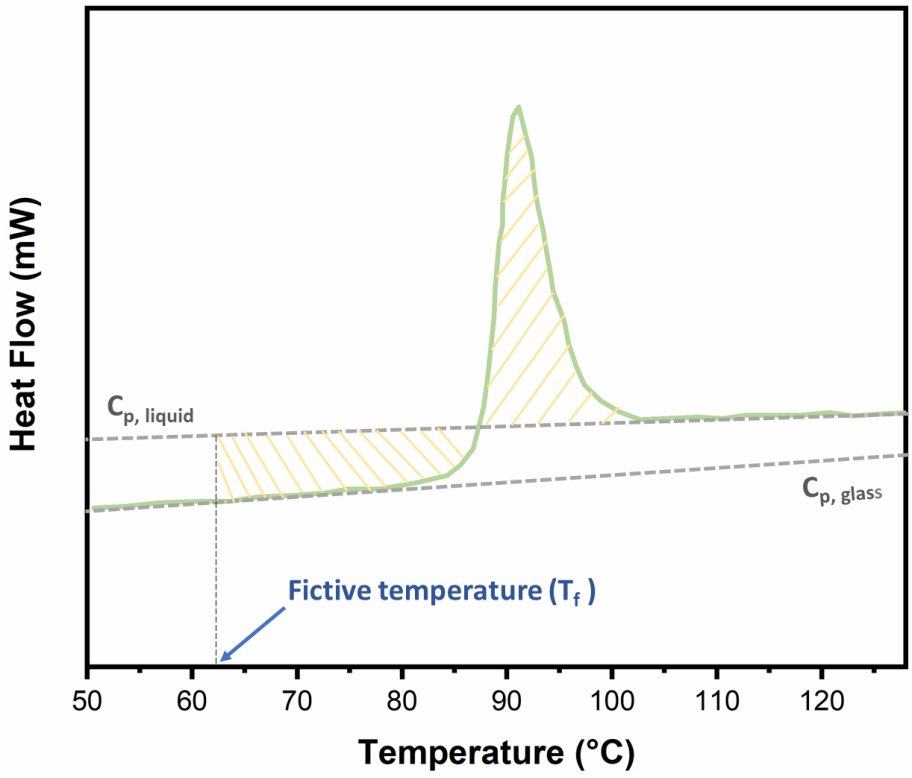

Figure 3.3 Schematic illustration of the matching area method used to estimate the fictive temperature; $C_{p, liquid}$ Heat capacity of the liquid state, $C_{p, glass}$ Heat capacity of the glassy state

In this chapter, the signature of the molecular orientation within PAN nanofiber mats has been tracked by investigating their amorphous phase through physical aging, crystalline phase through Wide-angle X-ray diffraction (WAXD) and chemical structure by Fourier Transform Infrared spectroscopy (FTIR). The latter are accompanied with relatively high uncertainties since they rely typically on large amount of material to get a sufficiently clear signal for interpretation. However, in this case, the resultant signals allowed the estimation of the crystalline phase and the identification of the molecular composition of each sample.

3.2 Evaluation of polymer chain orientation

3.1 Spectroscopic analysis

Polyacrylonitrile has been considered to have a low crystallinity degree because of its weak and diffuse X-ray diffraction pattern [13]. As a matter of fact, previous studies seem to be controversial regarding its microstructure. Among the proposed explanations, Dalton et al [14]

investigated PAN fibers and reported two main equatorial reflections indicating order perpendicular to the fiber axis, which have been interpreted as an hexagonal conformation. It has been stated as well that PAN microstructure is formed by a single para-crystalline phase, a "laterally ordered" phase, or a two phased structure with both ordered and disordered regions [15] [16]. Moreover, in a way to examine the crystalline structure of polyacrylonitrile, other studies have established a pattern as following; dry PAN-based structures such as powder, molded films and fibers possess a hexagonal packing with no chain axis order. On the other hand, PAN-based structure involving solvent use within their fabrication process, display an orthorhombic packing because of a distortion within the original hexagonal packing triggered by, in some cases, the co-crystallization of the solvent due to its involvement in hydrogen-bonding interaction with nitrile groups [17]. However, under certain circumstances like high drawing, the solvent is expected to be expelled and the chains to reorganize in a hexagonal conformation.

Due to the disagreement in literature about polyacrylonitrile crystal structure and its diffuse signal, it was worth investigating the X-ray diffraction pattern of PAN nanofiber mats in our study having the average nanofibers diameters 273, 482 and 800 nm.

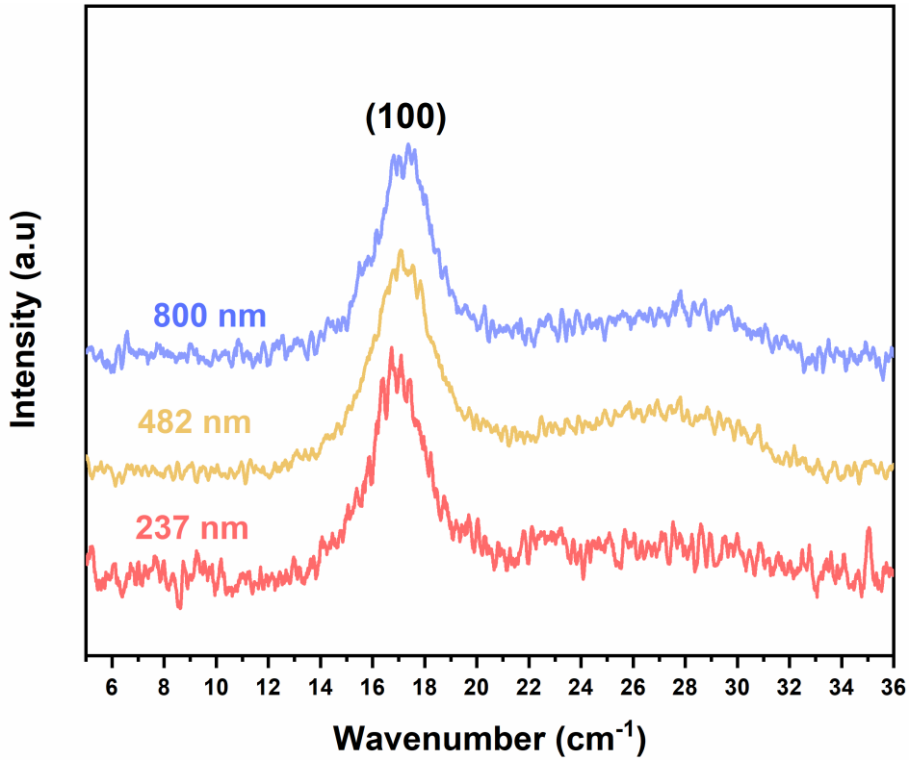

Figure 3.4 WAXD spectra of PAN nanofiber mats recorded at room temperature within a scan range of 5 to 36° and a step size of 0.01

The experimental WAXD spectra illustrated in *Figure 3.4* exhibit a main peak around 2θ= 17°, which may can be indexed as (100) reflection [18], with a diffraction spacing (d-spacing) around 0.52 nm that is followed by a broad halo centered around 2θ= 27°. As mentioned in the previous paragraph, it is difficult to ascertain the structure of polyacrylonitrile. However, in our case, the spectra present similarities with the XRD spectrum of PAN cast film and of drawn polyacrylonitrile investigated in earlier studies and considered to adopt a rod-like hexagonal conformation [17] [19]. Further analysis is presented in the following part estimating the degree of crystallinity of PAN nanofiber mats by the deconvolution of the corresponding WAXD spectra. The degree of crystallinity of each sample is estimated by dividing the area corresponding to the crystalline phase by the sum of the crystalline and the amorphous phases. It is noteworthy that the deconvolution parameters and crystallinity degree should not be considered as absolute values, they were used to describe the trend of crystalline phase.

Due to the lack of information in literature about the deconvolution of PAN spectra, several fits have been tested and two amorphous halos were finally used to depict the amorphous phase. The position of the amorphous halo was chosen based on a previous study in which the diffraction peak at 2θ= 17° was considered to include both the crystalline and amorphous contributions [20].

Table 3.1 Position 2θ, FWHM, crystallinity ratio obtained from fitting the WAXD experimental spectra of PAN nanofiber mats

Nanofibers diameters (nm)	**2θ (°)**			**FWHM (°)**			**Xc (%)**
	crystalline	**amorphous**		**crystalline**	**amorphous**		
237	17	17	26.4	2.16	8.47	11.77	28
482	17	17.39	26	2.43	8.24	11.7	30
800	17.2	16.92	26.8	2.29	7.98	10.59	33

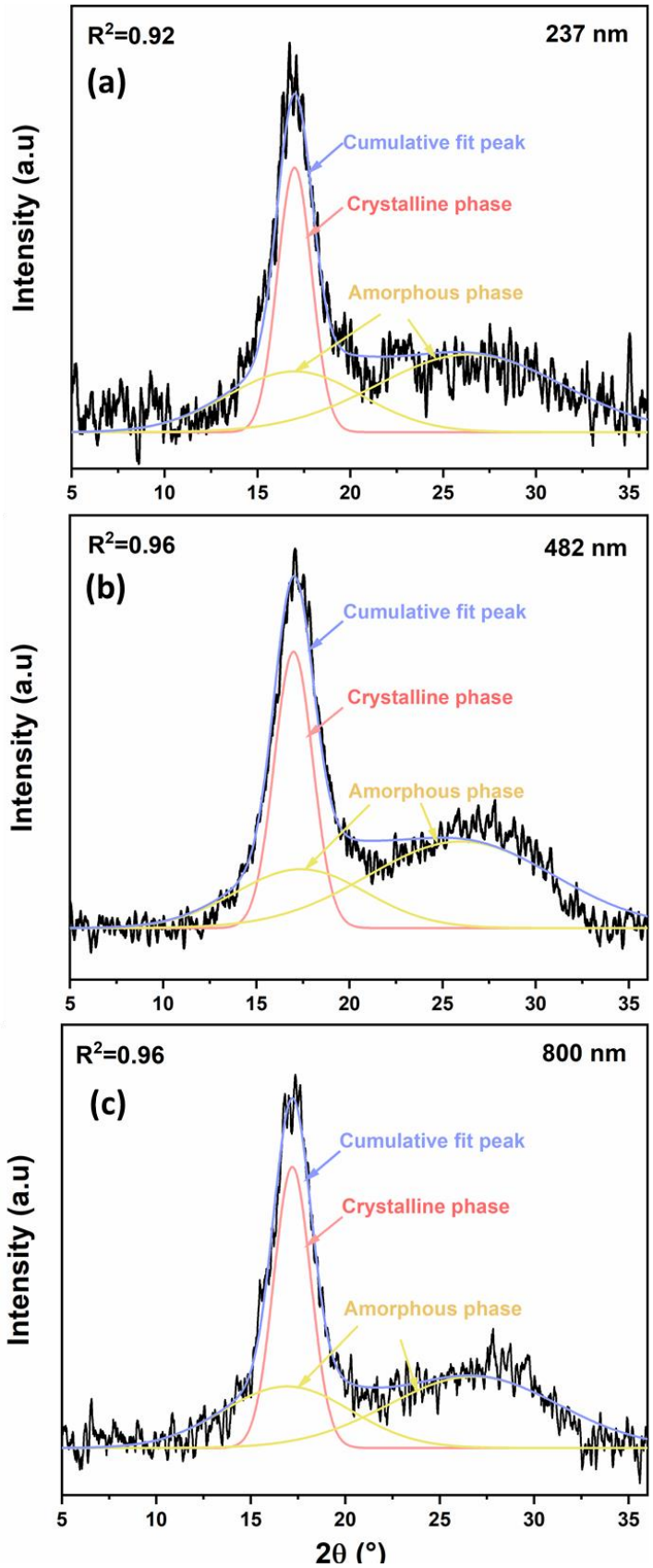

Figure 3.5 Deconvolution of WAXD spectra of PAN nanofiber mats (a) 237 nm, (b) 482 nm, (c) 800 nm

Figure 3.5 and *Table 3.1* show a crystallinity degree that decreases slightly when the average diameter of nanofiber mats decreases. An intuitive explanation of this behavior would be related to the electrospinning process during which the rapid solidification of polymer jet solution may have hindered the formation of crystals. Therefore, when the diameter of nanofibers decreases the impact of this rapid solidification is expected to be higher, considering the fact that thinner nanofibers, in our case, are electrospun from polymer solution less concentrated in PAN.

As mentioned in *section 3.1.1* , previous investigations conducted on PAN nanofiber mats by Papkov et al [3] [21] revealed a decrease of the crystallinity degree when decreasing nanofibers diameters. Combined with a simultaneous improvement of toughness and modulus, this behavior was attributed to a high molecular orientation along the fiber axis induced by the high elongation of polymer jet during electrospinning. The high orientation is expected to contribute to the increase of the modulus and the low crystallinity to the increase of the toughness. In the same context, Gu et al [22] investigated the molecular orientation of macroscopically aligned PAN nanofibers with an average diameter range of 130 to 280 nm. Contrarily to cast film, the 2D X-ray diffraction pattern of electrospun nanofibers illustrated arcs indicating preferred crystal orientation. Different observations were earlier noted by Fennessey et al [23] in their investigation of PAN nanofibers electrospun using a stationary and a rotating collector. They stated that in the first case, no sign of orientation was illustrated in the 2D WAXD pattern. However, when increasing the rotating speed of the collector higher crystallinity and molecular orientation were stated by the appearance of pronounced arcs on the WAXD pattern and the increase of an orientation factor along with the decrease of nanofibers diameters. They considered that molecular orientation was mostly triggered by mechanical forces resulting from the rotation of the collector, and that polymer chains may have been oriented during electrospinning on a stationary collector but lost this orientation due to their relaxation after electrospinning.

Based on the previous mechanical properties of PAN nanofibers within the same range of nanofibers diameters as ours, the hypothesis adopted in our study is that the slight decrease of crystallinity along with the decrease of nanofibers diameters is related to the molecular orientation of polymer chains within nanofibers, even though it could have been partially relaxed after electrospinning. Further investigations were conducted by FTIR spectroscopy and will be presented in the following part.

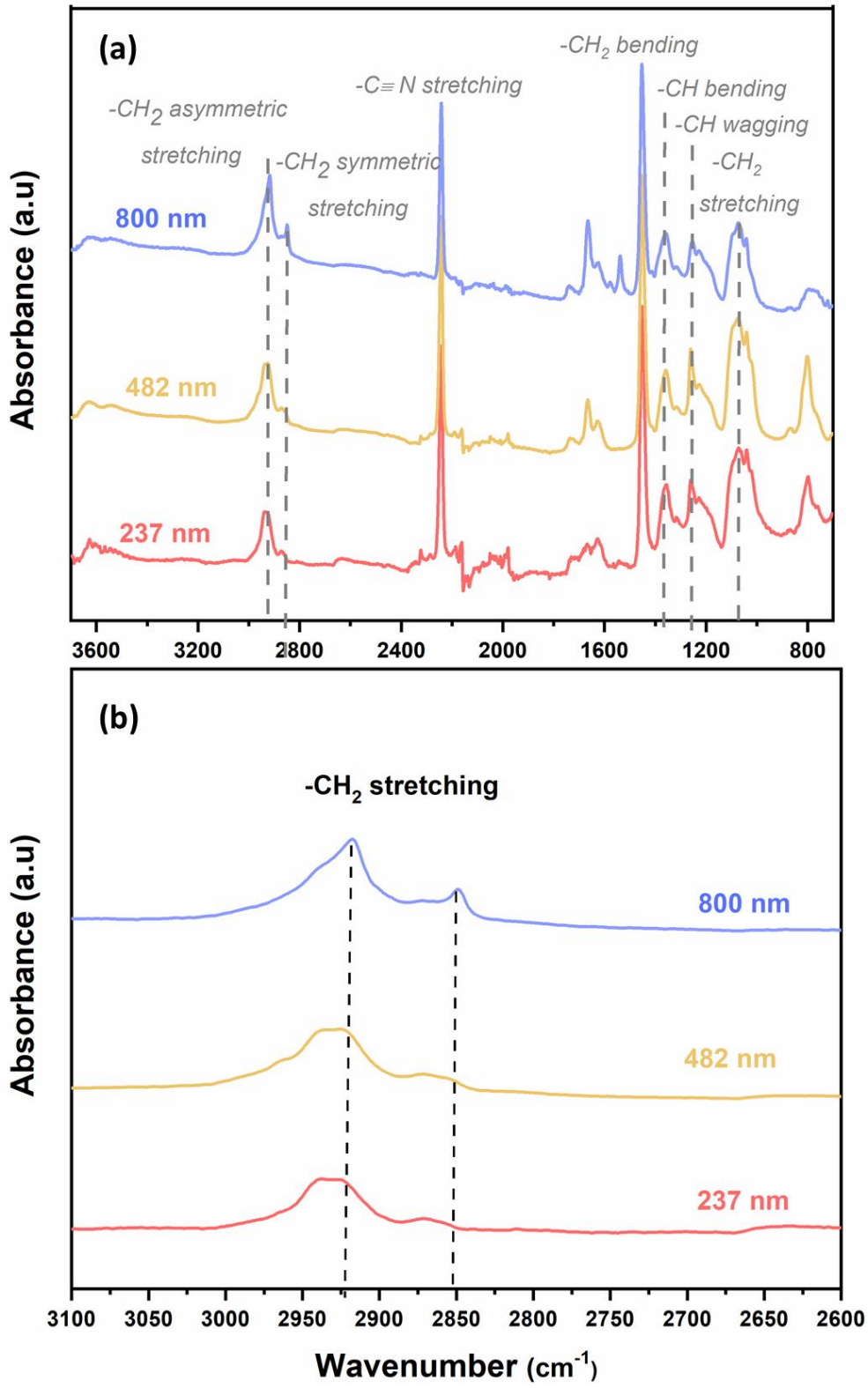

Figure 3.6 FTIR spectra of PAN electrospun nanofibers with average nanofiber diameter of 237, 482 and 800 nm (a) spectra with a wavenumber range of 800-3800 cm^{-1} (b)Spectra from 2200-3200 cm^{-1} to illustrate the evolution of (-CH2) functional group

Figure3.6.a illustrates the absorbance peaks and their corresponding functional groups of PAN electrospun nanofibers. The three nanofiber mats revealed two main peaks at 2242 cm^{-1} and 1454 cm^{-1} that were attributed in literature to the stretching of nitrile group and the bending of the methylene group respectively. It showed, also, peaks at 2930 $cm^{-1}$and 2870 cm^{-1} that were related to CH_2 stretching. At lower wavenumbers, the absorbance peak at 1360 cm^{-1} was related to -CH bending, the peak at 1260 cm^{-1} to -CH wagging and the peak at 1075 cm^{-1} was designated as -CH_2 stretching [24] [25]. Moreover, the presence of absorbance peaks in the wavenumber range of 1600-1745 cm^{-1} can be noticed for all the tested samples. These peaks are generally reported in literature to correspond to -C=O, C=C, N-H functional groups, which appearance is usually related either to the presence of additives or comonomers such as vinyl acetate (VA) and methyl methacrylate (MAA) [24] [26] [27], or during the first stages of thermal treatment of polyacrylonitrile in order to obtain carbon fibers [28] [29]. Considering that none of these conditions were present in our case, we suggest that these peaks may result either from a residual solvent (peak at 1600 cm^{-1}) or a probable chemical aging that took place during the storage of PAN nanofiber mats.

According to *Figure 3.6.b* the intensity of the absorbance peaks corresponding to -CH_2 at 2930 cm^{-1} and 2870 cm^{-1} decreases slightly with the decrease of nanofibers diameters. These functional groups were considered in previous studies to have transition dipole moment perpendicular to the polymer chain axis [25]. This might be considered as a signature of a conformational change of the polymer chain to be more oriented along the fiber axis. Furthermore, in an attempt to quantify this signature, we chose to estimate and compare the ratio ($I_{1260}/_{1450}$)of the intensity related to the peak at 1260 cm^{-1} *(I_{1260})* attributed to -CH wagging with a dipole moment parallel to the chain axis, by the intensity of the absorbance peak at 1450cm^{-1} *(I_{1450})* attributed to -CH_2. The value of ($I_{1260}/_{1450}$) was found to increase from 0.41 for the thickest nanofiber to 0.44 for the thinnest nanofiber, which goes along with the suggestion of the orientation according to the fiber axis.

Similar outcome has been stated for individual PAN nanofibers with diameters ranging from 300-500 nm investigated by polarized atomic force microscopy-infrared technique (AFM-IR), in which the dichroic ratio was obtained from the directional absorbance parallel and perpendicular for specific absorbance peaks; 1450 cm^{-1} related to -CH_2 bending and1264 cm^{-1} related to -CH wagging. For instance, the dichroic ratio of the perpendicular band at 1450 cm^{-1} was noticed to decrease when decreasing nanofibers diameters indicating a higher degree of

parallel orientation of the polyacrylonitrile backbone [30]. These results were considered to be consistent with a previous study conducted by Papkov et al [31] that used Raman spectroscopy and in which the orientation of polymer chains in the direction of the nanofiber axis was associated with the high strain experienced by the polymer jet during electrospinning.

As previously stated, we can conclude that PAN nanofibers in our case may have undergone a mild chemical degradation but still have a potential residual orientation. In the following part, we will investigate another aspect of these nanofibers which is related to their thermal behavior.

3.2 Thermal analysis

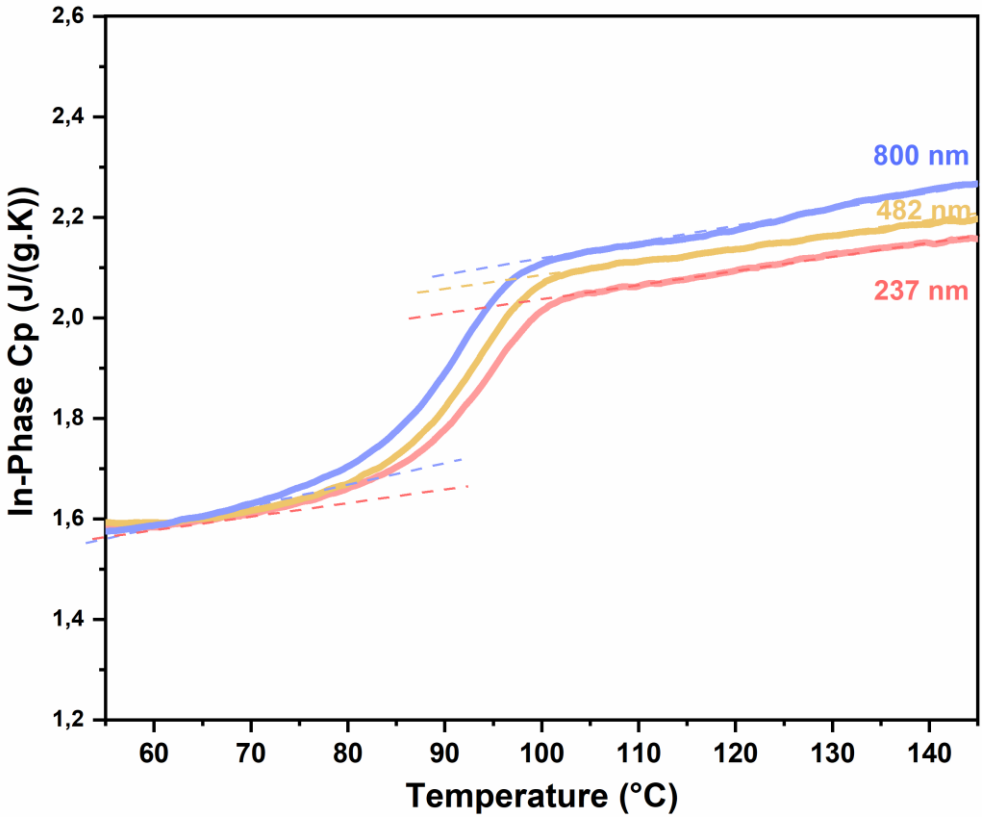

Figure 3.7 In-Phase heat capacity recorded at 1 K.min-1 with an amplitude of ±2.5 K and a period of 100s for PAN nanofiber mats with different diameters (dashed lines are put to show the baselines of glass heat capacity $C_{p,\,g}$ and liquid heat capacity $C_{p,\,L}$

Table 3.2 Characteristics of glass transition of PAN electrospun nanofibers obtained by MT-DSC

Nanofiber mat diameters (nm)	T_g (°C)	ΔC_p (J/(g.K))
237	93 ± 0.5	0.35 ± 0.01
482	91 ± 0.5	0.38 ± 0.01
800	90 ± 0.5	0.36 ± 0.01

Figure 3.7 illustrates the results of MT-DSC experiments conducted on the PAN nanofiber mats. And values of the obtained glass transition temperature (T_g) estimated at the mid-point of the heat capacity step as well as the corresponding heat capacity are stated in *Table 3.2*. Taking into consideration the uncertainties related to the estimation of these values, a slight increase of T_g is noticed when decreasing nanofibers diameters.

As mentioned in the first part of this chapter, this increase has been stated previously by Araujo et al [4] in their study of PAN nanofiber mats combining MT-DSC and DRS techniques. They revealed that by reducing nanofibers diameters, the glass transition gets wider and its mid-point evolves towards higher temperatures (an increase of 10°C) indicating a constrained amorphous phase. Moreover, DRS allowed the determination of the dielectric signature of the glass transition and indicated a slowdown of the relaxation dynamics of the amorphous phase for thinner nanofibers crossing the glass transition. This result was accounted for a higher polymer chain orientation. It is worth mentioning that the shift of the glass transition in the present work is less spectacular. This could be the consequence of a gradual loss of the orientation during the prolongated storage, which would be consistent with the signature of chemical structure evolution recorded in the infrared spectra *(Figure 3.6).*

Moreover, the slight increase in glass transition temperature revealed by MT-DSC, combined with the slight decrease in crystallinity obtained from WAXD experiments *(Table 3.1)* as the diameter of PAN nanofibers decreases, may be associated with a constrained amorphous phase through the effect of molecular orientation due to the extensional forces applied during electrospinning.

Further investigations were carried out on PAN nanofiber mats using Fast Scanning Calorimetry in order to determine their melting behavior. Indeed, it is known that polyacrylonitrile presents a high melting point whose investigation is highly challenging, due

to the fact that PAN undergoes degradation prior to melting or in the same range of temperature [32]. The origin of this degradation was accorded, in literature, to a crosslinking reaction within the polymer structure that takes place during heating. As a matter of fact, polyacrylonitrile can experience a structural modification involving the formation of aromatic cycles designated as a ladder structure that is thermally stable and therefore prevents melting [1] [33] [34].

Many researches have been realized in an attempt to determine the melting temperature of PAN. For instance, Frushour et al [35] studied the melting behavior of polyacrylonitrile by incorporating copolymers which led to a depression of PAN melting temperature and enthalpy. They developed a model according to which melting temperature was estimated as a function of copolymer composition and the amount of temperature depression. Bajaj et al [36] [37] have also attempted to estimate PAN melting temperature using water as a plasticizer, though the resulting temperature (170~180°C) seemed lower than the expected one. They have tried heating at relatively high rates at 160°C/min but it was reported that the recorded melting peak includes an overlapping of both an exothermic and an endothermic reaction. In this context our attempt to determine this temperature is presented in the following part.

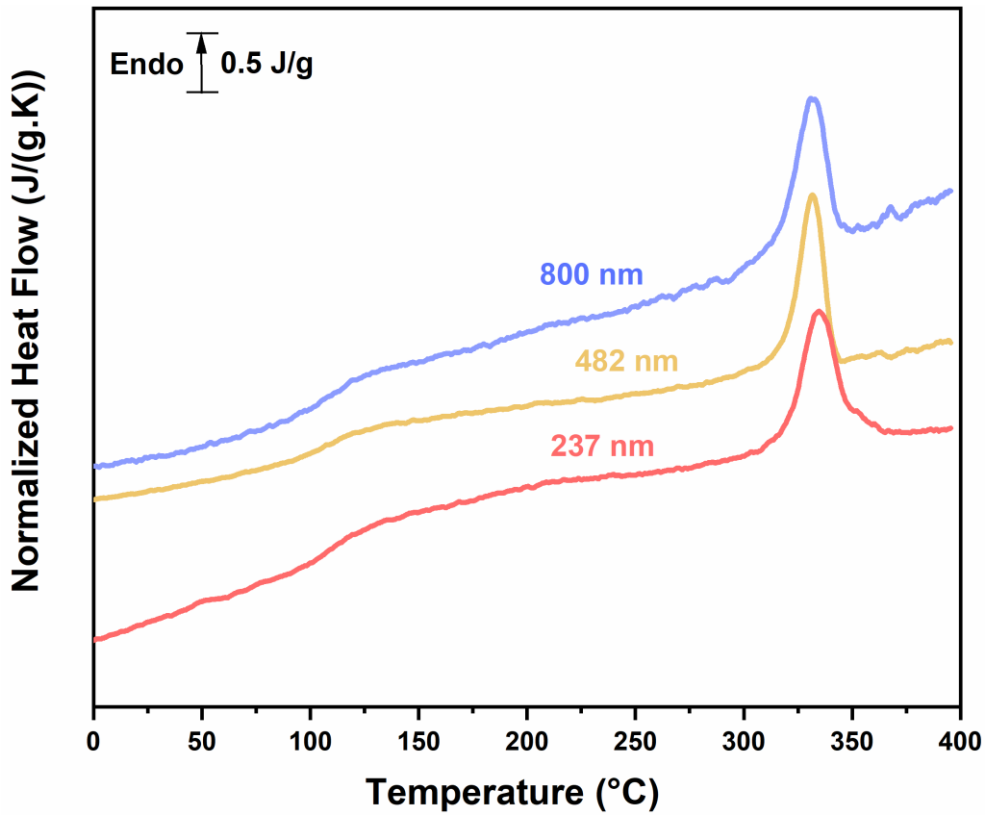

Figure 3.8 Heat flow recorded for PAN nanofiber mats obtained by FSC at 180 000 K/min normalized by the mass of each sample

Table 3.3 Glass transition, melting temperature and enthalpy of melting of PAN nanofibers mat obtained by FSC

Nanofiber mat diameters (nm)	T_g (°C)	T_m (°C)	ΔH_m (J/(g.K))
237	107 ± 1	333 ± 1	24
482	103 ± 1	331 ± 1	25
800	102 ± 1	332 ± 1	27

Figure 3.8 illustrates the heating scans of the nanofiber mats, showing a step-like signal corresponding to the glass transition, and a single endothermic peak around 332°C (depending on the fibers diameters) and no sign of an exothermic reaction. This may be explained by the very high heating rate 180 000 K/min allowing to avoid cold crystallization and cyclization of the molecular chain conformation that usually leads to the degradation of the samples. Similar results were obtained recently by Furushima et al [38] on polyacrylonitrile powder. In their work, they investigated the thermal behavior of PAN by heating at different scanning rates varying from 10 K/min till 200 K/min. The latter heating rate allowed the observation of an endothermic peak along with an exothermic one prior to melting. Further experiments were realized by FSC and heating at 120 000 K/min allowed the observation of a neat melting peak and values of melting temperature were around 350°C.

According to *Table 3.3*, the glass transition temperature presents the same trend as that obtained by MT-DSC, namely a slight increase as the nanofiber diameter decreases. The melting temperature is mainly the same regardless of the nanofiber size. The value of the enthalpy of melting was also estimated by integrating the area under the melting peaks and it was found to decrease with decreasing nanofibers diameters, which is consistent with the results obtained by WAXD. Therefore, we can assume that these results are consistent with the previous conclusion that they are related to the signature of a higher molecular orientation.

As mentioned above and in the second chapter, the Fast Scanning Calorimeter is used to investigate nano-sized samples with a high scanning rate. This induces a delay of the heat transfer between the heater and the sample which leads to a shift of the characteristic temperatures in a way that the measured thermal event appears to occur at higher temperatures. In this work, the values of characteristic temperatures were corrected after calculation of thermal lag according to the method explained in chapter 2 *(Table 3.4)*.

Table 3.4 Glass transition temperature and melting temperature after thermal lag correction

Nanofiber mat diameters (nm)	T_g (°C)	T_m (°C)
237	97 ± 1	323 ± 1
482	94 ± 1	322 ± 1
800	93 ± 1	323 ± 1

3.3 Study of structural relaxation of PAN nanofiber mats

Understanding the physical aging of glassy polymers and the evolution of their thermodynamic properties is generally crucial to gain knowledge about the evolution of their performances over the time, such as their mechanical or barrier properties.

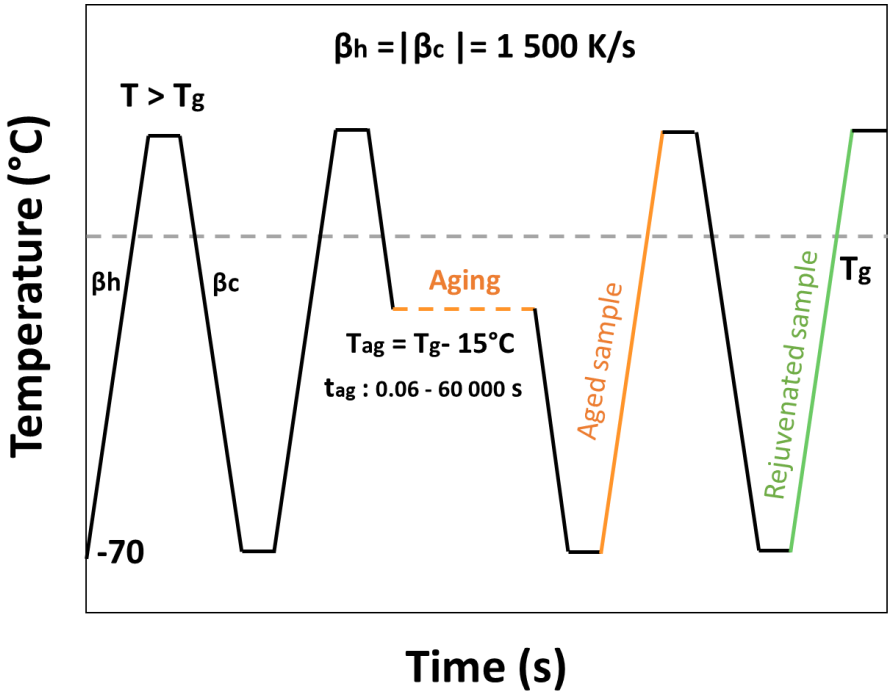

Figure 3.9 Schematic illustration of the aging protocol applied on PAN nanofiber mats

In this work, the physical aging of PAN nanofiber mats is investigated as a mean to monitor the evolution of the molecular mobility within nanofibers. The kinetics of structural relaxation are studied by aging three different PAN nanofiber mats as well as their bulk counterpart,15°C below their respective glass transition temperatures that were determined upon cooling (T_{ag} = $T_{g,\,cool}$ -15°C). The protocol associated to these experiments is illustrated in *Figure 3.9*. First, a heating up to 40°C above T_g, and a subsequent cooling ramp till -70°C were applied to remove any residual tension within nanofibers and determine glass transition temperature from cooling. A subsequent heating-cooling ramp was applied, this time, till 15°C below $T_{g,\,cool}$. This temperature was maintained for different aging durations t_{ag} = 0.001- 1000 min. Afterwards, two heating-cooling ramps were realized in order to record the response of the aged and rejuvenated system. Then, samples were heated until reaching the melting temperature and the same aging process was repeated for the bulk obtained from molten nanofiber mats. The whole process was realized with the same heating (β_h) and cooling rates (β_c), that is ± 1500 K/s.

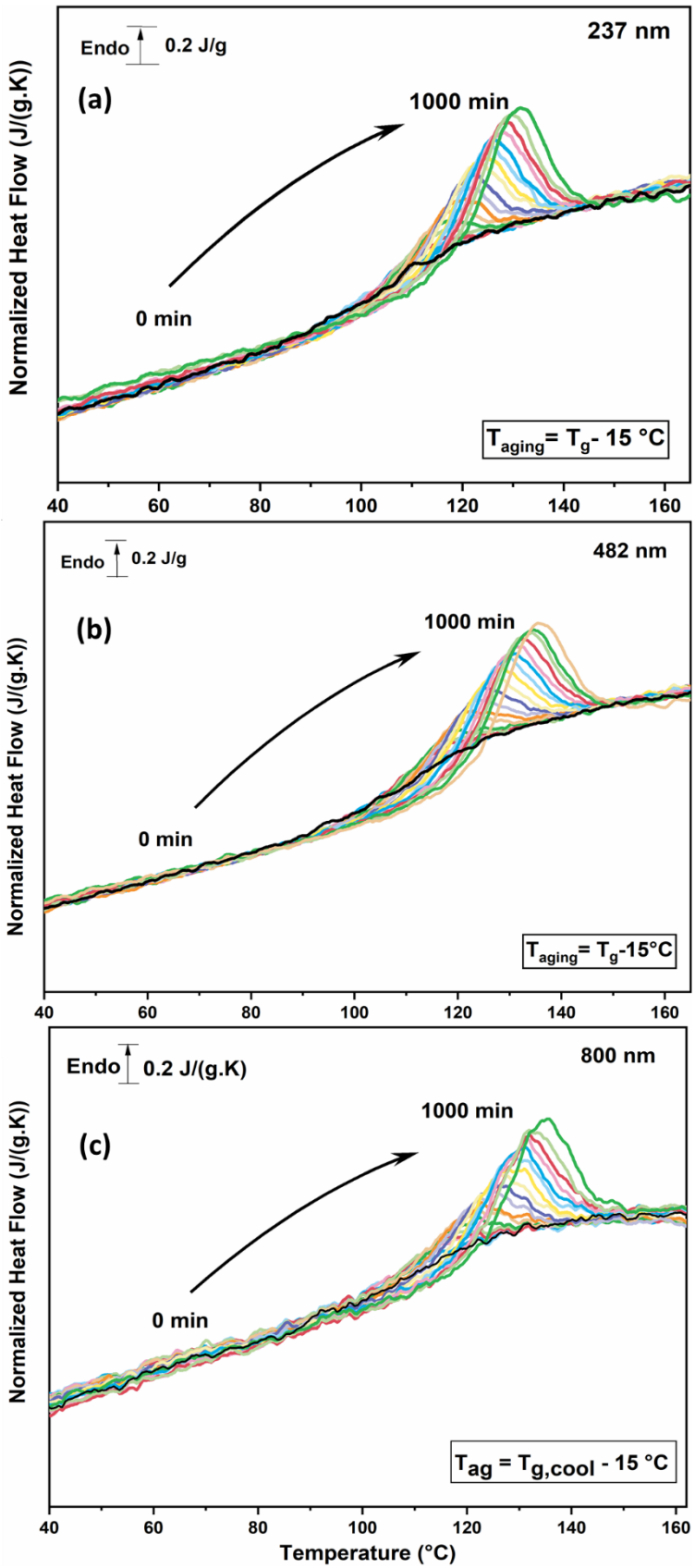

Figure 3.10 Heat flow recorded after aging of PAN nanofiber mats obtained by FSC at the same heating and cooling rate ±1500 K/s for different average nanofiber diameters (a) 237 nm (b) 482 nm (c) 800 nm

The normalized heat flow curves recorded upon physical aging for the different tested samples, are shown in *Figure 3.10* and reveals a sequence of endothermic peaks superimposed on the glass transition. It can be noticed that the enthalpy recovery increases with increasing aging time and its peak shifts towards higher temperatures. The same phenomenon has been classically reported in the literature, when studying the physical aging of several materials in the glassy state [8] [39].

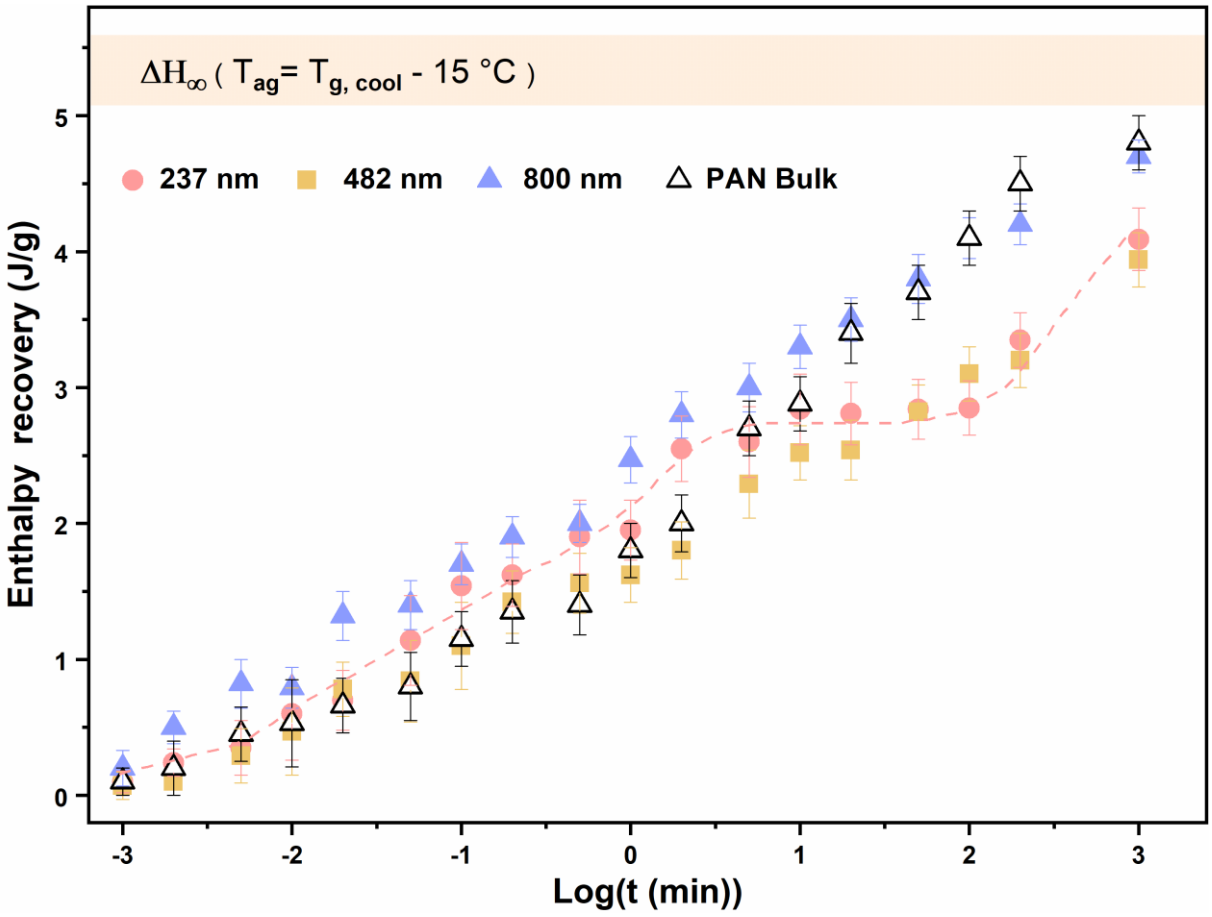

Figure 3.11 Enthalpy recovery as a function of aging times of PAN nanofibers with the average diameters 237nm (orange circles) 482 nm (yellow squares) 800 nm (blue triangles) bulk PAN (empty triangles), the pink dashed line is to guide the eye

Figure 3.11 illustrates the enthalpy recovery associated to the aged samples that was estimated by integrating the difference between heat capacities of the aged and the rejuvenated sample. Besides, the expected total enthalpy loss (ΔH_∞) was determined depending on the heat capacity step at the glass transition, the glass transition temperature, and the aging temperature, as explained in *section 3.1.2*. The estimated ΔH_∞ corresponding to the investigated samples was found to vary between 5.2 J/g and 5.7 J/g depending on the nanofiber diameter value.

It can be noticed that for short aging times, all the samples present nearly the same recovery kinetics. However, for longer aging times the kinetics are considerably different. This can be seen in the behavior of the thinnest nanofiber where the aging kinetics present a delay compared to the thickest nanofiber and the bulk, expressed by a plateau-like phenomenon mainly after 5 minutes of aging. On the other hand, the nanofiber mat with an average diameter of 800 nm showed one step aging kinetic with no clearly visible intermediate plateau. It is noteworthy that the behavior of the thickest nanofibers is more likely to resemble to the response of the bulk sample. Similar behavior to that of thin nanofibers was reported by Cangialosi et al [40] in their study of physical aging of Polystyrene (PS). Upon aging at temperatures close to the glass transition, two-step aging kinetics have been noted and explained as following; a first decay of the enthalpy recovery of secondary relaxation due to localized molecular mobility and a second decay related to the relaxation of the main polymer chain. Therefore, our hypothesis of explanation is that, this delay of aging kinetics within nanofibers when reducing their diameter is either related to a geometric confinement effect due to the nano-sized structure or to a restrained molecular mobility induced by the orientation of polymer chains during electrospinning.

The physical aging of confined structures has been widely investigated in literature and remains subject to controversy and dependent on the form of confined structure, whether it is free-standing or supported films, nanoparticles or nanocomposites [41] [42]. For instance, the study of physical aging of poly (methyl methacrylate) PMMA/silica and PS/silica nanocomposites revealed accelerated aging kinetics for both structures compared to their bulk counterparts. Meanwhile, the dynamics of segmental mobility probed by DRS showed no difference between the bulk PMMA, PS-based nanocomposites and bulk along with a decrease in the calorimetric glass transition temperature. This was explained by the free volume holes model described as a diffusion of free volume within a glassy out-of-equilibrium material due to its spontaneous densification towards its surface [43].

More recently, Perez-De-Eulate et al [44] studied the structural recovery of 3D confined structures; polystyrene nanospheres with diameters varying from 230 nm to 500 nm, using fast scanning calorimetry. The physical aging results revealed two aging mechanisms of equilibrium recovery similar to those mentioned in the previous paragraph. Faster aging kinetics for nanospheres compared to bulk PS and the increase of these kinetics when reducing nanospheres diameter were also found and attributed to a geometric confinement effect. Different observations were noted by Monnier et al [45] when investigating the physical aging kinetics of co-extruded

multilayer of amorphous polylactide (PLA) and polystyrene (PS), by means of FSC, and reported a decrease of the aging rate of constrained PLA within multilayer film in comparison with the amorphous bulk. This result was attributed to the presence of capped interfaces in multilayer systems, and partially to the fabrication process during which the samples underwent high elongation and shear rates.

Based on the previously reported studies and according to our results, we may conclude that the slowing down of aging kinetics with the reduction of nanofibers diameters cannot be explained a geometrical confinement effect but rather by a restrained molecular mobility that may be caused by a molecular orientation due to high elongational deformation during electrospinning.

3.4 Conclusion

In this chapter; electrospun polyacrylonitrile nanofibers with average diameters of 237nm, 482nm and 800nm were studied. WAXD results revealed a low crystallinity that decreased slightly with decreasing nanofibers diameters which can be intuitively explained by electrospinning process since it involves rapid solidification that hinders the crystallization.

Further investigations via FTIR spectroscopy allowed the estimation of specific infrared bands ratio leading to the hypothesis of a better orientation toward the fiber axis direction for thinner nanofibers. It showed also, the signature of a probable mild chemical degradation of PAN structure because of the storage. On the other hand, MT-DSC results illustrated a slight increase of the glass transition temperature determined at the mid-point of the heat capacity step. Combined with the decrease of the crystallinity and the probable preferential orientation along the fiber axis, this result was attributed to a restrained molecular mobility within the amorphous phase. Therefore, it was convenient to investigate the polymer chain mobility in the amorphous phase by the investigation of the physical aging of PAN nanofibers. These studies were conducted at aging temperature relatively close to the glass transition and for different aging times that resulted in two main findings. The first related to a double relaxation mechanism and the second to the slower aging kinetics both apparent in the thinner nanofibers contrarily to thicker nanofibers and bulk PAN which was justified in our case by a restrained mobility induced by the macromolecular orientation of polymer chains during electrospinning.

It is worth noting that studying PAN nanofibers using fat scanning calorimetry allowed the determination of their melting temperature, an information that is hardly accessible by conventional thermal analysis techniques since PAN undergoes degradation prior to its melting.

Overall, we believe that the different behavior of the thinnest nanofibers can be driven by a residual molecular orientation of polymer chain despite the probability of a partial relaxation of this orientation during storage.

3.5 References

[1] M. S. A. Rahaman, A. F. Ismail, and A. Mustafa, "A review of heat treatment on polyacrylonitrile fiber," *Polym. Degrad. Stab.*, vol. 92, no. 8, pp. 1421–1432, Aug. 2007, doi: 10.1016/j.polymdegradstab.2007.03.023.

[2] S. N. Arshad, M. Naraghi, and I. Chasiotis, "Strong carbon nanofibers from electrospun polyacrylonitrile," *Carbon*, vol. 49, no. 5, pp. 1710–1719, Apr. 2011, doi: 10.1016/j.carbon.2010.12.056.

[3] D. Papkov, Y. Zou, M. N. Andalib, A. Goponenko, S. Z. D. Cheng, and Y. A. Dzenis, "Simultaneously Strong and Tough Ultrafine Continuous Nanofibers," *ACS Nano*, vol. 7, no. 4, pp. 3324–3331, Apr. 2013, doi: 10.1021/nn400028p.

[4] S. Araujo, N. Delpouve, L. Delbreilh, D. Papkov, Y. Dzenis, and E. Dargent, "Dielectric and calorimetric signatures of chain orientation in strong and tough ultrafine electrospun polyacrylonitrile," *Polymer*, vol. 178, p. 121638, Sep. 2019, doi: 10.1016/j.polymer.2019.121638.

[5] J. M. Hutchinson, "Physical aging of polymers," *Prog. Polym. Sci.*, vol. 20, pp. 703–759, 1995.

[6] C. A. Angell, "Formation of Glasses from Liquids and Biopolymers," *Science*, vol. 267, no. 5206, pp. 1924–1935, Mar. 1995, doi: 10.1126/science.267.5206.1924.

[7] C. Fosse, "Compréhension du rôle de la fraction amorphe rigide dans les polyesters," Physique, Université de Rouen Normandie, 2020.

[8] D. Cangialosi, V. M. Boucher, A. Alegría, and J. Colmenero, "Physical aging in polymers and polymer nanocomposites: recent results and open questions," *Soft Matter*, vol. 9, no. 36, p. 8619, 2013, doi: 10.1039/c3sm51077h.

[9] B. Quelennec, "Investigation des dynamiques relaxationnelles dans des systèmes époxy pour apporter une meilleure compréhension des effets de vieillissement physiques et chimiques dans le cadre d'application structurale," Université de Rouen Normandie, 2022.

[10] I. M. Hodge, "Enthalpy relaxation and recovery in amorphous materials," *J. Non-Cryst. Solids*, vol. 169, no. 3, pp. 211–266, Apr. 1994, doi: 10.1016/0022-3093(94)90321-2.

[11] A. Q. Tool and C. G. Eicitlin, "Variations caused in the heating curves of glass by heat treatment," *J. Am. Ceram. Soc.*, vol. 14, no. 4, pp. 276–308, Apr. 1931, doi: 10.1111/j.1151-2916.1931.tb16602.x.

[12] C. T. Moynihan *et al.*, "Structural relaxation in vitreous materials," *Ann. N. Y. Acad. Sci.*, vol. 279, no. 1 The Glass Tra, pp. 15–35, Oct. 1976, doi: 10.1111/j.1749-6632.1976.tb39688.x.

[13] R. Chiang, "Crystallization and melting behavior of polyacrylonitrile," *J. Polym. Sci. A*, vol. 1, no. 9, pp. 2765–2775, Sep. 1963, doi: 10.1002/pol.1963.100010902.

[14] S. Dalton, F. Heatley, and P. M. Budd, "Thermal stabilization of polyacrylonitrile fibres," *Polymer*, vol. 40, no. 20, pp. 5531–5543, Sep. 1999, doi: 10.1016/S0032-3861(98)00778-2.

[15] B. G. Colvin and P. Storr, "The crystal structure of polyacrylonitrile," *Eur. Polym. J.*, vol. 10, no. 4, pp. 337–340, Apr. 1974, doi: 10.1016/0014-3057(74)90147-5.

[16] A. T. Kalashnik, T. N. Smirnova, O. P. Chernova, and V. V. Kozlov, "Properties and structure of polyacrylonitrile fibers," *Polym. Sci. Ser. A*, vol. 52, no. 11, pp. 1233–1238, Nov. 2010, doi: 10.1134/S0965545X10110180.

[17] Z. Bashir, "Co-crystallization of solvents with polymers: The x-ray diffraction behavior of solvent-containing and solvent-free polyacrylonitrile," *J. Polym. Sci. Part B Polym. Phys.*, vol. 32, no. 6, pp. 1115–1128, Apr. 1994, doi: 10.1002/polb.1994.090320616.

[18] I. Karacan and G. Erdoğan, "The role of thermal stabilization on the structure and mechanical properties of polyacrylonitrile precursor fibers," *Fibers Polym.*, vol. 13, no. 7, pp. 855–863, Sep. 2012, doi: 10.1007/s12221-012-0855-8.

[19] G. Hinrichsen, "On the Origin of Order-Disorder in Drawn Polyacrylonitrile," *J. Appl. Polym. Sci.*, vol. 17, pp. 3305–3321, 1973, doi: 10.1002/app.1973.070171106.

[20] V. Causin, C. Marega, S. Schiavone, and A. Marigo, "Employing glass refractive index measurement (GRIM) in fiber analysis: a simple method for evaluating the crystallinity of acrylics," *Forensic Sci. Int.*, vol. 149, no. 2–3, pp. 193–200, May 2005, doi: 10.1016/j.forsciint.2004.06.015.

[21] D. Papkov *et al.*, "Quantifying Polymer Chain Orientation in Strong and Tough Nanofibers with Low Crystallinity: Toward Next Generation Nanostructured Superfibers," *ACS Nano*, vol. 13, no. 5, pp. 4893–4927, May 2019, doi: 10.1021/acsnano.8b08725.

[22] S. Y. Gu, J. Ren, and Q. L. Wu, "Preparation and structures of electrospun PAN nanofibers as a precursor of carbon nanofibers," *Synth. Met.*, vol. 155, no. 1, pp. 157–161, Oct. 2005, doi: 10.1016/j.synthmet.2005.07.340.

[23] S. F. Fennessey and R. J. Farris, "Fabrication of aligned and molecularly oriented electrospun polyacrylonitrile nanofibers and the mechanical behavior of their twisted yarns," *Polymer*, vol. 45, no. 12, pp. 4217–4225, May 2004, doi: 10.1016/j.polymer.2004.04.001.

[24] H. Kakida and K. Tashiro, "Mechanism and Kinetics of Stabilization Reactions of Polyacrylonitrile and Related Copolymers IV. Effects of Atmosphere on Isothermal DSC Thermograms and FT-IR Spectral Changes during Stabilization Reaction of Acrylonitrile/Methacrylic Acid Copolymer," *Polym. J.*, vol. 30, no. 6, pp. 463–469, Jun. 1998, doi: 10.1295/polymj.30.463.

[25] I. Karacan and G. Erdogan, "The influence of thermal stabilization stage on the molecular structure of polyacrylonitrile fibers prior to the carbonization stage," *Fibers Polym.*, vol. 13, no. 3, pp. 295–302, Mar. 2012, doi: 10.1007/s12221-012-0295-5.

[26] V. Causin, C. Marega, S. Schiavone, and A. Marigo, "A quantitative differentiation method for acrylic fibers by infrared spectroscopy," *Forensic Sci. Int.*, vol. 151, no. 2–3, pp. 125–131, Jul. 2005, doi: 10.1016/j.forsciint.2005.02.004.

[27] P. Bajaj, T. V. Sreekumar, and K. Sen, "Structure development during dry-jet-wet spinning of acrylonitrile/vinyl acids and acrylonitrile/methyl acrylate copolymers," *J. Appl. Polym. Sci.*, vol. 86, no. 3, pp. 773–787, Oct. 2002, doi: 10.1002/app.10973.

[28] Z. Wangxi, L. Jie, and W. Gang, "Evolution of structure and properties of PAN precursors during their conversion to carbon fibers," *Carbon*, vol. 41, no. 14, pp. 2805–2812, 2003, doi: 10.1016/S0008-6223(03)00391-9.

[29] Y. Zou *et al.*, "Influence of pre-oxidation on mechanical properties of single electrospun polyacrylonitrile nanofiber," *Mater. Today Commun.*, vol. 26, p. 102069, Mar. 2021, doi: 10.1016/j.mtcomm.2021.102069.

[30] Z. Wang, B. Sun, X. Lu, C. Wang, and Z. Su, "Molecular Orientation in Individual Electrospun Nanofibers Studied by Polarized AFM–IR," *Macromolecules*, vol. 52, no. 24, pp. 9639–9645, Dec. 2019, doi: 10.1021/acs.macromol.9b01778.

[31] D. Papkov, C. Pellerin, and Y. A. Dzenis, "Polarized Raman Analysis of Polymer Chain Orientation in Ultrafine Individual Nanofibers with Variable Low Crystallinity," *Macromolecules*, vol. 51, no. 21, pp. 8746–8751, Nov. 2018, doi: 10.1021/acs.macromol.8b01869.

[32] R. B. Mathur, O. P. Bahl, and J. Mittal, "A new approach to thermal stabilisation of PAN fibres," *Carbon*, vol. 30, no. 4, pp. 657–663, 1992, doi: 10.1016/0008-6223(92)90185-Y.

[33] Thomas.J Xue, Michael A. McKinney, and Charles A. Wilkie*, "The thermal degradation of polyacrylonitrile," *Polym. Degrad. Stab.*, vol. 58, pp. 193–202, 1997.

[34] M. Wu, Q. Wang, K. Li, Y. Wu, and H. Liu, "Optimization of stabilization conditions for electrospun polyacrylonitrile nanofibers," *Polym. Degrad. Stab.*, vol. 97, no. 8, pp. 1511–1519, Aug. 2012, doi: 10.1016/j.polymdegradstab.2012.05.001.

[35] BruceG. Frushour, "Melting behavior of polyacrylonitrile copolymers," *Polym. Bull.*, vol. 11, no. 4, 1984, doi: 10.1007/BF00254277.

[36] P. Bajaj, T. V. Sreekumar, and K. Sen, "Thermal behaviour of acrylonitrile copolymers having methacrylic and itaconic acid comonomers," *Polymer*, vol. 42, no. 4, pp. 1707–1718, Feb. 2001, doi: 10.1016/S0032-3861(00)00583-8.

[37] K. Sen, P. Bajaj, and T. V. Sreekumar, "Thermal behavior of drawn acrylic fibers," *J. Polym. Sci. Part B Polym. Phys.*, vol. 41, no. 22, pp. 2949–2958, Nov. 2003, doi: 10.1002/polb.10609.

[38] Y. Furushima, M. Nakada, H. Takahashi, and K. Ishikiriyama, "Study of melting and crystallization behavior of polyacrylonitrile using ultrafast differential scanning calorimetry," *Polymer*, vol. 55, no. 13, pp. 3075–3081, Jun. 2014, doi: 10.1016/j.polymer.2014.05.015.

[39] X. Monnier, A. Saiter, and E. Dargent, "Physical aging in PLA through standard DSC and fast scanning calorimetry investigations," *Thermochim. Acta*, vol. 648, pp. 13–22, Feb. 2017, doi: 10.1016/j.tca.2016.12.006.

[40] D. Cangialosi, V. M. Boucher, A. Alegrıa, and J. Colmenero, "Direct Evidence of Two Equilibration Mechanisms in Glassy Polymers," *Phys. Rev. Lett.*, p. 5, 2013.

[41] C. Zhang, Y. Guo, and R. D. Priestley, "Confined glassy properties of polymer nanoparticles," *J. Polym. Sci. Part B Polym. Phys.*, vol. 51, no. 7, pp. 574–586, Apr. 2013, doi: 10.1002/polb.23268.

[42] J. E. Pye and C. B. Roth, "Two Simultaneous Mechanisms Causing Glass Transition Temperature Reductions in High Molecular Weight Freestanding Polymer Films as Measured by Transmission Ellipsometry," *Phys. Rev. Lett.*, vol. 107, no. 23, p. 235701, Nov. 2011, doi: 10.1103/PhysRevLett.107.235701.

[43] D. Cangialosi, V. M. Boucher, A. Alegría, and J. Colmenero, "Enhanced physical aging of polymer nanocomposites: The key role of the area to volume ratio," *Polymer*, vol. 53, no. 6, pp. 1362–1372, Mar. 2012, doi: 10.1016/j.polymer.2012.01.033.

[44] N. G. Perez-De-Eulate and D. Cangialosi, "Double Mechanism for Structural Recovery of Polystyrene Nanospheres," *Macromolecules*, vol. 51, no. 9, pp. 3299–3307, May 2018, doi: 10.1021/acs.macromol.8b00502.

[45] X. Monnier *et al.*, "Reduced physical aging rates of polylactide in polystyrene/polylactide multilayer films from fast scanning calorimetry," *Polymer*, vol. 150, pp. 1–9, Aug. 2018, doi: 10.1016/j.polymer.2018.07.017.

Chapter 4 Size effect of nanofibers: Impact on polymorphic crystalline structure

Size effect on the polymorphic crystalline structure of PA6 nanofiber mats

Polyamide 6 (PA6), also known as Nylon 6, is amongst the first synthetic polymers to be developed. It was patented in 1938 by I.G. Farbenindustrie in Germany and gained interest because of its important role in the history of polymers, particularly during the second world war when its industrial development was accelerated to be used in military applications [1]. Later on, improvement of the processability of nylon 6 helped broadening the range of its application to include both apparel and industrial fields [2]. For instance, its high elastic recovery and abrasive resistance led to its wide use in garments, carpet fibers and ropes [3]. Moreover, its high tensile strength and impact resistance have brought it to be largely used as a thermoplastic polymer for engineering applications [4] [5] [6].

The growing interest in improving polyamide 6 properties was the incentive to discover the potential of its nanofibrous form, owing to its lightweight and high surface-to-volume ratio among other compelling features. [7] As mentioned in the first chapter, depending on the manufacturing parameters, several polymer nanofibers have shown impressive mechanical properties, and polyamide 6 nanofibers are not an exception to this behavior. It was reported that introducing PA6 nanofiber mats to a fiber glass/epoxy composite material resulted in higher shear stress and minimal formation of delamination cracks between glass fiber layers [8]. Further studies were realized on both mat and single PA6 nanofibers, and revealed interesting mechanical behavior such as a tensile strain of 250% [9]. Electrospun PA6 nanofibers have, also, presented a crystalline structure that differs from its bulk counterpart. Having a polymorphic structure, PA6 has been noted to form different ratios of the two main types of crystals constituting its crystalline structure. The understanding of this behavior, its dependence on electrospinning parameters and its impact on the mechanical properties of nanofibers has been the objective of previous studies [10] [11]. In this chapter, our approach for understanding the behavior of PA6 nanofibers will be presented through a combination of spectroscopic and thermal analysis.

A simple depiction of the microstructure of semi-crystalline polymers can be realized according to a "*two-phase model*", considering the microstructure to be formed by a crystalline phase in which polymer chains form crystal lattice, and an amorphous phase that is defined by the absence of a long-range order [12]. However, it was noted that the decoupling between crystalline and amorphous phases is incomplete due to the continuity of partially crystallized macromolecules through the phase boundary, leading to the formation of an intermediate nanophase. This interphase includes an amorphous portion of macromolecules with a restrained mobility because of the surrounding crystalline portion, and it is referred to as the rigid

amorphous fraction (RAF). Oppositely, the unconstrained part of the amorphous phase is defined as the mobile amorphous fraction (MAF) [13] [14] [15]. Together with the crystalline phase, these amorphous fractions define the "*three-phase model*". The amount of these fractions can be determined as following [15];

$$\boldsymbol{X_c = {\Delta H_f}/{\Delta H_f^\circ}} \quad (1)$$

Where X_C is the degree of crystallinity, ΔH_f is the enthalpy of melting of the studied material and can be determined experimentally and ΔH_f° is the enthalpy of melting of the 100% crystalline material which is, in the case of polyamide 6, equal to 240 J/g [16]. The amount of rigid amorphous fraction X_{RAF} and mobile amorphous fraction X_{MAF} can be determined from the degree of crystallinity X_C and the heat capacity step at glass transition ΔC_p according to the following equations;

$$\boldsymbol{X_{MAF} = {\Delta C_p}/{\Delta C_p^\circ}} \quad (2)$$

Where ΔC_p° is the heat capacity step at glass transition for a 100% amorphous material This value can be found in literature. In the case of polyamide 6, this value was extracted from the ATHAS data base and it is equal to 0.47 J/(g.K). [17]

$$\boldsymbol{X_{RAF} = 1 - X_{MAF}} \quad (3)$$

4.1 Glass transition in polyamide 6 nanofibers

The focus in this section lies on the glass transition, considering its importance to determine the end-use properties of the studied polymer and to understand potential structural modifications in the amorphous phase.

4.1.1 Impact of moisture absorption

As mentioned in Chapter 2, three nanofiber mats were electrospun from 16 wt%, 20 wt% and 28 wt% of polyamide6 in formic acid, resulting an average nanofiber diameter of 60, 133 and 325 nm respectively.

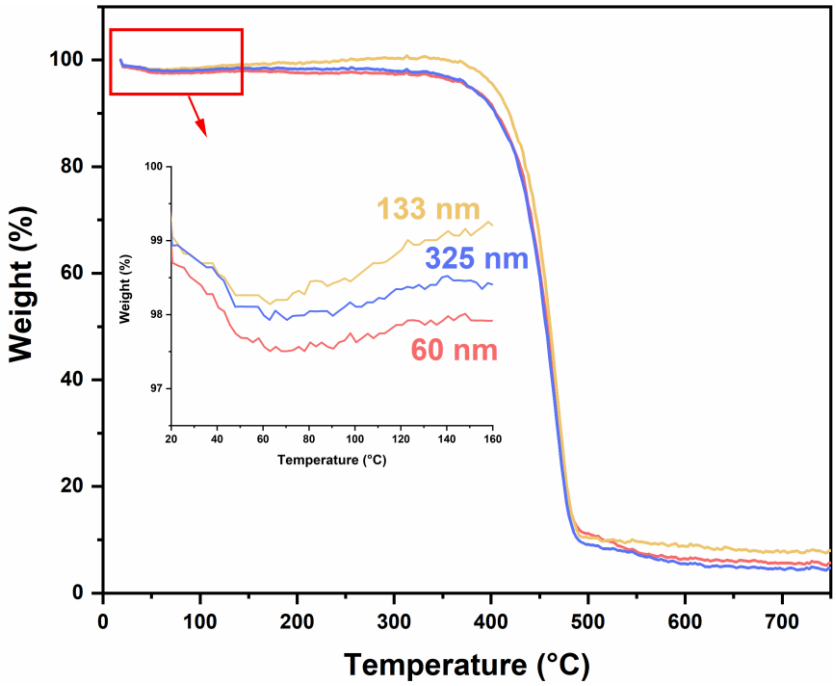

Figure 4.1 Heating scans of PA6 nanofiber mats recorded by TGA at 20 K.min^{-1}

Table 4.1 Degradation temperatures of PA6 nanofiber mats at 10% and 90% of weight loss

Nanofibers diameter (nm)	$T_{10\%}$ (°C)	$T_{90\%}$ (°C)	Maximum temperature of derivative curve (°C)
60	376	441	423
133	381	440	425
325	373	437	421

According to the results of thermogravimetric analysis presented in *Figure 4.1* and *Table 4.1*, all the tested samples display a one-step degradation with minor differences in onset temperature defined, in this work, as the temperature at 10 % of weight loss, and in endset temperature defined, in this work, as the temperature at 90% of weight loss. Additionally, a decrease of sample weight at low temperatures is noted and it may be explained by the presence of residual solvent or moisture within nanofiber mats.

It is noteworthy that the nanofiber mats investigated in this work were electrospun three years prior to the start of our current study, in the Department of Mechanical and Materials Engineering in the University of Nebraska Lincoln, and were tested by temperature modulated

DSC (MT-DSC) in our laboratory. Afterwards, the samples were stored at room humidity and temperature. In the current study, the same samples were investigated by means of MT-DSC before and after being dried in oven under 40°C for 24h and then put in a desiccator under vacuum.

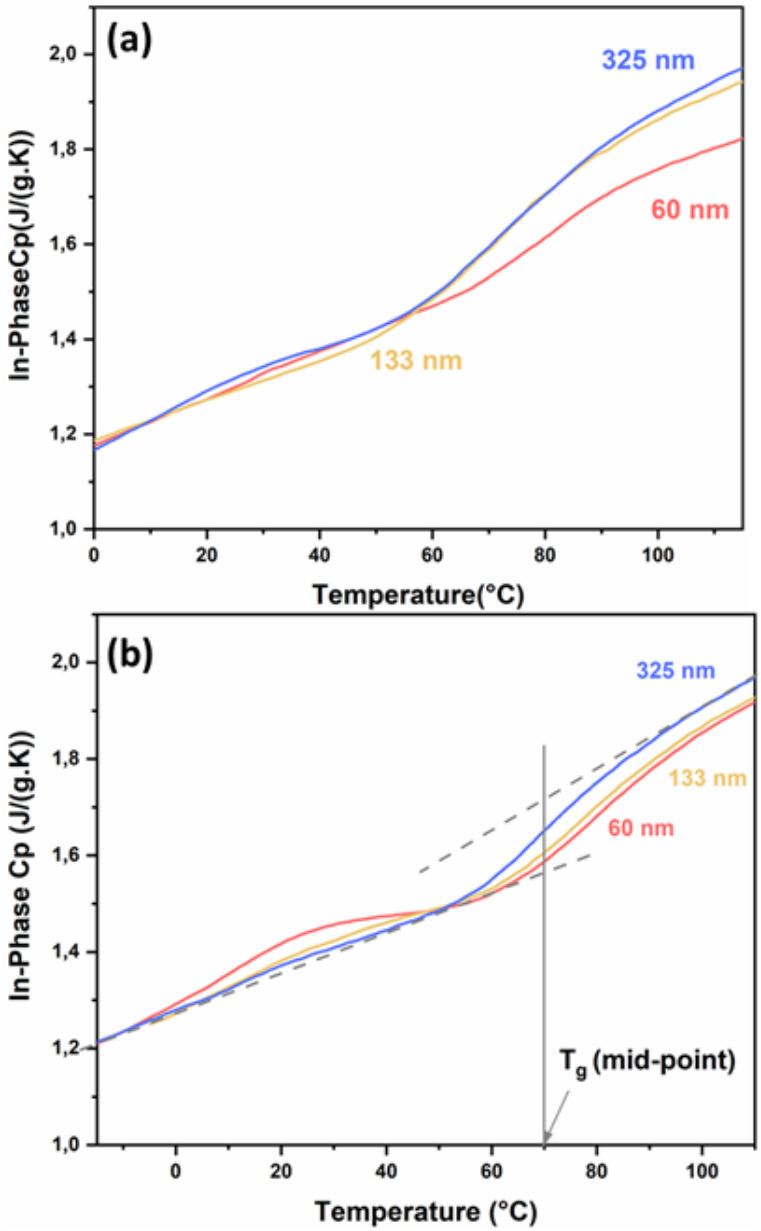

Figure 4.2 Heat capacity recorded by MT-DSC at 1 K.min^{-1} with a modulation amplitude of ±2.5 K and a period of 100 s(a) Results of experiments realized three years earlier to the current study (b) Results of the current study (dashed lines present baselines of the glassy and liquid state)

Table 4.2 Comparison of glass transition temperature estimated by MT-DSC for previous and current results

Nanofibers diameters (nm)	Glass transition temperature (°C)		
	Previous result (3 years ago)	current result	
		Before drying	After drying
60	78	73 ± 1	74 ± 0.5
133	74	70 ± 1	72 ± 0.4
325	74	68 ± 1	71 ± 0.4

Glass transition temperature (Tg) was determined at the mid-point of the heat capacity step for PA6 electrospun samples at different stages of this study as presented in *Figure 4.2* and *Table 4.2*. A remarkable decrease of Tg can be noted after three years of storage at room humidity and temperature, which increased later after drying the samples. An intuitive explanation of this behavior may be related to the absorption of the surrounding humidity that acted as a plasticizer leading to such a decrease in Tg values. This hypothesis is mostly plausible considering the hygroscopic nature of PA6 and its structure that is governed by hydrogen bonds

and polar groups facilitating the interaction with the surrounding environment. Therefore, by simple exposure to humidity, a part of hydrogen bonds may break and reconnects with water molecules. Acting like a plasticizer, these molecules induce an increase of chains mobility leading, in this case, to a decrease in glass transition temperature [18] [19].

Similar trends have been reported earlier while studying the hydration phenomenon and its impact on the mechanical properties of PA6 [20] [21] [22]. For instance, Parodi et al [23] investigated PA6 films placed under different relative humidity percentages 0, 35, 50 and 75 RH%, by means of dynamical mechanical thermal analysis (DMTA). They found that the values of glass transition temperature downshift from 60°C for a dry sample to -20°C for a sample soaked in water. This decrease was considered to be responsible for the decrease of the yield stress noted after tensile tests for the studied samples. The theory of explanation was that the hydration phenomenon led not only to an increase of the amorphous phase mobility but also to an increase of the amorphous structure at the boundaries with the crystalline phase, facilitating the deformation of crystal lamellae.

To conclude, exposing PA6 to a humid environment, depending on the temperature and relative humidity values, is considered to impact in a major part the amorphous phase by increasing its mobility that leads to the glass transition temperature depression, which has a direct impact on the mechanical properties such as the decrease of strength and stiffness, therefore, limiting its application in the engineering field [25].

4.1.2 Impact of nanofibers diameter

The glass transition temperature was noted to depend on the chemical structure, the preparation process, the annealing treatment and the geometry of the investigated polymer. A great focus was devoted to the understanding of the geometry, namely the size, effect on the glass transition behavior of polymers with reduced length scale in one or more dimensions, since a significant change of this transition's temperature was reported compared to their bulk corresponding material [26] [27]. This change of behavior was attributed, in previous studies, to the "confinement effect" implying that when decreasing a polymer material dimensions the near-surface region exhibits a behavior different from its inner part [28].

In our case, we investigated the reduced size of nanofibers and its impact on their physical properties by tracking the variation of the glass transition temperature, the degree of crystallinity X_C, the amount of the rigid amorphous fraction X_{RAF} and the mobile amorphous fraction X_{MAF} .

Table 4.3 Characteristics of glass transition determined by MT-DSC for different diameters of nanofiber mats after being dried

Nanofiber mats diameters (nm)	Tg (°C)	ΔC_p (J/ (g.K))	Xc (%)	X_{MAF} (%)	X_{RAF} (%)
60	74 ± 0.5	0.14± 0.001	33 ± 0.5	30 ± 0.1	37 ± 0.4
133	72 ± 0.4	0.14 ± 0.003	32 ± 0.5	30 ± 0.3	38 ± 0.5
325	71 ± 0.4	0.15 ± 0.001	31 ± 0.5	32 ± 0.3	37 ± 0.5

According to *Table 4.3* and considering the uncertainty of the estimated values, a slight increase of the glass transition temperature is noted while the degree of crystallinity remains almost the same when decreasing nanofibers diameters. The explanation of this behavior remains object of controversy in literature when it comes to investigating the size effect of polymer materials. For example, Wang et al [29] determined the glass transition temperature of single polyvinyl alcohol (PVA) nanofibers by means of AFM nanomechanical indentation and three point

bending, and revealed a decrease of 7°C of the glass transition temperature when decreasing nanofiber diameters from 600 nm to 100 nm. They explained this behavior by consideration of a probable polymer chain confinement at the fiber surface. In other words, they presumed that molecular chains with high mobility are present near the surface of the fiber with a volume fraction that increases when decreasing nanofibers diameter. Their results fitted a previous theoretical model and simulation highlighting size dependence of the glass transition temperature in spatially confined polymers [30] [31].The model itself was based on a phenomenon extensively studied in literature, that is the confinement effect in thin films. For these structures, the deviation of Tg from the bulk value was reported to be related to the presence of free interfaces which is the case of freestanding films, or the lack of free interfaces which is the case of films supported on a substrate [32]. As a matter of fact, the presence of the free surface was considered to enhance the local short-range mobility leading to a decrease of the glass transition temperature. On the other hand, for supported films and in the presence of a polymer surface-substrate interaction, the local short-range mobility is expected to be hindered leading to an increase in the glass transition temperature [26] [33] [34].

Regarding nanofibrous structures, another study conducted by Ji et al [35] reported no change in the glass transition temperature when varying polystyrene (PS) nanofibers diameter, however for a diameter range of 600 nm till 17µm. Their perception is that during electrospinning, the polymer jet solution undergoes high shear forces due to the applied electric field coupled with the rapid solidification of the polymer jet, leading to a high molecular orientation. Being heated, a gradual loss of this orientation takes place until reaching equilibrium at the glass transition temperature.

When compared to the abovementioned explanations, our results can be interpreted differently considering the slight increase of Tg contrarily to the trend reported for thin films and having nanofibers way thinner than those studied by Ji et al. In fact, the behavior of PA6 nanofibers in our work, can be accounted in part to the high molecular orientation of polymer chains in the amorphous phase due to the elongational forces and rapid solidification of the polymer jet, whose impact can be more significant for thinner nanofibers leading to a higher molecular orientation. The other part may be related to the formation and the slight increase of the rigid amorphous fraction (RAF) when decreasing nanofibers diameters as shown in *Table 4.3.*

In this matter, several studies have revealed the presence of a rigid amorphous fraction within semi-crystalline polymers and its impact on the polymer properties such as mechanical and gas

barrier properties [36] [37]. Being tightly related to the crystalline phase, the RAF was considered to behave similarly and act like a stress transfer point leading to an increase of the elastic modulus [38]. Though, with regards to the barrier properties, the RAF was considered to be closer to the behavior of an unconstrained amorphous phase due to its higher free volume comparing to the crystalline phase, resulting with different diffusion rates [37] [39]. It has been also mentioned that the formation of the rigid amorphous fraction is governed by the crystallization conditions such as the crystallization temperature and rate [40] [41]. Moreover, the presence of this fraction has been studied within nanosized structures such as nanocomposites of PMMA (polymethyl methacrylate)/SiO_2 (silicone dioxide) [42] and PTT (polytrimethylene terephthalate)/MWCNT (carbon nanotubes).[43] It was reported that adding MWCNTs to PET nanofibers induced an increase of the rigid amorphous fraction from 11% to 33% when the degree of crystallinity remained almost the same. This increase is thought to be related to the fact that adding MWCNTs created interfacial interactions with the polymer matrix that may have triggered a strong restriction of the polymer chain mobility that was emphasized by the orientation of MWCNTs along the fiber axis due to the high elongation of PTT/MWCNT jet during electrospinning [43] [44]. The presence of RAF was noted even in the absence of nanoparticle fillers within nanofibers. It is the case of highly aligned PLA electrospun nanofibers, for which an amount of 11% of RAF was determined when using a drum rotating with a rotation speed of 2500 rpm. This was explained by the molecular orientation induced by the mechanical force applied using a rotation drum as a collector, Columbic force due to the electric field applied during electrospinning coupled with the high surface to volume ratio and the air-polymer interface serving as “virtual” constraint leading to the formation of the non-crystalline oriented structure defined in this work as the RAF [45]. In the case of our study, the collector is a stationary plate but still the formation of the RAF can be attributed in part to the nanofibrous form that may have created a restrictive environment along with high elongational forces that hindered the mobility of polymer chain segments within the amorphous phase.

The orientational order in nanofibrous structure developed during electrospinning and the spatial restriction induced by the decrease of their diameters were considered, in this work, as driving forces for the slight increase of the glass transition temperature and the mobility restriction of a portion of the amorphous phase that was designated as the rigid amorphous fraction. For a better understanding of the impact of this behavior, a combination of thermal and WAXD analysis was conducted.

4.2 Crystalline structure of PA6 nanofibers: identification and distribution of crystalline population

Polyamide 6 is well known for its polymorphic structure, generated by strong intramolecular and intermolecular interactions such as hydrogen bonds. Its crystalline phase may consist of two or more forms depending on the crystallization and processing conditions [18]. Several crystalline and metastable forms were reported in literature such as the presence of a mesomorphic β form that was distinguished by a random distribution of hydrogen bond layers perpendicular to the main chain axis [46] [47]. However, two main forms are more frequently considered to figure in the crystalline structure of polyamide 6, α and γ forms *(Figure 4.3)* [48]. The α crystalline form is defined as a monoclinic lattice with hydrogen bonds formed between anti-parallel chains. It is considered to have a planar zigzag conformation with crystallographic reflections along (200), (002/202) planes and intersheet distance, or also called d-spacing, of $d_{(200)} \approx 0.37$ nm and $d_{(002/202)} \approx 0.44$ nm. On the other hand, the γ form is reported to have a pseudohexagonal packing with twisted conformation, hydrogen bonds formed between parallel chains and crystallographic reflections along (001), (200/201) and intersheet distance of $d_{(001)} \approx 0.41$ nm [16] [49] [50].

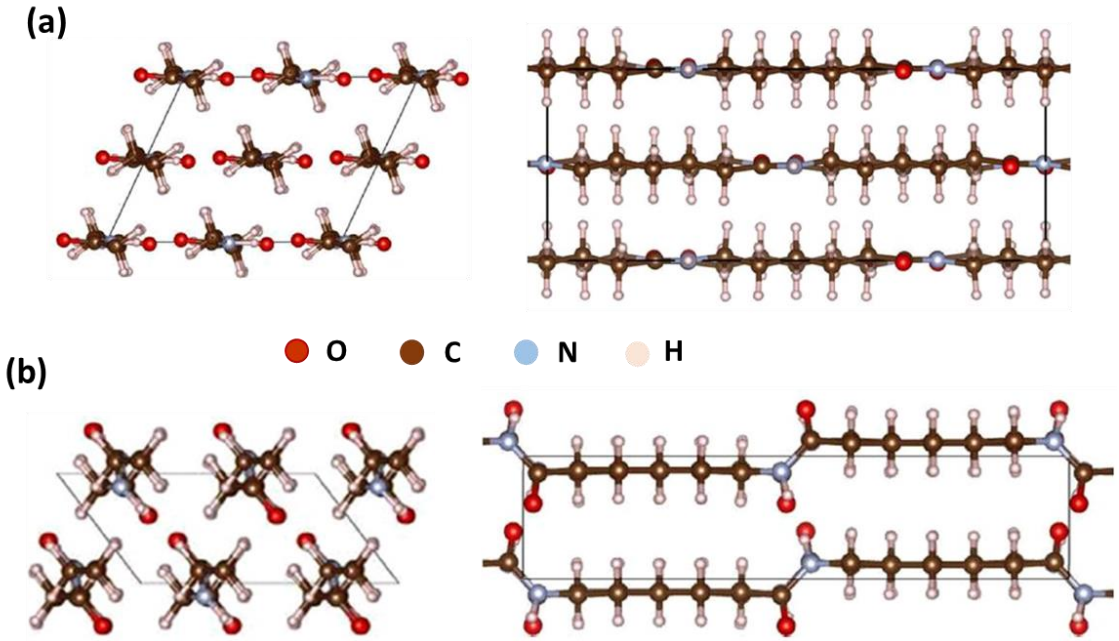

Figure 4.3 Schematic illustration of the atomic configuration of polyamide 6 (a)α and (b) γ crystalline forms [51]

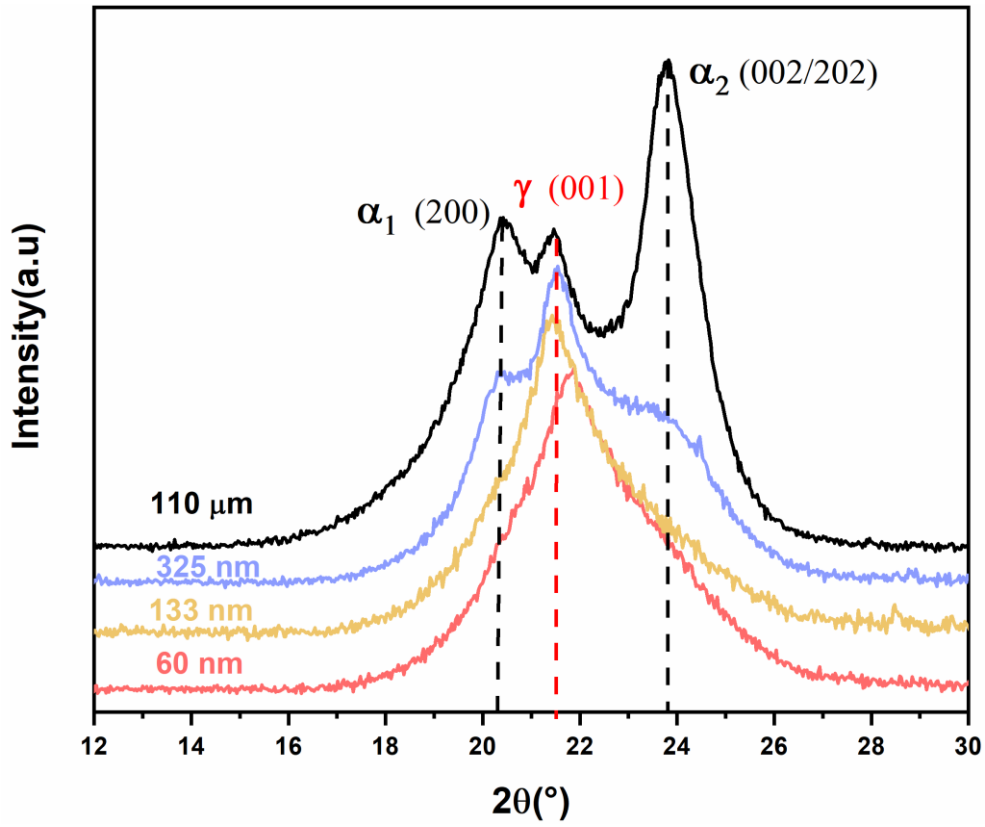

Figure 4.4 WAXD diffraction spectra of PA6 nanofiber mats and film. Dashed lines designate α (black lines) and γ (red line) diffraction peaks

Figure 4.4 illustrates the WAXD spectra of the electrospun PA6 nanofiber mats and a PA6 film with a thickness of 110 μm. The latter was formed by compression molding of PA6 pellets at melting temperature for 5 min and then cooled down at room temperature. The experimental spectrum of this film displays two external diffraction peaks at 2θ= 20.3° and 2θ= 23.8° corresponding to α-crystals and a third peak at 2θ= 21.4° that may correspond to the presence of γ-crystals [16] [52]. Regarding nanofiber mats, WAXD spectra present a pronounced central peak at 2θ= 21.4~21.7° corresponding to γ-crystals and two α-crystal peaks at 2θ=20.2° and 2θ=23~23.7°.

A difference between the spectra of nanofiber mats and of the film is noticeable; the intensity of α-crystal peaks is higher for the film and the γ-crystal peak is more pronounced in nanofiber mats. This can be related to the processing conditions of polyamide 6. Indeed, it is generally believed that slow cooling or isothermal crystallization at temperatures higher than 140°C promote the formation of α-crystals. Oppositely, it was reported that γ-crystals prevail when fast cooling, rapid crystallization or isothermal crystallization at temperatures lower than 130°C are involved in the manufacturing process such as melt spun fibers and cast films [53] [54] [55].

Being electrospun, PA6 nanofibers underwent rapid solidification due to the fast solvent evaporation which may have led to a predominance of γ-crystals comparing to the film [56] [57].

In order to investigate the crystalline conformation in the abovementioned electrospun nanofiber mats, deconvolution of their corresponding XRD spectra along with the estimation of the amount of each crystalline form within nanofibers are presented in the following part. Therefore, we defined A_α as the amount of α-crystals, A_γ as the amount of γ-crystals, $A\gamma_{/\alpha}$ as the ratio of the amount of γ by α crystals as a way to quantify the variation of the different crystalline conformations and X_C as the crystallinity degree. The amount of each crystalline conformation was estimated by dividing the area under the curve of each conformation by the sum of the areas corresponding to the crystalline phase. It is worth precising, that the deconvolution parameters and crystallinity ratios should not be considered as absolute values, they were used to describe the trend of crystalline phase and that the positions of the crystalline forms as well as the amorphous halo were chosen according to previous studies [16] [52].

Table 4.4 Position 2θ, FWHM (Full Width at Half Maximum), $A\gamma_{/\alpha}$ and X_C obtained from fitting of the WAXD experimental spectra of PA6 nanofiber mats

Nanofibers diameters (nm)	**2θ (°)**			**FWHM (°)**			**Aγ/ Aα**	**Xc (%)**
	α_1	**γ**	**α_2**	**α_1**	**γ**	**α_2**		
60	20.2	21.7	23.5	1	1.7	2.2	1.22	69
133	20.2	21.4	23.1	1.9	1.6	2.2	1.09	69
325	20.2	21.5	23.4	1.4	1.3	2.3	0.67	67

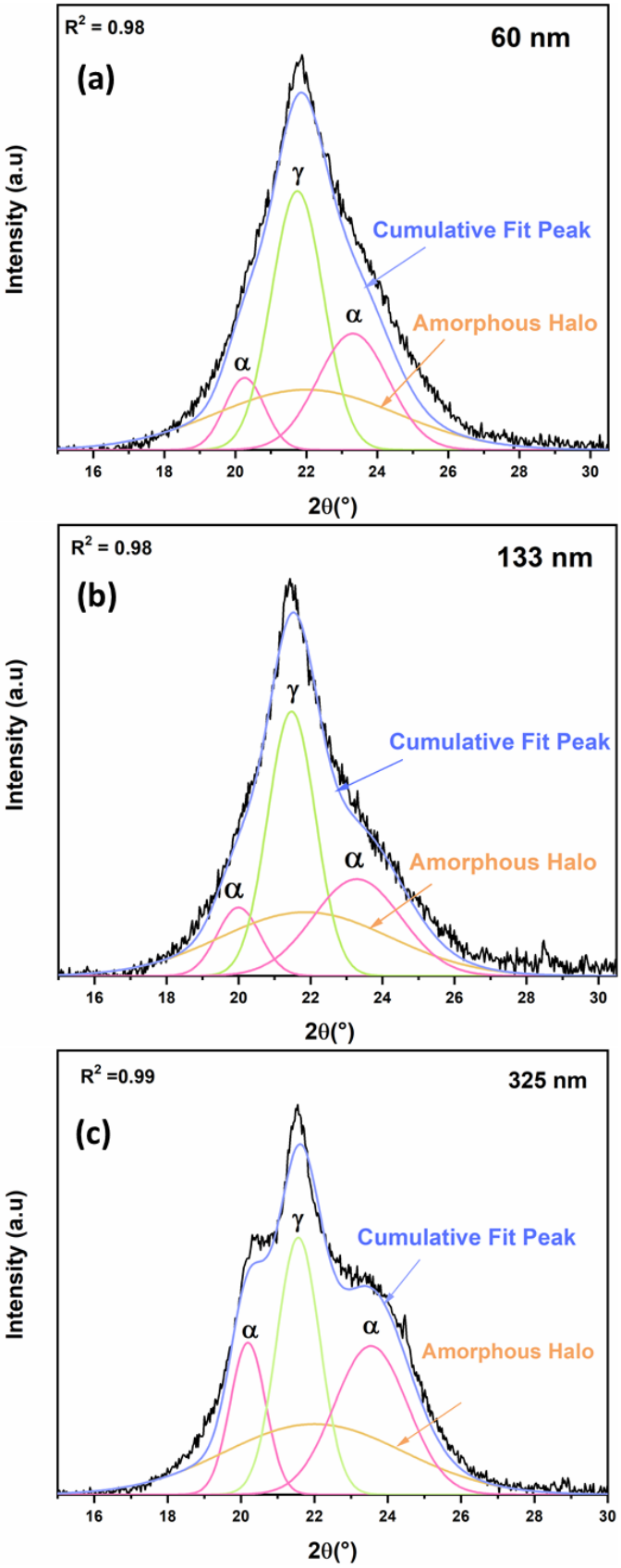

Figure 4.5 Deconvolution of WAXD spectra of nanofiber mats (a) 60 nm, (b) 133 nm, (c) 325 nm

According to *Figure 4.5* and *Table 4.4* , the value of $A_{\gamma/\alpha}$ increases when nanofibers diameter decreases suggesting that the microstructure of the thinnest nanofiber is governed mainly by γ-crystals. Similar observation was noted when investigating electrospun mat from 15% of PA6 in HFIP for which the Raman spectrum was found to be identical to a cast film treated in aqueous potassium iodine/iodine (KI/I_2) that is known to promote γ-crystals formation [58]. Moreover, by comparison to the Raman spectrum of bulk PA6, the peaks related to a C-C stretching, the signature of a trans-planar α conformation, decreased in intensity and shifted to a lower wavenumber and the peaks related to trans amide group weren't observed in PA6 electrospun spectrum, indicating a difference in the backbone of PA6 structure. Meanwhile, gel permeation chromatography (GPC) was applied on pre-spun and electrospun PA6 and showed that the molecular weight for both samples are within the accuracy of the technique highlighting the absence of any denaturing or polymer chain degradation. Therefore, the decrease of the Raman peak associated to α conformation with the change of the molecular arrangement of the polymer chain were believed to be a signature of the predominance of γ crystals that is considered to be resulting from the high stress applied during electrospinning prevailing the kinetics of α crystals formation [59].

To gain more insight into the predominance of this conformation it is necessary to explain the formation of both polymorphic α and γ forms within PA6 crystalline structure. As a matter of fact, a common concept was reported in literature explaining the formation of the crystalline phase according to a chain folded topology involving short molecular folding loops that connects adjacent chain stems [60] [61] [62]. It is believed that when chains are folded repeatedly, intramolecular hydrogen bonds are formed which inevitably cause the adjacent chain to be in opposite direction. This packing was considered to lead to the formation of α-conformation [61]. Depending on the crystallization conditions, an alternative packing, γ conformation, was also reported in literature whose major feature is the formation of hydrogen bonding between parallel chains. Being inconsistent with the chain-folding arrangement, the hydrogen bonds are expected to be intermolecular. The chain folded topology is believed to imply a high degree of crystallinity, because in the case of low crystallinity($X_C \leq 35\%$) the amorphous layers are believed to be as twice as thick as the crystalline lamellae of the semi-crystalline structure. Therefore, the contour length of a chain fold should be on average twice as long as the chain stem to which it is connected. In other words, an amorphous chain segment that exits the crystal will follow a random trajectory and has little chance to fold back to the closest adjacent chain stem forming a non-adjacent loose chain folding, hence the inability to

form a regular chain folding as described for high crystalline PA6 [54] [63]. It was also stated that the high or low degree of crystallinity does not favor any crystalline conformation, being highly dependent on the formation process and crystallization kinetics [54]. Electrospinning is among the techniques that was found to induce both high and low crystallinity degree nanofibers depending on the electrospinning parameters and the spun polymer [64]. The structures formed by electrospinning are described as very similar to those produced by processing techniques involving rapid crystallization such as melt-spinning, where the formation of γ crystals is thought to be faster and more prevalent than the formation of α crystals due to kinetic factors, rapid cooling conditions, and not specifically due to a strain-induced conformation [65]. In this context, Kim et al [66] investigated electrospun PA6 nanofibers with an average diameter of 60 nm by Wide angle X-ray scattering. The spectrum of this sample revealed two peaks at $2\theta = 10°$ and $2\theta = 21°$ attributed to γ crystal conformation, compared to a bulk PA6 with peaks attributed to both γ and α crystals. These results are consistent with the behavior of a melt-spun PA6 as described in previous studies [67]. They were explained by the high shear stress during electrospinning, that led to a change in the spatial arrangement of the molecules resulting in a twist of hydrogen bonds within the amide groups and leading to a shortening of the chains which is considered as a feature of γ crystal conformation. Indeed, nuclear magnetic resonance (NMR) and FTIR experiments have revealed the formation of shorter H-bonds within the γ conformation [61] [68]. However, Chung et al [57] revealed contradictory results when investigating PA6 nanofibers with an average diameter ranging from 70 to 370 nm for which WAXD patterns illustrated an increase of the intensity of peaks relative to α crystals when decreasing nanofibers diameters. This was explained by the formation of a highly packed crystalline phase that is believed to be induced by a high degree of chain stretching and packing due to the decrease of chain entanglement for low concentrated polymer solution. This might be related to mechanical forces applied on the polymer jet due to the use of a rotating collector.

The trend of the predominance of γ crystals within electrospun nanofibers has been reported in several studies, though the explanation of this trend was considered to be mainly kinetic. As a matter of fact, polymorphic phases of PA6 were noted to display different densities; $\rho(\alpha) = 2.13\ g/cm^3$ and $\rho(\gamma) = 1.18\ g/cm^3$ [69]. Having a higher density value, the α crystal conformation needs more crystallization time than the γ conformation, which means when rapid crystallization conditions are favored the PA6 structure is more likely to develop γ conformation.

Regarding our XRD results and according to the above-mentioned explanation about the arrangement of crystal conformation within PA6, we may suppose that α crystals are formed according to the chain folding topology. However, being electrospun, the polymer solution jet solidifies rapidly which means that the solvent evaporation rate is expected to be faster than the crystallization kinetics preventing the molecular chains to register in an anti-parallel arrangement. When reducing the diameter of the nanofibers by electrospinning a polymer solution that is less concentrated in PA6, the impact of rapid solidification should be even more pronounced. Subsequently, the likelihood of the molecular chains arranging in α conformation decreases as the diameter of nanofibers decreases.

It is worthy to mention, that in our case the degree of crystallinity obtained by WAXD *(Table 4.4)* are higher than that obtained by MT-DSC *(Table 4.3)* . At the same time, the sum of the value of the crystallinity degree together with the mesophase fraction or what we designated as rigid amorphous fraction in our work, is relatively close to the value of crystallinity degree determined by WAXD. This may be explained by an overestimation of the crystalline degree during the deconvolution considering the fact that we didn't assign a precise peak for this rigid amorphous fraction. More importantly, in both cases the degree of crystallinity do not vary considerably for the different nanofiber mats and as mentioned earlier the degree of crystallinity does not impact necessarily the distribution of the polymorphic crystalline conformations, being dependent mainly on the crystallization conditions [54].

In the following part, FTIR spectroscopy was performed on the nanofiber mats and the PA6 film to identify and distinguish, more precisely, these crystal conformations. All the spectra were normalized according to amide II absorbance band [70].

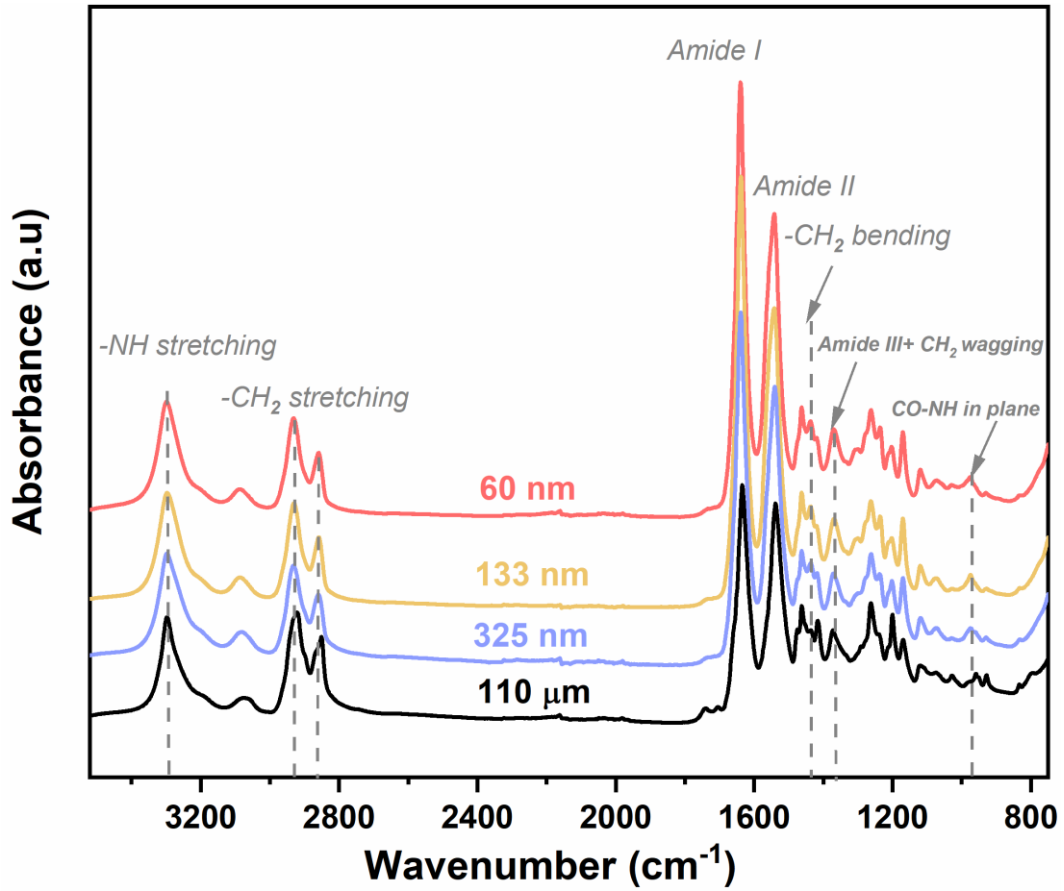

Figure 4.6 FTIR spectra of PA6 nanofiber mats with an average diameter of 60, 133 and 325 nm and a PA6 film with a thickness 110 µm

Figure 4.6 illustrates the absorbance peaks along with the corresponding functional groups classically found in PA6 [72]. All the investigated PA6 samples showed main absorbance peaks at; 3300 cm^{-1} related to hydrogen bonded -NH, 2932 and 2860 cm^{-1} related respectively to CH_2 asymmetric and symmetric stretching, 1640 cm^{-1} related to the carbonyl C=O stretching (amide I) and 1543 related to C-N stretching and -NH in plane bending [73]. To shed the light on the differences between FTIR spectra, we focused on the 1300-800 cm^{-1} wavenumber range, that has been used in previous studies to distinguish the two crystalline forms of PA6 *(Figure 4.7)* [70] [71].

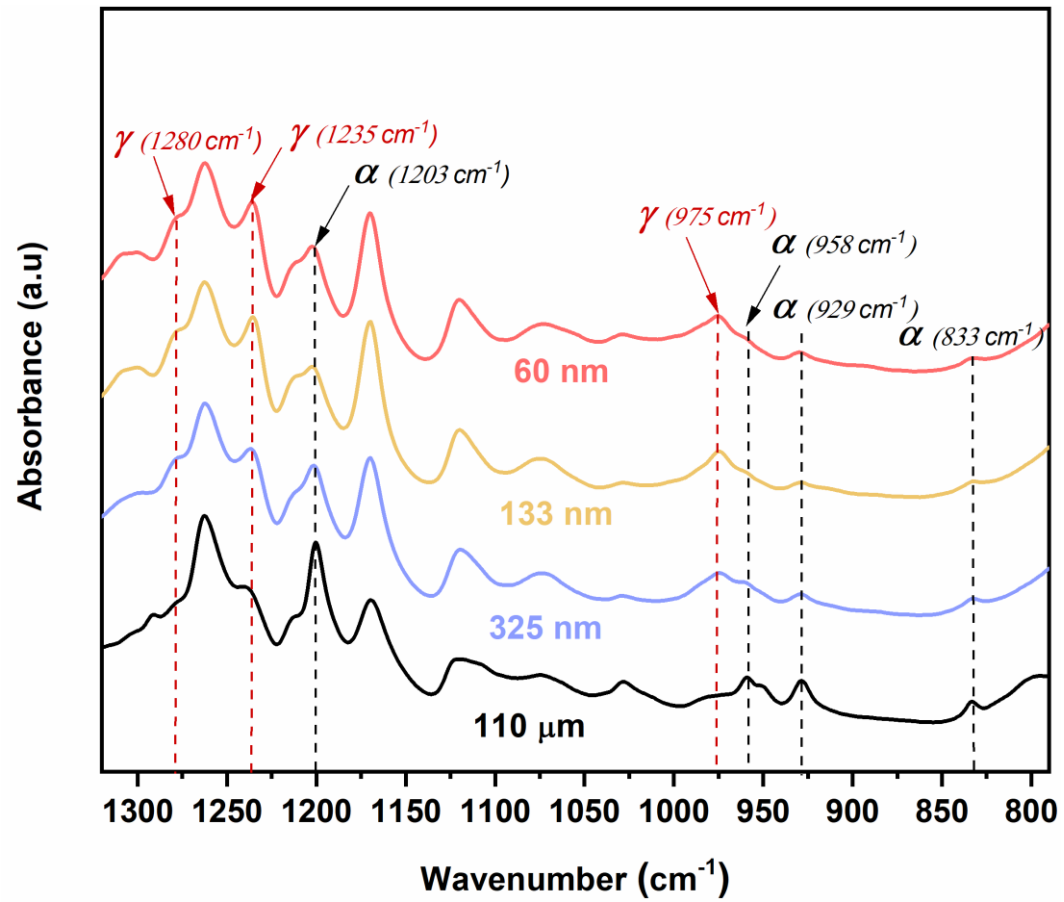

Figure 4.7 FTIR spectra with designation of α and γ absorbance peaks

Table 4.5 Assignement of FTIR absorbance peaks of α and γ crystal conformation[70] [71]

Wavenumber (cm^{-1})	Functional group	Crystal conformation
833	-CH_2 rocking	α
929	-CO – NH in plane	α
958	-CO – NH in plane	α
975	-CO – NH in plane	γ
1235	CH_2 wagging/twisting	γ
1280	CH_2 wagging and amide	γ

According to *Figure 4.7*, the intensity of the absorbance peaks at 975 cm^{-1}, 1235 cm^{-1} and 1280 cm^{-1} corresponding to the γ crystal conformation increases as the diameter of nanofibers decreases, and conversely, the intensity of the absorbance peaks corresponding to α conformation decreases with decreasing nanofiber diameter. In an attempt to quantify this variation, we chose to compare the absorbance at two wavenumbers 1235 cm^{-1} and 1203 cm^{-1} corresponding respectively to γ and α conformations. An absorbance ratio $I_{\gamma/\alpha}$ was determined and was found to increase from 1.09 to 1.27 when decreasing nanofiber diameter from 325 nm to 60 nm. Considering the uncertainties of these calculations we can assume that the microstructure of the thinnest nanofiber entitles a higher amount of γ crystals. This result can be considered as in accordance with the one obtained by WAXD (*Table 4.4)* despite the slight difference regarding the γ/α ratio where a higher amount of α crystals was noticed within the crystalline structure of the thickest nanofiber.

Similar investigations were conducted by Rabolt et al [74] on PA6 nanofibers electrospun by two different techniques "AFM probe-tip electrospinning" and "syringe-needle electrospinning", the first giving access to thinner nanofibers with low polymer solution concentration and higher electric potential. FTIR spectral data of both nanofiber mats, illustrated a higher absorbance peak at 977 cm^{-1}, attributed to γ crystal conformation, for the thinner nanofibers and lower absorbance peak at 1200 cm^{-1}, attributed to α crystal conformation. Though WAXD spectra revealed a predominance of γ crystals for both nanofiber mats comparing to a PA6 film obtained by spin coating of the same electrospinning solution, it is believed that the difference in FTIR spectra is due to a more pronounced impact of the rapid solvent evaporation and high stress on the polymer jet solution, considering the fact that the AFM-based process is supported by a higher localized electric potential. Meanwhile, Lee et al [73] stated different distribution of γ and α conformations when studying electrospun PA6 nanofibers collected on a rotating cylinder with a take-up ranging from 0 to 900 m/min, by means of polarized FTIR. A shift of the peak corresponding to the asymmetric CH_2 stretching (initially at 2930 cm^{-1}) to higher wavenumbers was revealed in the perpendicular polarized spectra while no change was noted in the parallel spectra, when increasing the take-up speed which means decreasing the diameter of nanofibers. This shift was attributed to a relatively higher content of α crystals, since the polymer chains are more tightly packed in this crystalline form. Therefore, they hypothesized that the take-up speed of the collector may have contributed to the molecular arrangement in the α form at the expense of the γ form. Similar outcome has been reported by Vasanthan [75] in his work about drawn PA6 fibers at different draw ratios

(DR= 1, 2, 3 and 4). Indeed, FTIR spectra illustrated an increase in the absorbance of the peak at 930 cm^{-1} corresponding to α crystals simultaneously with a decrease in the absorbance of the peak at 973 cm^{-1} corresponding to γ crystals when increasing the draw ratio. This trend was explained by a strain-induced crystallization of the α crystalline form combined with a crystal-crystal (γ-to- α) transformation at high draw ratio (DR=4). Strain-induced crystallization was also studied for uniaxially PA6 quenched films and it was reported that the crystalline structure formed initially by a predominance of a mesomorphic β conformation transforms into α conformation [76].

The above-mentioned discrepancy in the distribution of crystalline conformations within PA6 structure is mainly due to different crystallization and processing conditions. Indeed, it can be concluded that film or fiber drawing and even electrospinning using a rotating collector led to a strain-induced conformational changes favoring the formation of α crystals. In contrast, WAXD and FTIR spectra in our case illustrated a predominance of γ crystal conformation that is more pronounced for thinner nanofibers and that is mainly related to the rapid solidification of the polymer solution jet and mildly to the contribution of electric elongational deformation forces.

4.3 Temperature dependence of the crystalline structure

In this part, the thermal behavior of electrospun nanofiber mats is investigated to gain more insight into the thermal stability of the two polymorphic phases that form the crystalline phase of PA6 nanofibers. The analysis was performed using means of MT-DSC, FSC and high temperature WAXD.

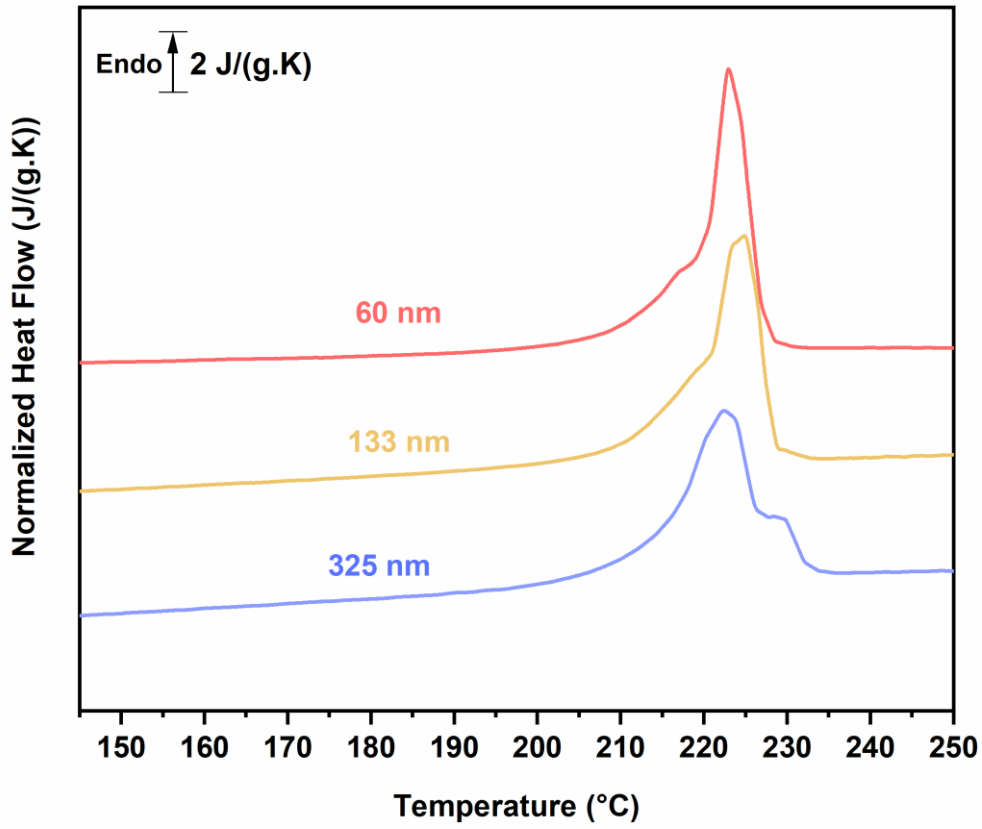

Figure 4.8 Heat flow recorded by MT-DSC at 2 K.min^{-1} with an amplitude of ±0.32 K and a period of 60s for PA6 nanofiber mats

Table 4.6 Melting temperature, Enthalpy of melting and crystallinity degree of PA6 nanofiber mats

Nanofiber mats diameters (nm)	T_f (°C)	$\Delta H_f (J/g)$	X_C(%)
60	223	79	33
133	224	77	32
325	222	75	31

Figure 4.8 illustrates a complex melting behavior of nanofiber mats including a melting peak accompanied with a shouldering. For the thinnest nanofiber mat, a shouldering appears at 217°C followed by a main peak at 223°C. Similar behavior was noted for nanofibers with an average diameter of 133 nm with a shouldering at 219°C followed by a main peak at 224°C. Unlikely, the thickest nanofiber mat presents an inversion of this shouldering-peak trend revealing a main peak at 222°C followed by a shouldering at 228°C. Two main hypotheses may explain the origin of this behavior; the polymorphic structure of PA6 with α and γ crystalline forms melting at different temperatures or the melting of crystallites of the same crystalline form, but with different degree of imperfection due to the electrospinning process.

Previous studies revealed similar complex melting behavior for polyamide 6 samples processed under different conditions. For instance, PA6 film prepared by melt-pressing and quenching in liquid nitrogen was heated till melting at 10°C/min. The DSC curve illustrated a main peak at 220°C neighbored with a melting shoulder around 193°C. It was stated that quenching the sample prevented a full growth of the crystallites which led to the formation of crystals with different degree of defects. Therefore, after high temperature WAXD experiments, it was concluded that the small shoulder may correspond to the melting of imperfect α and γ crystals and the higher temperature peak corresponds the melting of less-defected α and γ crystals [77]. In the same work, the DSC results of PA6 powder obtained from a nylon 6 resin dissolved in formic acid and precipitated in water, showed the shoulder-peak phenomenon that was attributed in this case to the melting of α crystals with different degree of perfection. Moreover, thermal dependence of the polymorphic structure of PA6 crystallized from the molten state was widely analyzed [78] [79]. In this context, the melting behavior of PA6 yarn from the molten state was assessed, by varying the annealing temperature, duration and scanning rate. Proceeding at low heating rates (10 K/min) after annealing for 15 min at a temperature range from 90°C to 150°C, a sharp endothermic peak with a shouldering was observed. Two hypotheses were suggested to explain this behavior; the first one attributed both shouldering and sharp peak to the melting of reorganized crystals and metastable crystals formed during slow heating, and the second hypotheses accorded the shouldering to a mesophase-crystal transition followed by the melting of the reorganized crystals [80].

Another illustration of this phenomenon was reported for electrospun nylon 6 nanofibers with two different diameters; 100 and 250 nm. Both samples were tested in DSC with a heating rate of 10°C/min and showed a sharp melting peak with two small endothermic events prior and following the melting phenomenon [81]. Considering that the microstructure of these

nanofibers was thought to be mainly formed by γ-crystals, the first endothermic event and the main peak were assigned to the melting of this crystalline conformation, deriving from the high degree of elongational deformation during electrospinning. The higher temperature shouldering was attributed to the melting of the small amount of α-crystals within the microstructure. Although, 1D XRD didn't show a well-defined α-form peak, the existence of this crystalline form was confirmed by 2D X-ray diffraction and FTIR. These findings support the observation of a previous study conducted by Liu et al [82] in which the shoulder-peak melting phenomenon of PA6 nanofibers was explained by either melting of γ crystals followed by the melting of α crystals , or a melting-recrystallization phenomenon of γ into α crystalline form.

The melting temperature of both polymorphic forms has been subject to controversy. Indeed, their thermodynamic melting temperatures, considered as the melting of perfectly organized α and γ crystals, were determined theoretically and found to display a minor difference $T_m^o\ (\alpha)\approx$ 228 °C and $T_m^o\ (\gamma)\approx$ 225°C, contrarily to usual experimental observation of a notably lower melting temperature of γ crystals followed by a probable organization into α crystalline form. Therefore, in the case of our study, high temperature WAXD experiments were conducted to provide a clear understanding of the thermal stability of the crystalline structure of electrospun nanofibers.

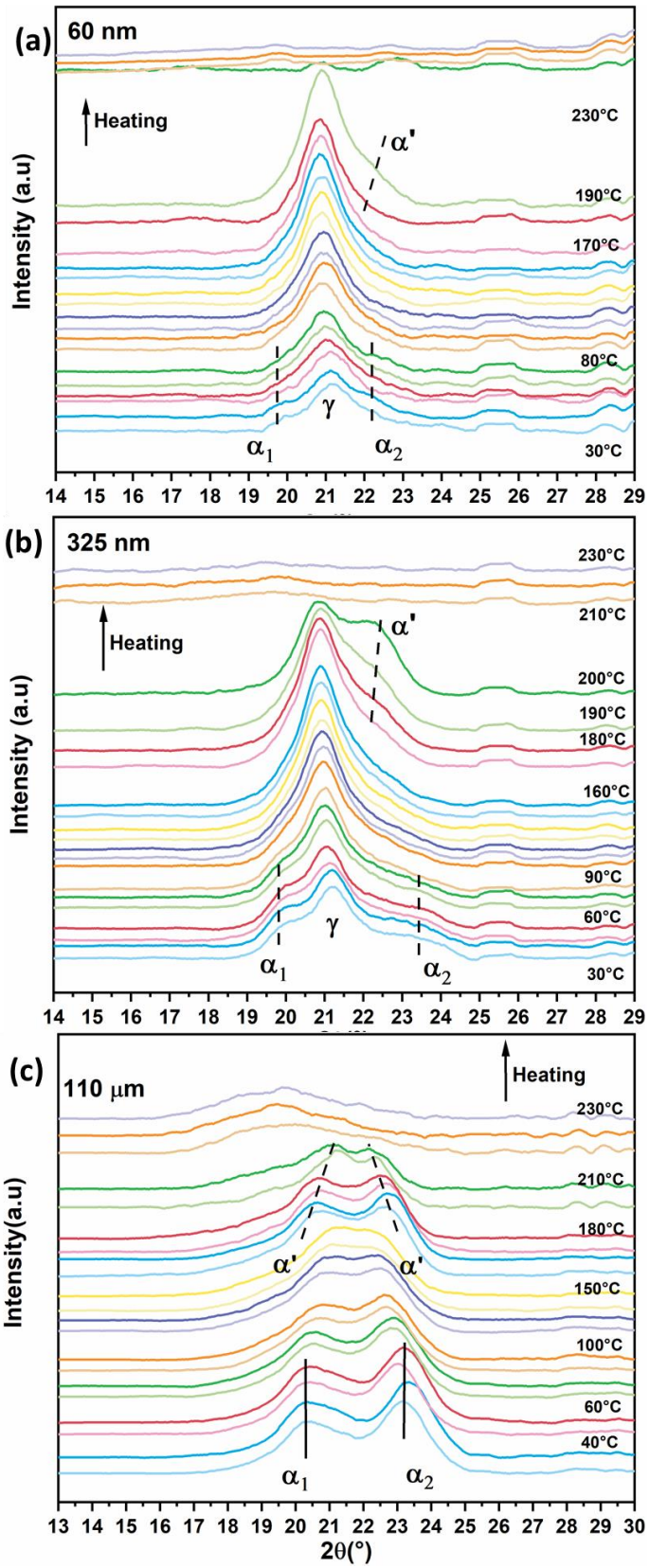

Figure 4.9 WAXD intensity profiles of heated samples from room temperature until 230°C at 2 K/min, XRD scans were recorded every 10°C for electrospun PA6 nanofibers with diameters of (a) 60 nm (b) 325 nm and (c) PA6 film with a thickness of 110 μm

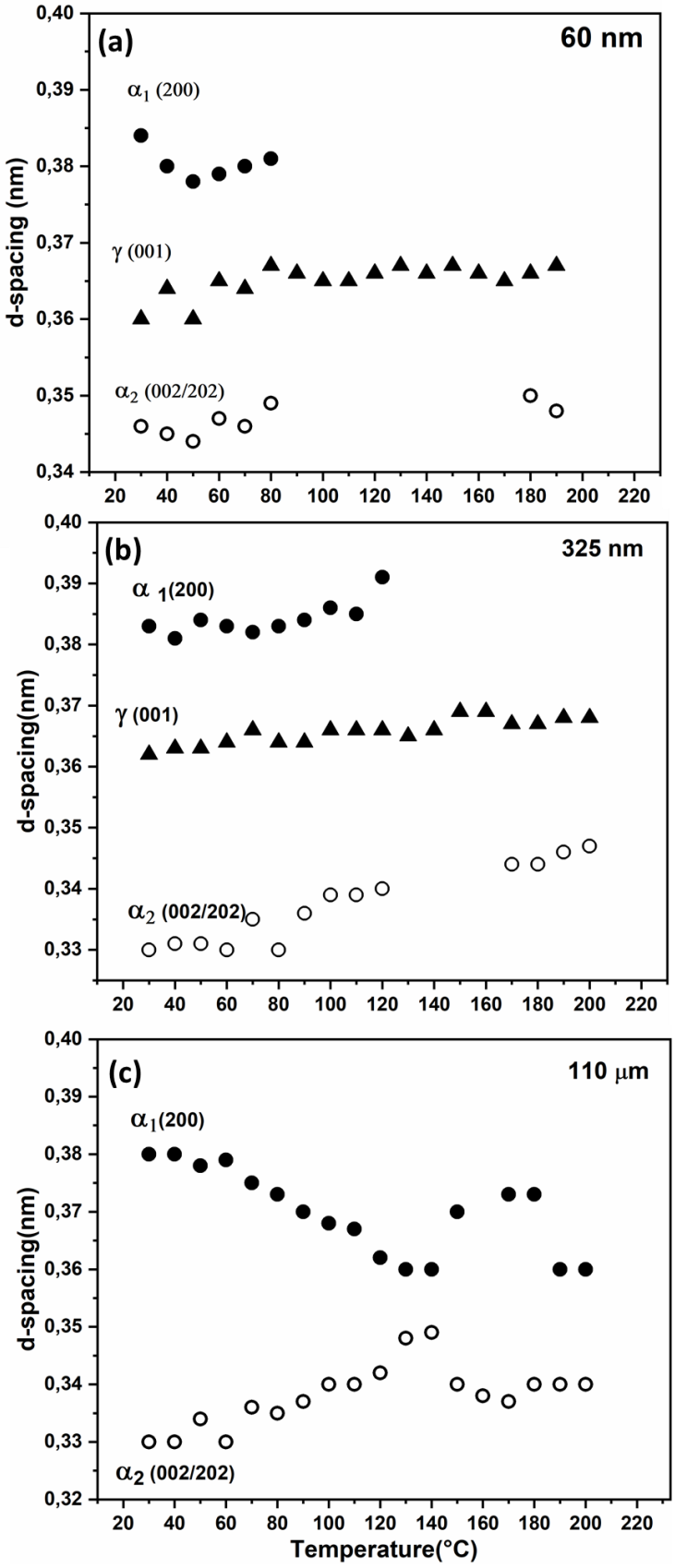

Figure 4.10 Temperature dependence of diffraction spacing (d-spacing) of electrospun PA6 nanofibers with the following diameters (a) 60 nm (b) 325 nm and PA6 film with a thickness of (c) 110 μm

Figure 4.9.a illustrates the WAXD intensity profile of electrospun nanofiber mat with an average diameter of 60 nm. Upon heating, the diffraction peaks related to α crystalline conformation initially reported at room temperature at 2θ (α_1) = 20° and 2θ (α_2) ≈23°, were noted to disappear at temperatures around 100°C and a new peak appears at 170°C at 2θ = 22°. Meanwhile the diffraction peak corresponding to γ crystals at 2θ =21° remains almost the same until melting. Similar phenomenon is noted for electrospun nanofibers with an average diameter of 325 nm *(Figure 4.9.b),* though with higher intensity of the peaks related to α conformation and the one appearing near melting temperature. The WAXD profile of PA6 film *(Figure 4.9.c)* revealed different feature with two peaks at 2θ (α_1) = 20.2° and 2θ (α_2) = 23°, corresponding to α crystals, that decreased in intensity as the temperature increases. At 110°C, both peaks grow closer and slightly merge to form a one large peak at 140°C. On further heating, new peaks appear at 2θ = 20.7° and 2θ = 22.5° until melting.

The thermal dependence of Bragg spacing (d-spacing) was also determined for these samples. For both electrospun nanofibers *(Figure 4.10.a , Figure 4.10.b)* d-spacings of α_1 (200) and α_2 (002/202) slightly decrease and then increase upon heating which can be related to thermal expansion of the crystal lattice [83]. On the other hand, the d-spacing corresponding to γ crystals for both nanofiber mats revealed minor increase, though remained steady until the melting temperature. Regarding the PA6 film *(Figure 4.10.c)* d-spacing related to α_1 (200) decreases along with an increase of the d-spacing related to α_2 (002/202) until 140°C. On further heating d-spacings values evolve inversely until reaching the melting temperature.

Similar observations to those as described have been reported in literature. For instance, the intensity profile of a PA6 powder showed the same phenomenon noted for PA6 film in our study, of the disappearance of peaks related to the α-crystalline conformation and the appearance of two peaks at different positions at higher temperatures, designated as α_1' at 2θ =21° and α_2' at 2θ =22.7°. This behavior was attributed to a transition, triggered by heating, from low-temperature monoclinic crystalline structure α to a high-temperature crystalline structure α′, that was estimated to be also monoclinic [84]. Moreover, the d-spacings were noted to vary and it was related to a modification of the distance between the planes of the H-bonded chains and H-bonded sheets. However, the presence of both peaks at high temperatures was thought to be related to the maintain of the integrity of H-bonds during heating. This suggestion was confirmed by NMR experiments revealing a change of the C-C bonds linked to amide groups from a trans-conformation to gauche conformation that may result from rotational vibrations of the molecules in the crystal over a small angular range due to the increase of

temperature. Therefore, it was suggested that during heating the sample undergoes a conformational structural change while maintaining its integrity. This crystal-crystal (α - α′) transition was noted as a feature of the Brill transition within polyamide 6. Later, this phenomenon was further studied for different polyamides such as PA6, PA66 and PA11 and several hypothesis were suggested to explain the Brill transition like the presence of crystallites of various stabilities, rotational vibration of the methylene group induced by a high chain mobility when heating or the modification of the H-bonds distribution to be randomly arranged, though keeping the same density throughout the heating process [83] [85] [86].

In the same context, Ramesh et al [87] investigated PA6 film chemically treated by potassium-iodine/iodine treatment (KI/I) to obtain a crystalline structure deemed to be formed strictly by γ conformation. The high temperature WAXD profile of this sample illustrated a peak at 2θ =21.47° that was maintained almost the same until the melting temperature along with its corresponding d-spacing. This behavior was attributed to the stability of the γ crystals that is related to the stability of the intersheet H-bonds. Similarities with these results have been reported for quenched PA6 film, where γ conformation was noted to persist to high temperatures though with a slight decrease in intensity and the development of an α-like high crystalline structure around 180°C [77].

Further studies were conducted by Cho et al [81] by means of high temperature WAXD on PA6 electrospun nanofibers from solution and from melt. The resulting intensity profiles suggested that nanofibers electrospun from solution illustrated a stable γ crystalline conformation along with an appearance of peaks related to the α conformation prior to melting, contrarily to nanofibers electrospun from the melt illustrating a γ to α transition around 185°C. It was concluded that despite being electrospun from the melt, the polymer jet underwent rapid quenching due to enhanced heating transfer which led to the formation of a metastable γ crystals that transforms into a stable α crystals on heating. Another example of studies conducted on PA6 electrospun nanofibers was introduced by Wang et al [88]. They investigated nanofibers with different average diameters. For instance, the WAXD intensity profile of nanofibers with an average diameter of 310 nm, illustrated both peaks corresponding to α crystals at room temperature that vanished on the temperature range from 100 and 180°C and the central peak at 21° corresponding to γ crystals that was preserved up to its melting suggesting, also, its thermal stability.

Based on the findings of the previous studies, the temperature-dependent WAXD profiles of PA6 electrospun nanofibers in our case suggest a high thermal stability of the γ crystalline

structure till its melting contrarily to a transition of the α crystals to a high temperature form α´. Accordingly, the complex melting phenomenon illustrated in *Figure 4.8.* may be attributed as following;

- For PA6 nanofibers with an average diameter of 60 nm, the shouldering and the melting peak may correspond to that of the high temperature α´ followed by the melting of γ crystals. This assignment can be true for 133 nm diameter nanofibers.
- For nanofibers with an average diameter of 325 nm, the main peak may be related to the melting phenomenon and the shouldering at higher temperature to the α´ crystals.

Thus far, the thermal behavior and the stability of polymorphic phases have been studied by MT-DSC and high-temperature WAXD that enabled an explanation of the complex melting phenomenon. These experiments were realized at low heating rate leading to the reorganization of the formed crystals during heating. Therefore, in the following part the samples are further investigated by Fast Scanning Calorimetry using a higher heating rate to prevent this reorganization and have a visualization that is as accurate as possible of the melting point of each polymorphic phase.

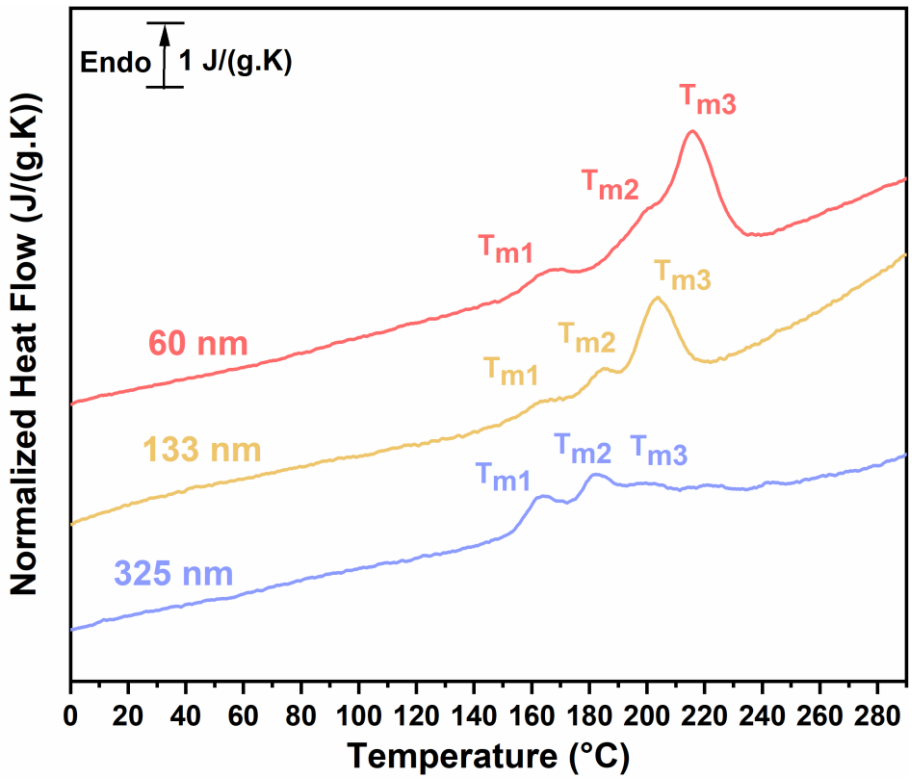

Figure 4.11 FSC heating scans of PA6 nanofiber mats with different nanofibers diameters normalized to the sample mass and the heating rate 120 000 K.min^{-1}

Table 4.7 Melting temperature values of PA6 nanofiber mats obtained by FSC experiment with a heating rate of 120 000 K.min^{-1}

Nanofiber mats diameters (nm)	$T_{m\,1}$ (°C)	$T_{m\,2}$ (°C)	$T_{m\,3}$ (°C)
60	166	200	215
133	164	185	203
325	164	182	200

Figure 4.11 and *Table 4.7* illustrate several melting temperature values for the studied electrospun nanofiber mats. Three main peaks can be distinguished with different temperature values; a first peak around 164°C, a second peak that varies from 180°C for the thickest nanofiber mat to 200°C for the thinnest nanofiber mat and a third melting peak ≥ 200°C depending on the fiber diameter.

Comparing to results obtained by heating the nanofiber mats at 2 $K.min^{-1}$ (*Table 4.6)*, the maximum melting peak shifted to lower values when heated at 120 000 $K.min^{-1}$ which may indicate the hindering of crystal perfectioning by reorganization. Similar explanation was stated by Steyaert et al [89] when investigating PA6 electrospun nanofibers at different scanning rates ranging from 20 to 1000 $K.min^{-1}$ and by Furushima et al [80] for isothermally crystallized PA6 film, where the maximum melting point was noted to shift to lower temperatures. Furthermore, with regard to results obtained by high temperature WAXD that show a disappearance of α crystals justified by its gradual transition to a higher temperature α´ structure along the temperature range of 100-180°C, we might consider that by fast heating this transition was hindered, suggesting that T_{m1} T_{m2} may correspond to the melting of α crystals, and the T_{m3} would correspond to the melting of γ crystals considering its thermal stability that is justified by the interpretations stated earlier in this section.

Overall, the investigation of the melting behavior of PA6 electrospun nanofibers at both high and low heating rates in our study suggest a high thermal stability of the γ crystalline conformation, specifically for the thinnest nanofiber mat presenting the highest melting peak. This finding might seem contradictory considering the fact that nanofibers are produced by electrospinning, a technique that involves rapid solidification of the polymer jet due to fast solvent evaporation on extremely short timeline, leading to the formation of crystals with relatively high degree and different levels of imperfection. This contradiction is thought to be related to the presence of hydrogen-bonds within the crystalline structure of PA6. Though it remains subject of controversy, several studies suggested that the H-bonds are stronger in γ than in the α crystalline structure using NMR, FTIR and molecular dynamics [90] [91], which can contribute to the fact that γ crystals remain mainly unchanged until its melting. This behavior can also be accounted for a high orientational order within the microstructure of nanofibers, as explained in section *4.1.2*, triggered by a combination of relatively high and rapid elongational deformation along the fiber axis [89] [11].

4.4 Conclusion

The crystalline structure of polyamide 6 electrospun nanofiber mats with average nanofiber diameter of 60 nm, 133 nm and 325 nm were investigated. MT-DSC analysis revealed a slight increase of the glass transition temperature and a restriction of the mobility of a portion of the amorphous phase that was identified as a rigid amorphous fraction, when the diameter of nanofibers decreased. The degree of crystallinity being mainly the same for the nanofibers, these phenomena were accorded to a high molecular mobility induced by the stretching of the polymer jet that has a higher impact on the less concentrated polymer solution and to spatial restriction induced by the decrease of their diameters, respectively.

Then, the impact of the diameter of nanofibers on the polymorphic structure of PA6 was studied by WAXD and FTIR. The fractions of γ and α crystals were quantified for each sample, and an increase of the amount of γ crystals was noted, along with the appearance of a more pronounced peak intensity associated with the γ crystals when decreasing the diameter of nanofibers. The decrease of the probability of molecular chains arranging in α conformation was explained by slow crystallization kinetics of this conformation comparing to γ crystals, implying that the PA6 structure is more likely to develop the γ conformation under fast crystallization conditions.

Furthermore, the polymorphic phase stability was investigated through the melting behavior of PA6 nanofiber mats. Low heating rate experiments conducted by MT-DSC revealed a complex melting behavior that was further explained by high-temperature WAXD. Results illustrated a high thermal stability of γ crystals remaining mostly unchanged until their melting, compared to a probable melting/reorganization phenomenon that accompanied the transition of α crystals to a higher temperature α′ crystalline conformation. Being electrospun, the crystalline structure presents relatively high imperfections and heating at low scanning rates would allow their perfectioning. Therefore, FSC experiments were conducted at a high scanning rate to approximate the perfection-free melting of the crystals and the results confirmed the suggestion of the thermal stability of the γ crystalline conformation. This was attributed to the H-bonds being stronger in γ conformation helping to maintain its integrity until melting.

Overall, thermal stability of γ crystals and their predominance with the decrease of nanofibers diameters can be attributed to the orientational order of polymer chains along the fiber axis generated by elongational electric forces combined with a spatial restriction due to the small size of the electrospun nanofibers.

4.5 References

[1] P. Matthies and W. F. Seydl, “History and Development of Nylon 6,” in High Performance Polymers: Their Origin and Development, R. B. Seymour and G. S. Kirshenbaum, Eds. Dordrecht: Springer Netherlands, 1986, pp. 39–53. doi: 10.1007/978-94-011-7073-4_4.

[2] B. L. Deopura, “Polyamide fibers,” in Polyesters and polyamides, Woodhead Publishing in Textiles, 2008, pp. 41–61.

[3] B. L. Deopura and N. V. Padaki, “Synthetic Textile Fibres,” in Textiles and Fashion, Elsevier, 2015, pp. 97–114. doi: 10.1016/B978-1-84569-931-4.00005-2.

[4] X.-C. Hu and H. H. Yang, “Polyamide and Polyester Fibers,” in Comprehensive Composite Materials, Elsevier, 2000, pp. 327–344. doi: 10.1016/B0-08-042993-9/00060-7.

[5] J. Rowe, Advanced materials in automative engineering. Woodhead Publishing Limited, 2012.

[6] F. Chavarria and D. R. Paul, “Comparison of nanocomposites based on nylon 6 and nylon 66,” Polymer, vol. 45, no. 25, pp. 8501–8515, Nov. 2004, doi: 10.1016/j.polymer.2004.09.074.

[7] J. Xue, T. Wu, Y. Dai, and Y. Xia, “Electrospinning and Electrospun Nanofibers: Methods, Materials, and Applications,” Chem. Rev., vol. 119, no. 8, pp. 5298–5415, Apr. 2019, doi: 10.1021/acs.chemrev.8b00593.

[8] B. De Schoenmaker, S. Van der Heijden, I. De Baere, W. Van Paepegem, and K. De Clerck, “Effect of electrospun polyamide 6 nanofibres on the mechanical properties of a glass fibre/epoxy composite,” Polym. Test., vol. 32, no. 8, pp. 1495–1501, Dec. 2013, doi: 10.1016/j.polymertesting.2013.09.015.

[9] M. B. Bazbouz and G. K. Stylios, “The tensile properties of electrospun nylon 6 single nanofibers,” J. Polym. Sci. Part B Polym. Phys., vol. 48, no. 15, pp. 1719–1731, Jun. 2010, doi: 10.1002/polb.21993.

[10] M. V. Jose et al., “Morphology and mechanical properties of Nylon 6/MWNT nanofibers,” Polymer, vol. 48, no. 4, pp. 1096–1104, Feb. 2007, doi: 10.1016/j.polymer.2006.12.023.

[11] M. Richard-Lacroix and C. Pellerin, “Molecular Orientation in Electrospun Fibers: From Mats to Single Fibers,” Macromolecules, vol. 46, no. 24, pp. 9473–9493, Dec. 2013, doi: 10.1021/ma401681m.

[12] C. Fosse, “Compréhension du rôle de la fraction amorphe rigide dans les polyesters,” Physics, University of Rouen Normandy, Rouen, 2020.

[13] R. Androsch and B. Wunderlich, "The link between rigid amorphous fraction and crystal perfection in cold-crystallized poly(ethylene terephthalate)," Polymer, vol. 46, no. 26, pp. 12556–12566, Dec. 2005, doi: 10.1016/j.polymer.2005.10.099.

[14] M. C. Righetti, E. Tombari, and M. L. D. Lorenzo, "Crystalline, mobile amorphous and rigid amorphous fractions in isotactic polystyrene," Eur. Polym. J., vol. 44, no. 8, pp. 2659–2667, Aug. 2008, doi: 10.1016/j.eurpolymj.2008.05.026.

[15] X. Monnier, "Etude de la mobilité moléculaire dans des systèmes polymères complexes anisotropes et confinés," Université de Rouen Normandie, Rouen, 2017.

[16] T. D. Fornes and D. R. Paul, "Crystallization behavior of nylon 6 nanocomposites," Polymer, vol. 44, no. 14, pp. 3945–3961, Jun. 2003, doi: 10.1016/S0032-3861(03)00344-6.

[17] B. Wunderlich, "The ATHAS database on heat capacities of polymers," Pure Appl. Chem., vol. 67, no. 6, pp. 1019–1026, Jan. 1995, doi: 10.1351/pac199567061019.

[18] N. S. Murthy, "Hydrogen bonding, mobility, and structural transitions in aliphatic polyamides," J. Polym. Sci. Part B Polym. Phys., vol. 44, no. 13, pp. 1763–1782, Jul. 2006, doi: 10.1002/polb.20833.

[19] T. S. Ellis, "Moisture-induced plasticization of amorphous polyamides and their blends," J. Appl. Polym. Sci., vol. 36, no. 3, pp. 451–466, Jul. 1988, doi: 10.1002/app.1988.070360301.

[20] N. S. Murthy, M. Stamm, J. P. Sibilia, and S. Krimm, "Structural changes accompanying hydration in nylon 6," Macromolecules, vol. 22, no. 3, pp. 1261–1267, Mar. 1989, doi: 10.1021/ma00193a043.

[21] I. Boukal, "Effect of water on the mechanism of deformation of nylon 6," J. Appl. Polym. Sci., vol. 11, no. 8, pp. 1483–1494, Aug. 1967, doi: 10.1002/app.1967.070110811.

[22] V. Miri, O. Persyn, J.-M. Lefebvre, and R. Seguela, "Effect of water absorption on the plastic deformation behavior of nylon 6," Eur. Polym. J., vol. 45, no. 3, pp. 757–762, Mar. 2009, doi: 10.1016/j.eurpolymj.2008.12.008.

[23] E. Parodi, "Structure properties relations for polyamide 6," Technische Universiteit Eindhoven, 2017.

[24] E. Parodi, G. Peters, and L. Govaert, "Structure–Properties Relations for Polyamide 6, Part 1: Influence of the Thermal History during Compression Moulding on Deformation and Failure Kinetics," Polymers, vol. 10, no. 7, p. 710, Jun. 2018, doi: 10.3390/polym10070710.

[25] N. Jia and V. A. Kagan, "Mechanical Performance of Polyamides with Influence of Moisture and Temperature – Accurate Evaluation and Better Understanding," in Plastics Failure Analysis and Prevention, Elsevier, 2001, pp. 95–104. doi: 10.1016/B978-188420792-1.50014-7.

[26] C. Zhang, Y. Guo, and R. D. Priestley, "Confined glassy properties of polymer nanoparticles," J. Polym. Sci. Part B Polym. Phys., vol. 51, no. 7, pp. 574–586, Apr. 2013, doi: 10.1002/polb.23268.

[27] R. D. Priestley, D. Cangialosi, and S. Napolitano, "On the equivalence between the thermodynamic and dynamic measurements of the glass transition in confined polymers," J. Non-Cryst. Solids, vol. 407, pp. 288–295, Jan. 2015, doi: 10.1016/j.jnoncrysol.2014.09.048.

[28] J. L. Keddie, R. A. L. Jones, and R. A. Cory, "Size-Dependent Depression of the Glass Transition Temperature in Polymer Films," Europhys. Lett. EPL, vol. 27, no. 1, pp. 59–64, Jul. 1994, doi: 10.1209/0295-5075/27/1/011.

[29] W. Wang and A. H. Barber, "Measurement of size-dependent glass transition temperature in electrospun polymer fibers using AFM nanomechanical testing," J. Polym. Sci. Part B Polym. Phys., vol. 50, no. 8, pp. 546–551, Apr. 2012, doi: 10.1002/polb.23030.

[30] J. A. Forrest and J. Mattsson, "Reductions of the glass transition temperature in thin polymer films: Probing the length scale of cooperative dynamics," Phys. Rev. E, vol. 61, no. 1, pp. R53–R56, Jan. 2000, doi: 10.1103/PhysRevE.61.R53.

[31] S. Curgul, K. J. Van Vliet, and G. C. Rutledge, "Molecular Dynamics Simulation of Size-Dependent Structural and Thermal Properties of Polymer Nanofibers," Macromolecules, vol. 40, no. 23, pp. 8483–8489, Nov. 2007, doi: 10.1021/ma0714666.

[32] R. D. Priestley, C. J. Ellison, L. J. Broadbelt, and J. M. Torkelson, "Structural Relaxation of Polymer Glasses at Surfaces, Interfaces, and In Between," Science, vol. 309, no. 5733, pp. 456–459, Jul. 2005, doi: 10.1126/science.1112217.

[33] Q. Jiang, H. X. Shi, and J. C. Li, "Finite size effect on glass transition temperatures," Thin Solid Films, vol. 354, no. 1–2, pp. 283–286, Oct. 1999, doi: 10.1016/S0040-6090(99)00537-4.

[34] J. A. Forrest and K. Dalnoki-Veress, "The glass transition in thin polymer films," Adv. Colloid Interface Sci., vol. 94, no. 1–3, pp. 167–195, Nov. 2001, doi: 10.1016/S0001-8686(01)00060-4.

[35] Y. Ji, B. Li, S. Ge, J. C. Sokolov, and M. H. Rafailovich, "Structure and Nanomechanical Characterization of Electrospun PS/Clay Nanocomposite Fibers," Langmuir, vol. 22, no. 3, pp. 1321–1328, Jan. 2006, doi: 10.1021/la0525022.

[36] I. Kolesov and R. Androsch, "The rigid amorphous fraction of cold-crystallized polyamide 6," Polymer, vol. 53, no. 21, pp. 4770–4777, Sep. 2012, doi: 10.1016/j.polymer.2012.08.017.

[37] A. Guinault, C. Sollogoub, V. Ducruet, and S. Domenek, "Impact of crystallinity of poly(lactide) on helium and oxygen barrier properties," Eur. Polym. J., vol. 48, no. 4, pp. 779–788, Apr. 2012, doi: 10.1016/j.eurpolymj.2012.01.014.

[38] M. C. Righetti, M. Laus, and M. L. Di Lorenzo, "Rigid amorphous fraction and melting behavior of poly(ethylene terephthalate)," Colloid Polym. Sci., vol. 292, no. 6, pp. 1365–1374, Jun. 2014, doi: 10.1007/s00396-014-3198-8.

[39] N. Delpouve, G. Stoclet, A. Saiter, E. Dargent, and S. Marais, "Water Barrier Properties in Biaxially Drawn Poly(lactic acid) Films," J. Phys. Chem. B, vol. 116, no. 15, pp. 4615–4625, Apr. 2012, doi: 10.1021/jp211670g.

[40] R. Androsch and B. Wunderlich, "The link between rigid amorphous fraction and crystal perfection in cold-crystallized poly(ethylene terephthalate)," Polymer, vol. 46, no. 26, pp. 12556–12566, Dec. 2005, doi: 10.1016/j.polymer.2005.10.099.

[41] M. L. Di Lorenzo and M. C. Righetti, "Crystallization-induced formation of rigid amorphous fraction," Polym. Cryst., vol. 1, no. 2, p. e10023, Aug. 2018, doi: 10.1002/pcr2.10023.

[42] A. Sargsyan, A. Tonoyan, S. Davtyan, and C. Schick, "The amount of immobilized polymer in PMMA SiO2 nanocomposites determined from calorimetric data," Eur. Polym. J., vol. 43, no. 8, pp. 3113–3127, Aug. 2007, doi: 10.1016/j.eurpolymj.2007.05.011.

[43] Q. Ma and P. Cebe, "Phase structure of electrospun poly(trimethylene terephthalate) composite nanofibers containing carbon nanotubes," J. Therm. Anal. Calorim., vol. 102, no. 2, pp. 425–434, Nov. 2010, doi: 10.1007/s10973-010-0977-4.

[44] H. Chen, Z. Liu, and P. Cebe, "Chain confinement in electrospun nanofibers of PET with carbon nanotubes," Polymer, vol. 50, no. 3, pp. 872–880, Jan. 2009, doi: 10.1016/j.polymer.2008.12.030.

[45] Q. Ma, M. Pyda, B. Mao, and P. Cebe, "Relationship between the rigid amorphous phase and mesophase in electrospun fibers," Polymer, vol. 54, no. 10, pp. 2544–2554, Apr. 2013, doi: 10.1016/j.polymer.2013.03.019.

[46] F. Auriemma, V. Petraccone, L. Parravicini, and P. Corradini, "Mesomorphic Form (β) of Nylon 6," Macromolecules, vol. 30, no. 24, pp. 7554–7559, Dec. 1997, doi: 10.1021/ma970828e.

[47] D. R. Holmes, C. W. Bunn, and D. J. Smith, "The crystal structure of polycaproamide: Nylon 6," J. Polym. Sci., vol. 17, no. 84, pp. 159–177, Jun. 1955, doi: 10.1002/pol.1955.120178401.

[48] M. Kyotani and S. Mitsuhashi, "Studies on crystalline forms of nylon 6. II. Crystallization from the melt," J. Polym. Sci. Part -2 Polym. Phys., vol. 10, no. 8, pp. 1497–1508, Aug. 1972, doi: 10.1002/pol.1972.160100807.

[49] S. Dasgupta, W. B. Hammond, and W. A. Goddard, "Crystal Structures and Properties of Nylon Polymers from Theory," J. Am. Chem. Soc., vol. 118, no. 49, pp. 12291–12301, Jan. 1996, doi: 10.1021/ja944125d.

[50] D. Kobayashi and A. Takahara, “Interphase crystal structure of polyamide 6 on carbon materials revealed by grazing incidence X-ray diffraction with synchrotron radiation,” Polymer, vol. 97, pp. 174–178, Aug. 2016, doi: 10.1016/j.polymer.2016.05.028.

[51] S. Arabnejad and S. Manzhos, “Defects in alpha and gamma crystalline nylon6: A computational study,” AIP Adv., vol. 5, no. 10, p. 107123, Oct. 2015, doi: 10.1063/1.4934575.

[52] J. P. Parker and P. H. Lindenmeyer, “On the crystal structure of nylon 6,” J. Appl. Polym. Sci., vol. 21, no. 3, pp. 821–837, Mar. 1977, doi: 10.1002/app.1977.070210322.

[53] N. S. Murthy, R. G. Bray, S. T. Correale, and R. A. F. Moore, “Drawing and annealing of nylon-6 fibres: studies of crystal growth, orientation of amorphous and crystalline domains and their influence on properties,” Polymer, vol. 36, no. 20, pp. 3863–3873, Jan. 1995, doi: 10.1016/0032-3861(95)99780-X.

[54] R. Seguela, “Overview and critical survey of polyamide6 structural habits: Misconceptions and controversies,” J. Polym. Sci., vol. 58, no. 21, pp. 2971–3003, Nov. 2020, doi: 10.1002/pol.20200454.

[55] C. Ibanes, L. David, M. De Boissieu, R. Séguéla, T. Epicier, and G. Robert, “Structure and mechanical behavior of nylon-6 fibers filled with organic and mineral nanoparticles. I. Microstructure of spun and drawn fibers: Nanoparticle-Filled Nylon-6 Structure. I,” J. Polym. Sci. Part B Polym. Phys., vol. 42, no. 21, pp. 3876–3892, Nov. 2004, doi: 10.1002/polb.20217.

[56] N. Kimura, H.-K. Kim, B.-S. Kim, K.-H. Lee, and I.-S. Kim, “Molecular Orientation and Crystalline Structure of Aligned Electrospun Nylon-6 Nanofibers: Effect of Gap Size: Molecular Orientation and Crystalline Structure of Aligned …,” Macromol. Mater. Eng., vol. 295, no. 12, pp. 1090–1096, Dec. 2010, doi: 10.1002/mame.201000235.

[57] J. Chung, J. W. Chung, R. D. Priestley, and S.-Y. Kwak, “Confinement-Induced Change in Chain Topology of Ultrathin Polymer Fibers,” Macromolecules, vol. 51, no. 11, pp. 4229–4237, Jun. 2018, doi: 10.1021/acs.macromol.8b00023.

[58] H. Arimoto, M. Ishibashi, M. Hirai, and Y. Chatani, “Crystal structure of the γ-form of nylon 6,” J. Polym. Sci. A, vol. 3, no. 1, pp. 317–326, Jan. 1965, doi: 10.1002/pol.1965.100030132.

[59] J. S. Stephens, D. B. Chase, and J. F. Rabolt, “Effect of the Electrospinning Process on Polymer Crystallization Chain Conformation in Nylon-6 and Nylon-12,” Macromolecules, vol. 37, no. 3, pp. 877–881, Feb. 2004, doi: 10.1021/ma0351569.

[60] S. Adhikari and M. Muthukumar, “Theory of statistics of ties, loops, and tails in semicrystalline polymers,” J. Chem. Phys., vol. 151, no. 11, p. 114905, Sep. 2019, doi: 10.1063/1.5113595.

[61] Y. Li and W. A. Goddard, "Nylon 6 Crystal Structures, Folds, and Lamellae from Theory," Macromolecules, vol. 35, no. 22, pp. 8440–8455, Oct. 2002, doi: 10.1021/ma020815n.

[62] N. A. Jones, P. Sikorski, E. D. T. Atkins, and M. J. Hill, "Nature and Structure of Once-Folded Nylon 6 Monodisperse Oligoamides in Lamellar Crystals," Macromolecules, vol. 33, no. 11, pp. 4146–4154, May 2000, doi: 10.1021/ma9921394.

[63] M. Gilbert, "Aliphatic Polyamides," in Brydson's Plastics Materials, Elsevier, 2017, pp. 487–511. doi: 10.1016/B978-0-323-35824-8.00018-9.

[64] O. Ero-Phillips, M. Jenkins, and A. Stamboulis, "Tailoring Crystallinity of Electrospun Plla Fibres by Control of Electrospinning Parameters," Polymers, vol. 4, no. 3, pp. 1331–1348, Jun. 2012, doi: 10.3390/polym4031331.

[65] R. H. Somani, L. Yang, L. Zhu, and B. S. Hsiao, "Flow-induced shish-kebab precursor structures in entangled polymer melts," Polymer, vol. 46, no. 20, pp. 8587–8623, Sep. 2005, doi: 10.1016/j.polymer.2005.06.034.

[66] G.-M. Kim, G. H. Michler, F. Ania, and F. J. B. Calleja, "Temperature dependence of polymorphism in electrospun nanofibres of PA6 and PA6/clay nanocomposite," Polymer, vol. 48, no. 16, pp. 4814–4823, Jul. 2007, doi: 10.1016/j.polymer.2007.05.082.

[67] N. S. Murthy, S. M. Aharoni, and A. B. Szollosi, "Stability of the γ form and the development of the α form in nylon 6," J. Polym. Sci. Polym. Phys. Ed., vol. 23, no. 12, pp. 2549–2565, Dec. 1985, doi: 10.1002/pol.1985.180231212.

[68] R. Konishi and M. Ito, "Relation between ductility and segmental mobility of nylon-6," Polymer, vol. 45, no. 15, pp. 5191–5198, Jul. 2004, doi: 10.1016/j.polymer.2004.04.034.

[69] B. Wunderlich, "The Defect Crystal," in Macromolecular Physics, Elsevier, 1973, pp. 380–522. doi: 10.1016/B978-0-12-765601-4.50009-3.

[70] N. Vasanthan and D. R. Salem, "FTIR spectroscopic characterization of structural changes in polyamide-6 fibers during annealing and drawing," J. Polym. Sci. Part B Polym. Phys., vol. 39, no. 5, pp. 536–547, Mar. 2001, doi: 10.1002/1099-0488(20010301)39:5<536::AID-POLB1027>3.0.CO;2-8.

[71] S. S. Nair and C. Ramesh, "Studies on the Crystallization Behavior of Nylon-6 in the Presence of Layered Silicates Using Variable Temperature WAXS and FTIR," Macromolecules, vol. 38, no. 2, pp. 454–462, Jan. 2005, doi: 10.1021/ma048860d.

[72] G. Rotter and H. Ishida, "FTIR separation of nylon-6 chain conformations: Clarification of the mesomorphous and γ-crystalline phases," J. Polym. Sci. Part B Polym. Phys., vol. 30, no. 5, pp. 489–495, Apr. 1992, doi: 10.1002/polb.1992.090300508.

[73] K.-H. Lee, K.-W. Kim, A. Pesapane, H.-Y. Kim, and J. F. Rabolt, "Polarized FT-IR Study of Macroscopically Oriented Electrospun Nylon-6 Nanofibers," Macromolecules, vol. 41, no. 4, pp. 1494–1498, Feb. 2008, doi: 10.1021/ma701927w.

[74] G. Gururajan, S. P. Sullivan, T. P. Beebe, D. B. Chase, and J. F. Rabolt, "Continuous electrospinning of polymer nanofibers of Nylon-6 using an atomic force microscope tip," Nanoscale, vol. 3, no. 8, p. 3300, 2011, doi: 10.1039/c1nr10033e.

[75] N. Vasanthan, "Orientation and structure development in polyamide 6 fibers upon drawing," J. Polym. Sci. Part B Polym. Phys., vol. 41, no. 22, pp. 2870–2877, Nov. 2003, doi: 10.1002/polb.10605.

[76] L. Penel-Pierron et al., "Structural and mechanical behavior of nylon-6 films. II. Uniaxial and biaxial drawing: Nylon-6 Films. II," J. Polym. Sci. Part B Polym. Phys., vol. 39, no. 11, pp. 1224–1236, Jun. 2001, doi: 10.1002/polb.1096.

[77] Y. Zhang et al., "Phase stability and melting behavior of the α and γ phases of nylon 6," J. Appl. Polym. Sci., vol. 120, no. 4, pp. 1885–1891, May 2011, doi: 10.1002/app.33047.

[78] X.-Y. Zhao and B.-Z. Zhang, "The effects of annealing (solid and melt) on the time evolution of the polymorphic structure of polyamide 6," J. Appl. Polym. Sci., vol. 115, no. 3, pp. 1688–1694, Feb. 2010, doi: 10.1002/app.31190.

[79] X. Hu and X. Zhao, "Effects of annealing (solid and melt) on the time evolution of polymorphic structure of PA6/silicate nanocomposites," Polymer, vol. 45, no. 11, pp. 3819–3825, May 2004, doi: 10.1016/j.polymer.2004.03.055.

[80] Y. Furushima et al., "Two crystal populations with different melting/reorganization kinetics of isothermally crystallized polyamide 6," J. Polym. Sci. Part B Polym. Phys., vol. 54, no. 20, pp. 2126–2138, Oct. 2016, doi: 10.1002/polb.24123.

[81] D. Cho, E. Zhmayev, and Y. L. Joo, "Structural studies of electrospun nylon 6 fibers from solution and melt," Polymer, vol. 52, no. 20, pp. 4600–4609, Sep. 2011, doi: 10.1016/j.polymer.2011.07.038.

[82] Y. Liu et al., "Crystalline Morphology and Polymorphic Phase Transitions in Electrospun Nylon-6 Nanofibers," Macromolecules, vol. 40, no. 17, pp. 6283–6290, Aug. 2007, doi: 10.1021/ma070039p.

[83] R. Androsch, M. Stolp, and H.-J. Radusch, "Crystallization of amorphous polyamides from the glassy state," Acta Polym., vol. 47, no. 23, pp. 99–104, Feb. 1996, doi: 10.1002/actp.1996.010470206.

[84] N. S. Murthy, S. A. Curran, S. M. Aharoni, and H. Minor, "Premelting crystalline relaxations and phase transitions in nylon 6 and 6,6," Macromolecules, vol. 24, no. 11, pp. 3215–3220, May 1991, doi: 10.1021/ma00011a027.

[85] C. Ramesh, A. Keller, and S. J. E. A. Eltink, "Studies on the crystallization and melting of nylon-6,6: 1. The dependence of the Brill transition on the crystallization temperature," Polymer, vol. 35, no. 12, pp. 2483–2487, Jun. 1994, doi: 10.1016/0032-3861(94)90367-0.

[86] J. Pepin, V. Miri, and J.-M. Lefebvre, "New Insights into the Brill Transition in Polyamide 11 and Polyamide 6," Macromolecules, vol. 49, no. 2, pp. 564–573, Jan. 2016, doi: 10.1021/acs.macromol.5b01701.

[87] C. Ramesh and E. B. Gowd, "High-Temperature X-ray Diffraction Studies on the Crystalline Transitions in the α- and γ-Forms of Nylon-6," Macromolecules, vol. 34, no. 10, pp. 3308–3313, May 2001, doi: 10.1021/ma0006979.

[88] C. Wang, S.-Y. Tsou, and H.-S. Lin, "Brill transition of nylon-6 in electrospun nanofibers," Colloid Polym. Sci., vol. 290, no. 17, pp. 1799–1809, Nov. 2012, doi: 10.1007/s00396-012-2724-9.

[89] I. Steyaert, M.-P. Delplancke, G. Van Assche, H. Rahier, and K. De Clerck, "Fast-scanning calorimetry of electrospun polyamide nanofibres: Melting behaviour and crystal structure," Polymer, vol. 54, no. 25, pp. 6809–6817, Nov. 2013, doi: 10.1016/j.polymer.2013.10.032.

[90] Y. Li and W. A. Goddard, "Nylon 6 Crystal Structures, Folds, and Lamellae from Theory," Macromolecules, vol. 35, no. 22, pp. 8440–8455, Oct. 2002, doi: 10.1021/ma020815n.

[91] M. Z. Brela et al., "Study of hydrogen bond dynamics in Nylon 6 crystals using IR spectroscopy and molecular dynamics focusing on the differences between α and γ crystal forms," Int. J. Quantum Chem., vol. 118, no. 14, p. e25595, Jul. 2018, doi: 10.1002/qua.25595.

Conclusions and perspectives

Electrospun nanofibers have gained a huge amount of interest for the last few years by paving unprecedented advancements in several emerging applications, due to high tunability of their properties. More recently, nanofibers have evidenced compelling mechanical performance compared to bulk commercialized materials that were related to a high molecular orientation. However, the understanding of the microstructure-properties relationship within nanofibers is still fragmentary and the study of the molecular orientation remains challenging.

In this context, this research work was conducted in order to bring more understanding to the microstructure of nanofibers by investigating the signature of molecular orientation within two different nanofibrous polymers; polyamide 6 (PA6) and polyacrylonitrile (PAN). These polymers were chosen for their wide application in engineering and technical use such as carbon nanofibers in the case of polyacrylonitrile. Investigations were carried out using spectroscopic and thermal analysis that have provided crucial knowledge about the impact of the nanosized structure on the crystalline phase of PA6 and the tunability of its polymorphic aspect and on the amorphous phase of PAN nanofibers by investigating its structural relaxation kinetics.

In the first part of the work, three PAN nanofiber mats with different average diameter were investigated. According to results obtained by WAXD a low crystallinity was revealed with a slight decrease of its value when decreasing nanofibers diameters. Concurrently, MT-DSC revealed a slight increase of the glass transition temperature. Together with the FTIR results illustrating a preferential orientation in the direction of the fiber axis, the decrease of the crystallinity coupled with the increase of the glass transition temperature as the nanofibers diameter decreases was accorded to a restrained molecular mobility in the amorphous phase. Then, physical aging studies were conducted in order to track the signature of this molecular mobility restriction. Interestingly and in contrast to the behavior of other nanoscaled structures like nanocomposites and nanospheres, our results revealed a slower aging kinetics for the thinner nanofibers. This was explained by a higher molecular orientation induced by high and rapid elongational deformation of the polymer jet solution during electrospinning. Also, the melting behavior of PAN nanofibers was investigated by means of Fast Scanning Calorimetry that allowed, through high scanning rates faster than the crystallization kinetics, to avoid or retard the degradation of this material which usually takes place prior to melting. The enthalpy of melting determined by this experiment supports results obtained by WAXD.

Conclusions and perspectives

To the best of our knowledge, physical aging of polymer nanofibers was investigated for the first time within the framework of our study as well as the determination of PAN nanofibers melting temperature.

Then, two main aspects related to PA6 electrospun nanofiber mats with three different average diameters were studied. First, the glass transition temperature was evaluated by MT-DSC which illustrated a slight increase of its value as the diameter of nanofiber decrease along with the restriction of the mobility of a portion of the amorphous phase that we designated as rigid amorphous fraction. The crystallinity degree being almost the same for all the samples, this aspect was accorded to a higher molecular orientation induced by the stretching of the polymer jet, that has a higher impact on the less concentrated polymer solution which means as the diameter of the nanofibers decreases. On the other hand, the polymorphic aspect of PA6 nanofiber mats was investigated. WAXD and FTIR experiments allowed the quantification of the amount of γ and α crystalline conformations and revealed an increase of the γ/α ratio when nanofibers diameters decrease, which was explained by slow crystallization kinetics of α conformation comparing to γ crystals, implying that the PA6 structure is more likely to develop the γ conformation under fast crystallization conditions. Thermal stability of both conformations was analyzed by investigated the melting behavior of PA6 using MT-DSC which evidenced a complex melting behavior resulting from the reorganization of crystals with relatively high degree of imperfection formed during electrospinning. This phenomenon was further clarified using High Temperature WAXD that illustrated a high thermal stability of γ crystals remaining mostly unchanged until their melting, compared to a probable melting/reorganization phenomenon that accompanied the transition of α crystals to a higher temperature α´ crystalline conformation. Heating at high scanning rate using FSC helped preventing the reorganization phenomenon and results confirmed the suggestion of the thermal stability of the γ crystalline conformation that was attributed to the orientational order of polymer chains along the fiber axis generated by elongational electric forces.

This work allowed to investigate a particular feature of the crystalline structure of PA6 electrospun nanofibers which can be of great interest for the choice of application of PA6, since both polymorphic crystalline phases showed different mechanical behavior in previous studies. Therefore, by changing electrospinning parameters it is possible to tune the crystalline composition within nanofibers.

It is worth mentioning that in this study, the investigated electrospun nanofiber mats were developed several years prior to the investigation which may have led to a gradual relaxation of the molecular orientation. Therefore, as a short-term perspective, it would be interesting to investigate newly electrospun nanofiber mats with the same electrospinning parameters as ours to track the impact of environmental aging at room temperature conditions, i.e., under possibly combined actions of UV, oxygen and humidity, which is of an extreme interest for applications requiring a long-time use.

Another perspective would be related to the newly developed characterization methods that are more suitable for single nanofiber investigations and can provide more accurate understanding of the nanofibers features by avoiding the averaging over several hundreds of nanofibers within a mat. Working on a unitary nanofiber would allow a straightforward correlation between the orientation state and the investigated physical properties, whereas the distribution of orientation among the fibers is essentially unavoidable with the current means of investigation as they are designed to characterize mats. Finally, it would be interesting to extend this research work on a wider range of polymer systems including recycled or bio-based materials, to investigate a possible generalization of the structural relaxation kinetic slowing down with the nanofiber diameter decrease.

Abstract

Electrospun nanofibers have emerged as a new class of materials that combines both lightweight and compelling mechanical properties, promising a new area of less expensive and more efficient materials to be used in a wide range of applications. However, the structure-properties aspect of nanofibers has not been fully elucidated due to difficulties associated with their nanostructure. The aim of this research is to contribute to the understanding of a particular feature of nanofibers which is the molecular orientation, a feature that is generally mentioned to explain the properties of electrospun fibers, by the study of the polyamide 6 (PA6) and polyacrylonitrile (PAN) nanofiber mats. This study was conducted using spectroscopic techniques and thermal techniques. The Fast Scanning Calorimetry (FSC) allowed to trace the signature of molecular orientation in PAN nanofiber mats by the investigation of their structural relaxation kinetics, that was found to be slower as nanofibers diameters decrease. The study of the crystalline structure of PA6 nanofiber mats revealed the predominance of a polymorphic crystalline conformation and its higher thermal stability for thinner nanofibers, which illustrated the tunability of the nanofibers crystalline structure when varying their processing parameters.
Keywords: nanofibers, structural relaxation, polymorphic structure, fast scanning calorimetry

Resumé

Les nanofibres électrofilées représentent une nouvelle classe de matériaux combinant à la fois légèreté et propriétés mécaniques exceptionnelles ayant un énorme potentiel d'application dans plusieurs domaines. Cependant, l'aspect structure-propriétés des nanofibres n'est pas encore maîtrisé en raison des difficultés liées à leur structure nanométrique. L'objectif de ce travail est de contribuer à la compréhension d'une caractéristique particulière des nanofibres qui est l'orientation macromoléculaire, un critère généralement cité quand il s'agit des propriétés des nanofibres, par l'étude des mats de nanofibres en polyamide 6 (PA6) et polyacrylonitrile (PAN). Cette étude a été menée à l'aide de techniques spectroscopiques thermiques. La calorimétrie différentielle à balayage rapide (FSC) a permis de sonder la signature de l'orientation macromoléculaire dans les mats de nanofibres de PAN par l'étude de leur cinétique de relaxation structurale, qui s'est avérée plus lente lorsque le diamètre des nanofibres diminue. L'étude de la structure cristalline des mats de nanofibres de PA6 a révélé la prédominance d'une conformation cristalline polymorphe avec une meilleure stabilité thermique pour les nanofibres les plus fines.
Mots clés : nanofibre, relaxation structurale, structure polymorphique, calorimétrie différentielle à balayage rapide